

**BRANCH DEPENDENT SHEAR COEFFICIENTS AND
THEIR INFLUENCE ON THE FREE VIBRATION OF
MINDLIN PLATES**

BY JOSEPH M. LAKAWICZ

A thesis submitted to the
Graduate School—New Brunswick
Rutgers, The State University of New Jersey
in partial fulfillment of the requirements
for the degree of
Master of Science
Graduate Program in Mechanical & Aerospace Engineering

Written under the direction of

William J. Bottega

and approved by

New Brunswick, New Jersey

January, 2016

© 2016

JOSEPH M. LAKAWICZ
ALL RIGHTS RESERVED

ABSTRACT OF THE THESIS

**BRANCH DEPENDENT SHEAR COEFFICIENTS AND
THEIR INFLUENCE ON THE FREE VIBRATION OF
MINDLIN PLATES**

by **JOSEPH M. LAKAWICZ**

Thesis Director:

William J. Bottega

The effect of the shear correction coefficient on the branches of the frequency spectrum for the free vibrations of plates using Mindlin plate theory is studied. Each of the three branches of the frequency spectrum for the Mindlin plate is identified through comparison with the frequency spectrum of the infinite elastodynamic plate. The use of branch dependent shear correction coefficients is proposed, in order to bring each of the three branches of the Mindlin plate into best agreement with their corresponding elastodynamic branches. The general solution presented is applied to plates with simply-supported, simply-supported/clamped, and simply-supported/free edges and representative results for the frequency spectrum and modal plots for each of the boundary conditions is discussed. It is shown that the use of branch dependent shear correction coefficients improves the frequency predictions for the free vibrations of Mindlin plates when compared to other studies in the literature. The branches of the frequency spectrum contribute differently to the calculation of the natural frequencies of the vibration modes of the plate for the various boundary conditions considered. The insight gained into the interactions of the frequency branches improves upon the physical understanding and interpretation, as well as the analysis of the free vibration of the Mindlin plate, even for the classical case when a single shear correction coefficient is employed.

Acknowledgements

I would first and foremost like to thank my advisor, Dr. William J. Bottega, for his teachings, guidance, and assistance in the research and writing of this thesis. I would also like to thank Dr. Haym Benaroya and Dr. Haim Baruh for serving on my thesis committee and for their thoughts and comments in their review of the thesis.

Cynthia Cartegna is to be thanked for her help and support in the submission process. Also, thanks to my peers, Michael Pavlou and Peter Balogh, for their thoughts on and contributions to my research.

Lastly, I would like to acknowledge and thank my wife, Alaina, for her love and support throughout my academic studies as well as the love and support of all of my family members.

Table of Contents

Abstract	ii
Acknowledgements	iii
List of Tables	vi
List of Figures	vii
1. Introduction	1
1.1. Thesis Outline	4
2. A Review of Plate Theory	5
2.1. Kinematic Relations	5
2.2. Constitutive Relations and Stress Resultants	8
2.2.1. The Shear Correction Coefficient	10
2.3. Mindlin Plate Theory	12
2.3.1. Boundary and Initial Conditions	14
2.4. Kirchhoff Plate Theory	15
2.4.1. Boundary and Initial Conditions	16
3. The Infinite Elastodynamic Plate	17
3.1. The Frequency Spectrum	25
4. The General Free Vibration Response for the Mindlin Plate	30
4.1. The Eigenvalue Problem and Non-Dimensionalization	30
4.2. Solution Procedure	32
4.3. The Modal Functions	38
4.4. The Frequency Spectrum and Selection of the Shear Correction Coefficient	44

5. Mindlin Theory Applied for Specific Boundary Conditions	48
5.1. Simply-Supported Boundary Conditions in the \bar{x} -direction	48
5.2. Simply-Supported Boundary Conditions in the \bar{y} -direction	51
5.3. Clamped Boundary Conditions in the \bar{y} -direction	55
5.4. Free Boundary Conditions in the \bar{y} -direction	59
6. Results and Discussion	64
6.1. Simply-Supported Boundary Conditions in the \bar{y} -direction	64
6.1.1. Modal Plots	69
6.2. Clamped Boundary Conditions in the \bar{y} -direction	76
6.2.1. Modal Plots	79
6.3. Free Boundary Conditions in the \bar{y} -direction	81
6.3.1. Modal Plots	87
7. Conclusions	93
References	95

List of Tables

6.1. Natural frequencies for the first <i>flexural</i> branch of the simply-supported Mindlin plate with sides $\bar{a} = \bar{b} = 10$ and $\nu = 0.3$	65
6.2. Natural frequencies for the second <i>flexural</i> branch of the simply-supported Mindlin plate with sides $\bar{a} = \bar{b} = 10$ and $\nu = 0.3$	67
6.3. Natural frequencies for the <i>anti-symmetric shear</i> branch of the simply-supported Mindlin plate with sides $\bar{a} = \bar{b} = 10$ and $\nu = 0.3$	68
6.4. Natural frequencies for the present study of the simply-supported/clamped Mindlin plate with sides $\bar{a} = \bar{b} = 10$ and $\nu = 0.3$	78
6.5. Natural frequencies from Hashemi and Arsanjani [7] for the simply-supported/clamped Mindlin plate with sides $\bar{a} = \bar{b} = 10$ and $\nu = 0.3$	78
6.6. Natural frequencies for the present study of the simply-supported/free Mindlin plate with sides $\bar{a} = \bar{b} = 10$ and $\nu = 0.3$	86
6.7. Natural frequencies from Hashemi and Arsanjani [7] for the simply-supported/free Mindlin plate with sides $\bar{a} = \bar{b} = 10$ and $\nu = 0.3$	86

List of Figures

2.1. Plate with coordinate system.	5
3.1. The horizontal shear frequency spectrum for the infinite elastodynamic plate with $\nu = 0.3$	26
3.2. The Rayleigh-Lamb frequency spectrum for the infinite elastodynamic plate with $\nu = 0.3$	27
3.3. The complete frequency spectrum for the infinite elastodynamic plate with $\nu = 0.3$	28
4.1. Comparison of the Mindlin plate frequency spectrum to that of the infinite elastodynamic plate for two values of the shear coefficient with $\nu = 0.3$. . .	45
4.2. Comparison of the frequency spectrum for Kirchhoff plate theory, Mindlin plate theory, and the infinite elastodynamic plate for $\kappa_1 = 5/(6 - \nu)$ and $\kappa_2 = \kappa_s = \pi^2/12$	46
5.1. Plate with coordinate system and dimensions.	48
6.1. The vibration modes for the simply-supported Mindlin plate with sides $\bar{a} = \bar{b} = 10$ and $\nu = 0.3$	69
6.2. The modal functions for the first vibration mode of the first <i>flexural</i> branch for the simply-supported Mindlin plate with sides $\bar{a} = \bar{b} = 10$ and $\nu = 0.3$. .	70
6.3. The modal functions for the first vibration mode of the second <i>flexural</i> branch for the simply-supported Mindlin plate with sides $\bar{a} = \bar{b} = 10$ and $\nu = 0.3$. .	70
6.4. The modal functions for the first vibration mode of the <i>anti-symmetric shear</i> branch for the simply-supported Mindlin plate with sides $\bar{a} = \bar{b} = 10$ and $\nu = 0.3$	70
6.5. The modal shear angles for the first vibration mode of the first <i>flexural</i> branch for the simply-supported Mindlin plate with sides $\bar{a} = \bar{b} = 10$ and $\nu = 0.3$. .	71

6.6.	The modal shear angles for the first vibration mode of the second <i>flexural</i> branch for the simply-supported Mindlin plate with sides $\bar{a} = \bar{b} = 10$ and $\nu = 0.3$	72
6.7.	The modal displacements for several representative vibration modes of the first <i>flexural</i> branch for the simply-supported Mindlin plate with sides $\bar{a} = \bar{b} = 10$ and $\nu = 0.3$	73
6.8.	The modal bending rotations in the \bar{x} -direction for several representative vibration modes of the first <i>flexural</i> branch for the simply-supported Mindlin plate with sides $\bar{a} = \bar{b} = 10$ and $\nu = 0.3$	74
6.9.	The modal bending rotations in the \bar{y} -direction for several representative vibration modes of the first <i>flexural</i> branch for the simply-supported Mindlin plate with sides $\bar{a} = \bar{b} = 10$ and $\nu = 0.3$	75
6.10.	Modal wave number combinations for the simply-supported/clamped Mindlin plate with sides $\bar{a} = \bar{b} = 10$ and $\nu = 0.3$	76
6.11.	Frequency spectrum for the simply-supported/clamped Mindlin plate with sides $\bar{a} = \bar{b} = 10$ and $\nu = 0.3$	79
6.12.	The modal functions for the first vibration mode of the simply-supported/clamped Mindlin plate with sides $\bar{a} = \bar{b} = 10$ and $\nu = 0.3$	80
6.13.	The modal shear angles for the first vibration mode of the simply-supported/clamped Mindlin plate with sides $\bar{a} = \bar{b} = 10$ and $\nu = 0.3$	81
6.14.	The modal displacements for several representative vibration modes of the simply-supported/clamped Mindlin plate with sides $\bar{a} = \bar{b} = 10$ and $\nu = 0.3$	82
6.15.	The modal bending rotations in the \bar{x} -direction for several representative vibration modes of the simply-supported/clamped Mindlin plate with sides $\bar{a} = \bar{b} = 10$ and $\nu = 0.3$	83
6.16.	The modal bending rotations in the \bar{y} -direction for several representative vibration modes of the simply-supported/clamped Mindlin plate with sides $\bar{a} = \bar{b} = 10$ and $\nu = 0.3$	84

6.17. Modal wave number combinations for the simply-supported/free Mindlin plate with sides $\bar{a} = \bar{b} = 10$ and $\nu = 0.3$	85
6.18. Frequency spectrum for the simply-supported/free Mindlin plate with sides $\bar{a} = \bar{b} = 10$ and $\nu = 0.3$	87
6.19. The modal functions for the first vibration mode of the simply-supported/free Mindlin plate with sides $\bar{a} = \bar{b} = 10$ and $\nu = 0.3$	88
6.20. The modal shear angles for the first vibration mode of the simply-supported/free Mindlin plate with sides $\bar{a} = \bar{b} = 10$ and $\nu = 0.3$	88
6.21. The modal displacements for several representative vibration modes of the simply-supported/free Mindlin plate with sides $\bar{a} = \bar{b} = 10$ and $\nu = 0.3$	90
6.22. The modal bending rotations in the \bar{x} -direction for several representative vibration modes of the simply-supported/free Mindlin plate with sides $\bar{a} = \bar{b} = 10$ and $\nu = 0.3$	91
6.23. The modal bending rotations in the \bar{y} -direction for several representative vibration modes of the simply-supported/free Mindlin plate with sides $\bar{a} = \bar{b} = 10$ and $\nu = 0.3$	92

Chapter 1

Introduction

An elastic plate is mathematically a two-dimensional continuum that represents a thin and flat three-dimensional body. This type of structure resists bending and in-plane shear, while also resisting in-plane tension and compression. This thesis studies the free vibration of plates in accordance with the theories of Kirchhoff and Mindlin. The three-dimensional theory of elasticity is also studied in order to better understand the vibration frequency spectrum predicted by Mindlin plate theory.

The classical theory of the bending of plates is attributed to Kirchhoff [12], as he is credited with developing a theory which is mathematically well-posed with regard to boundary conditions. The Kirchhoff theory, however, neglects the effects of transverse shear stress and is known to lose accuracy for high frequency (short wave-length) flexural vibration modes. To improve upon the classical theory, R.D. Mindlin [17] and E. Reissner [26] separately introduced theories for the bending of plates that account for the effects of transverse shear deformation. Mindlin's theory also accounts for the rotatory inertia of the plate and will be the focus of study in this thesis.

While the Kirchhoff theory is formulated with the transverse displacement as the sole measure of motion of the plate, the motion predicted by Mindlin theory is determined by the transverse displacement as well as the transverse shear angles (or equivalently the rotations due to bending of a cross-section with normal in the x and y -directions for a rectangular plate). Mindlin [17] proposes a solution to his plate theory by expressing the transverse displacement and bending rotations in terms of potentials. Mindlin *et al.* [18] use this proposed solution to investigate the free vibration of a rectangular plate with four simply-supported edges as well as a plate with free edges in one direction. The authors found three anti-symmetric branches of the frequency spectrum for the vibration of the

plate which they classified as flexural, thickness-shear, and thickness-twist. Many authors proceeded to study the simply-supported Mindlin plate to address its accuracy or to attempt to improve upon its results, some of which will be commented upon shortly. Hashemi and Arsanjani [7] appear to be the first to consider a Mindlin plate simply-supported in one direction with all other combinations of simply-supported, clamped, or free boundaries in the opposite direction. The authors in that study applied the solution procedure of Mindlin *et al.* [18]. Mindlin and Medick [19] later presented an alternate theory which included the lowest symmetric thickness-stretch and thickness-shear frequency branches.

The most prominent method for analyzing the accuracy of a given plate theory in predicting the free vibration response of a plate, is to compare the results to that predicted by the three-dimensional theory of elasticity. A general elastodynamic solution for a finite plate of rectangular geometry is not known due to the difficulty of applying boundary conditions at the edges around the periphery of the plate. Srinivas *et al.* [28] present an exact solution satisfying the three-dimensional elastodynamic theory for the rectangular plate with all four edges simply-supported, but the solution is not valid for other combinations of boundary conditions. For finite plates of circular geometry, solutions have also been obtained for specific boundary conditions, such as in Hutchinson [9] for stress free edges and in Lange and Bottega [14] for rigid smooth boundaries. Due to the lack of a general elastodynamic solution for all boundary conditions, it is common to compare the results found from plate theory to that of the infinite plate.

The frequency spectrum, from elastodynamic theory, for wave propagation in an infinite plate with traction free surfaces is attributed to Rayleigh [22] and Lamb [13]. They arrived at the well known Rayleigh-Lamb frequency equations that govern the propagation of continuous straight crested waves in the infinite plate. The Rayleigh-Lamb frequency equations cannot be solved analytically, which resulted in much research into the frequency spectrum that they predict. Mindlin [20] summarized the contributions of various researchers in studying the Rayleigh-Lamb frequency spectrum and presents the spectrum for both real and imaginary wave numbers. Meeker and Meitzler [16] studied the general frequency spectrum for the infinite elastodynamic plate by including the contributions of horizontal shear waves with the vertical shear and longitudinal extensional waves of the Rayleigh-Lamb

spectrum. A thorough derivation and summary of the frequency spectrum for the infinite elastodynamic plate appears in Graff [6]. A review of the study of elastodynamics up to the year 1983, which covers many of these developments, is presented by Pao [21].

The frequency spectrum from the three-dimensional theory of elasticity is also prominently employed in determining the shear correction coefficient for the Mindlin plate. The shear correction coefficient is used in many plate theories that include transverse shear deformation to account for the non-uniform distribution of the transverse shear stress through the thickness of the plate. A summary of the various shear correction coefficients found in the literature appears within Chapter 2 of this thesis. In the previously mentioned study by Srinivas *et al.* [28], the authors used their results from the three-dimensional elastodynamic theory for the rectangular plate with all four edges simply-supported to determine the accuracy of the natural frequencies predicted by Mindlin *et al.* [18]. The results of Srinivas *et al.* have been subsequently used as accepted values by many studies, but again, can only be applied when analyzing plates with simply-supported bounding edges.

Mindlin plate theory is considered a first-order shear deformation theory as it allows for a constant shear stress distribution through the thickness of the plate, with only the shear correction coefficient allowing for the non-uniform distribution of the shear stress. Higher-order shear deformation theories allow for a more complex distribution of the shear stress through the thickness of the plate. Reddy [23] proposed a higher-order shear deformation theory that allows for a parabolic distribution of the shear stress and hence, did not require a shear correction coefficient. Reddy and Phan [24] presented exact solutions to that higher-order theory for rectangular plates with four simply-supported edges and showed that their results compared better to the exact results of Srinivas *et al.* [28] than did those of Mindlin *et al.* [18].

A brief history of some notable studies in the literature for plate theories including shear deformation with exact analytical solutions has been given here. A more complete summary of the work done on shear deformable plate theories up to the year 1993, including research done with approximate and finite element solution procedures, can be found in Liew *et al.* [15]. The focus of more recent research has been on developing a shear deformable plate theory that uses the transverse displacement due to bending and the transverse displacement

due to shear as the two variables that define the motion of the plate rather than the total transverse displacement and the rotations due to bending. Some examples of this research can be found in Shimpi and Patel [27], Endo and Kimura [3], and Xiang and Xing [32].

1.1 Thesis Outline

There are seven chapters to this thesis. In the first chapter, an introduction to the history of Mindlin plate theory is presented. Emphasis is placed upon research reported in the literature using exact analytical solutions. The second chapter provides the kinematic, constitutive, and kinetic relations for the Mindlin and Kirchhoff plate theories. A summary of prominent values used for the shear correction coefficient used in the literature is included. Chapter Three reviews the derivation of the frequency spectrum for the infinite elastodynamic plate. In the fourth chapter, a general solution for the free vibration of the Mindlin plate is presented, leading to the modal functions for the plate. A thorough analysis of the frequency spectrum for the Mindlin plate is included, leading to the selection of branch dependent shear correction coefficients—a major component of this thesis. Chapter Five applies the derived general solution to the Mindlin plate for specific boundary conditions to obtain the frequency equation and modal functions for each specific geometry. Square plates with simply-supported boundaries in the x -direction and simply-supported, clamped, or free boundaries in the y -direction are considered. In Chapter Six, the frequency equation for each specific geometry of the plate is solved to obtain the natural frequencies for each geometry. The natural frequencies obtained are used to plot the modal functions for several of the vibration modes of the plate. Results are compared to those of relevant studies published in the literature. The seventh chapter summarizes conclusions drawn from the results of Chapter Six. The thesis concludes with a complete list of cited references.

Chapter 2

A Review of Plate Theory

In this chapter, the kinematic relations, constitutive relations, governing equations, and requisite boundary conditions for the plate theories attributed to Mindlin and Kirchhoff are presented.

2.1 Kinematic Relations

We begin by considering a thin flat uniform, isotropic structure that lies with its mid-plane in the xy -cartersian coordinate plane when in the undeformed configuration, with the z -axis perpendicular to this plane as shown in Figure 2.1. The structure has a uniform thickness, h , in the z -direction that is small when compared to the characteristic length scale, L , in either direction of the mid-plane ($h/L \ll 1$). The plate is hence defined in the xy -plane with its faces located at $z = \pm h/2$.

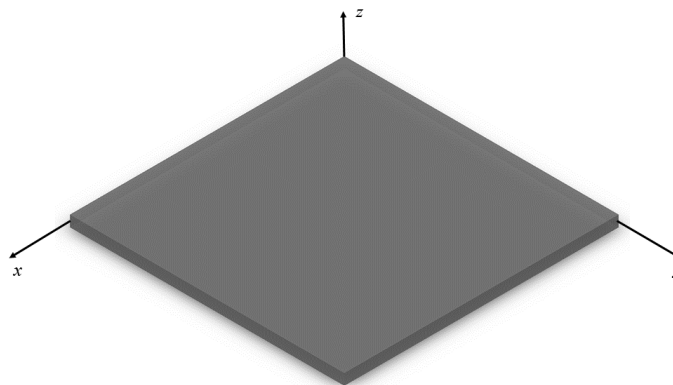


Figure 2.1: Plate with coordinate system.

We assume a linear variation of the in-plane displacements through the thickness in accordance with the Kirchhoff kinematic assumptions, with the deflections of the mid-plane

of the plate given by $u_x^{(0)}(x, y, t)$, $u_y^{(0)}(x, y, t)$, and $w(x, y, t)$ in the x , y , and z -directions respectively. Hence,

$$\begin{aligned} u_x(x, y, z, t) &= u_x^{(0)}(x, y, t) - z\varphi_x(x, y, t) \\ u_y(x, y, z, t) &= u_y^{(0)}(x, y, t) - z\varphi_y(x, y, t) \\ u_z(x, y, z, t) &= w(x, y, t) \end{aligned} \quad (2.1)$$

where $u_x(x, y, z, t)$, $u_y(x, y, z, t)$, and $u_z(x, y, z, t)$ are the displacements at any point through the thickness of the plate and φ_x and φ_y are the rotations due to bending of a cross section of the plate whose normal is in the direction indicated by the subscript.

In both the classical Kirchhoff plate theory and Mindlin plate theory, we incorporate linear strain-displacement relationships consistent with infinitesimal small strain, small rotation deformation. Hence, the normal strains are given by

$$\begin{aligned} \varepsilon_{xx} &= \frac{\partial u_x}{\partial x} \\ \varepsilon_{yy} &= \frac{\partial u_y}{\partial y} \end{aligned} \quad (2.2)$$

and

$$\varepsilon_{zz} = \frac{\partial u_z}{\partial z} = \frac{\partial w}{\partial z} = 0 \quad (2.3)$$

Since the normal strain in the z -direction vanishes identically, there is no change in thickness of the plate as it deforms. The in-plane shear strain, also common to both theories, is given by

$$\varepsilon_{xy} = \varepsilon_{yx} = \frac{1}{2}\gamma_{xy} = \frac{1}{2} \left\{ \frac{\partial u_y}{\partial x} + \frac{\partial u_x}{\partial y} \right\} \quad (2.4)$$

where γ_{xy} is the in-plane shear angle.

Under the classical Kirchhoff theory of plates, the influence of transverse shear stress is neglected and hence both transverse shear strain components are taken to be zero. In Mindlin plate theory, the effects of transverse shear are included and hence the transverse shear strains are given by

$$\varepsilon_{xz} = \varepsilon_{zx} = \frac{1}{2}\gamma_{xz} = \frac{1}{2} \left\{ \frac{\partial u_z}{\partial x} + \frac{\partial u_x}{\partial z} \right\} \quad (2.5)$$

and

$$\varepsilon_{yz} = \varepsilon_{zy} = \frac{1}{2}\gamma_{yz} = \frac{1}{2} \left\{ \frac{\partial u_z}{\partial y} + \frac{\partial u_y}{\partial z} \right\} \quad (2.6)$$

where γ_{xz} and γ_{yz} are the transverse shear angles.

Substitution of Eqs. (2.1) into Eqs. (2.2) and (2.4) yields the distribution of the in-plane strains through the thickness of the plate in accordance with the Kirchhoff kinematic assumptions. Hence,

$$\begin{aligned}\varepsilon_{xx}(x, y, z, t) &= \varepsilon_{xx}^{(0)}(x, y, t) - z\chi_{xx}(x, y, t) \\ \varepsilon_{yy}(x, y, z, t) &= \varepsilon_{yy}^{(0)}(x, y, t) - z\chi_{yy}(x, y, t) \\ \varepsilon_{xy}(x, y, z, t) &= \varepsilon_{yx}(x, y, z, t) = \varepsilon_{xy}^{(0)}(x, y, t) - z\chi_{xy}(x, y, t)\end{aligned}\quad (2.7)$$

where $\varepsilon_{xx}^{(0)}$, $\varepsilon_{yy}^{(0)}$, and $\varepsilon_{xy}^{(0)}$ are the in-plane strains at the reference mid-plane of the plate and are defined by

$$\begin{aligned}\varepsilon_{xx}^{(0)} &= \frac{\partial u_x^{(0)}}{\partial x} \\ \varepsilon_{yy}^{(0)} &= \frac{\partial u_y^{(0)}}{\partial y} \\ \varepsilon_{xy}^{(0)} &= \frac{1}{2} \left\{ \frac{\partial u_y^{(0)}}{\partial x} + \frac{\partial u_x^{(0)}}{\partial y} \right\}\end{aligned}\quad (2.8)$$

and where

$$\begin{aligned}\chi_{xx} &= \frac{\partial \varphi_x}{\partial x} \\ \chi_{yy} &= \frac{\partial \varphi_y}{\partial y} \\ \chi_{xy} = \chi_{yx} &= \frac{1}{2} \left\{ \frac{\partial \varphi_y}{\partial x} + \frac{\partial \varphi_x}{\partial y} \right\}\end{aligned}\quad (2.9)$$

are the changes of curvature of the reference surface in the direction indicated by the subscript. The linear displacement distribution given by Eqs. (2.1) results in a linear distribution of the in-plane strains through the thickness of the plate as given by Eqs. (2.7).

The transverse shear strain distribution through the thickness of the Mindlin plate is obtained from substitution of Eqs. (2.1) into Eqs. (2.5) and (2.6). Hence,

$$\varepsilon_{xz}(x, y, z, t) = \varepsilon_{xz}^{(0)}(x, y, t) = \frac{1}{2}\gamma_{xz}^{(0)}(x, y, t) = \frac{1}{2} \left[\frac{\partial w(x, y, t)}{\partial x} - \varphi_x(x, y, t) \right] \quad (2.10)$$

and

$$\varepsilon_{yz}(x, y, z, t) = \varepsilon_{yz}^{(0)}(x, y, t) = \frac{1}{2}\gamma_{yz}^{(0)}(x, y, t) = \frac{1}{2} \left[\frac{\partial w(x, y, t)}{\partial y} - \varphi_y(x, y, t) \right] \quad (2.11)$$

where $\varepsilon_{xz}^{(0)}$ and $\varepsilon_{yz}^{(0)}$ are the transverse shear strains at the reference mid-plane and $\gamma_{xz}^{(0)}$ and $\gamma_{yz}^{(0)}$ are the transverse shear angles at the reference mid-plane of the plate. For the Mindlin plate, Eqs. (2.10) and (2.11) show that the Kirchhoff kinematic assumptions for displacements predict a uniform distribution of the transverse shear strain and shear angle through the thickness of the plate.

2.2 Constitutive Relations and Stress Resultants

In our analysis of plates, we will consider plates that exhibit linearly elastic and isotropic material behavior. The stress-strain relationships for such materials are governed by Hooke's Law. Plate theory also assumes that the out-of-plane normal stress is negligible when compared with the in-plane normal stresses ($\sigma_{zz} \ll \sigma_{xx}$ and $\sigma_{zz} \ll \sigma_{yy}$). Hence, the in-plane constitutive relations are reduced to the following form

$$\begin{aligned}\sigma_{xx} &= \frac{E}{1-\nu^2} (\varepsilon_{xx} + \nu\varepsilon_{yy}) \\ \sigma_{yy} &= \frac{E}{1-\nu^2} (\varepsilon_{yy} + \nu\varepsilon_{xx}) \\ \sigma_{xy} &= 2G\varepsilon_{xy}\end{aligned}\tag{2.12}$$

The constitutive relations for the transverse shear stresses are

$$\begin{aligned}\sigma_{xz} &= 2G\varepsilon_{xz} \\ \sigma_{yz} &= 2G\varepsilon_{yz}\end{aligned}\tag{2.13}$$

where in both sets of equations

$$G = \frac{E}{2(1+\nu)}\tag{2.14}$$

In the above equations, E is the Young's modulus, ν is the Poisson's ratio, and G is the shear modulus.

Substitution of Eqs. (2.10) and (2.11) into Eqs. (2.13) when considering Mindlin plate theory, results in a predicted transverse shear stress distribution that is uniform through the thickness of the plate. Under general loading, the actual transverse shear stress acting on the plate will not be uniformly distributed through the thickness. Mindlin introduced a shear correction coefficient similar to the Timoshenko shear correction coefficient used in beam theory to account for this discrepancy. The effective transverse shear angles found in Eqs. (2.10) and (2.11), which result from the Kirchhoff assumptions, are defined as the weighted average of the actual transverse shear angle distribution. Hence,

$$\begin{aligned}\gamma_{xz}^{(0)}(x, y, t) &= \frac{1}{\kappa h} \int_{-h/2}^{h/2} \gamma_{xz}(x, y, z, t) dz \\ \gamma_{yz}^{(0)}(x, y, t) &= \frac{1}{\kappa h} \int_{-h/2}^{h/2} \gamma_{yz}(x, y, z, t) dz\end{aligned}\tag{2.15}$$

where κ is the shear correction coefficient for the Mindlin plate. Evaluation of the shear correction coefficient will be discussed in the next section.

The stress resultants are resultant forces and moments that are statically equivalent to the distribution of stresses through the thickness of the plate and are found by integrating the stresses and their moments through the thickness of the plate. The resultant membrane forces per unit length are found by integrating the stresses through the thickness of the plate, with the strain distributions given by Eqs. (2.7). Hence,

$$\begin{aligned} N_{xx}(x, y, t) &= \int_{-h/2}^{h/2} \sigma_{xx} dz = C \left(\varepsilon_{xx}^{(0)} + \nu \varepsilon_{yy}^{(0)} \right) \\ N_{yy}(x, y, t) &= \int_{-h/2}^{h/2} \sigma_{yy} dz = C \left(\varepsilon_{yy}^{(0)} + \nu \varepsilon_{xx}^{(0)} \right) \\ N_{xy}(x, y, t) &= \int_{-h/2}^{h/2} \sigma_{xy} dz = (1 - \nu) C \varepsilon_{xy}^{(0)} \end{aligned} \quad (2.16)$$

where the membrane stiffness, C , is given by

$$C = \frac{Eh}{1 - \nu^2} \quad (2.17)$$

The resultant bending and twisting moments per unit length are found by integrating the moments of the stresses through the thickness of the plate, with the strain distribution again given by Eqs. (2.7). Hence,

$$\begin{aligned} M_{xx}(x, y, t) &= \int_{-h/2}^{h/2} \sigma_{xx} z dz = -D (\chi_{xx} + \nu \chi_{yy}) \\ M_{yy}(x, y, t) &= \int_{-h/2}^{h/2} \sigma_{yy} z dz = -D (\chi_{yy} + \nu \chi_{xx}) \\ M_{xy}(x, y, t) &= \int_{-h/2}^{h/2} \sigma_{xy} z dz = -(1 - \nu) D \chi_{xy} \end{aligned} \quad (2.18)$$

where the bending stiffness, D , is given by

$$D = \frac{Eh^3}{12(1 - \nu^2)} = \frac{Ch^2}{12} \quad (2.19)$$

The resultant transverse shear forces per unit length are found by integrating the transverse shear stresses through the thickness of the plate.

$$\begin{aligned} Q_x(x, y, t) &= \int_{-h/2}^{h/2} \sigma_{xz} dz = G \int_{-h/2}^{h/2} \gamma_{xz}(x, y, z, t) dz \\ Q_y(x, y, t) &= \int_{-h/2}^{h/2} \sigma_{yz} dz = G \int_{-h/2}^{h/2} \gamma_{yz}(x, y, z, t) dz \end{aligned} \quad (2.20)$$

Substitution of Eqs. (2.15) into Eqs. (2.20) gives the resultant transverse shear forces as

$$\begin{aligned} Q_x(x, y, t) &= k \gamma_{xz}^{(0)}(x, y, t) \\ Q_y(x, y, t) &= k \gamma_{yz}^{(0)}(x, y, t) \end{aligned} \quad (2.21)$$

where the shear stiffness, k , is given by

$$k = \kappa Gh \quad (2.22)$$

Further, substitution of Eqs. (2.10) and (2.11) into Eqs. (2.21) gives the resultant transverse shear force per unit length in terms of the transverse displacement and the rotations due to bending as

$$Q_x(x, y, t) = k \left(\frac{\partial w}{\partial x} - \varphi_x \right) \quad (2.23a)$$

$$Q_y(x, y, t) = k \left(\frac{\partial w}{\partial y} - \varphi_y \right) \quad (2.23b)$$

In the next section we provide a discussion of the shear correction coefficient.

2.2.1 The Shear Correction Coefficient

The shear correction coefficient, κ appearing in Eqs. (2.15) and (2.22) is used in plate theories that include the effects of transverse shear deformation to account for the non-uniform distribution of transverse shear stress through the thickness of the structure. The correction coefficient appears in Mindlin's mathematically two-dimensional plate theory, as well as the mathematically one-dimensional analog-Timoshenko beam theory.

Values for the shear correction coefficient are often determined by theoretical or experimental study of Timoshenko beams with transverse shear deformation. Timoshenko [30] first determined a shear correction coefficient of $\kappa = 2/3$ by taking the effect of shear on a rectangular beam to be equal to the shear angle of the centroidal surface. In a later paper, Timoshenko [31] used $\kappa = 8/9$ to better bring his results into agreement with those obtained using two-dimensional elasticity theory. Timoshenko used this value based on the theoretical results of Filon [4]. Filon [5] later experimentally verified his own theoretical results by studying the transmission of polarized light through a glass beam of rectangular cross-section. Kaneko [11] states that although it is not explicitly presented, Timoshenko [31] suggests the following relation for the shear correction coefficient for a beam under the assumption of plane stress.

$$\kappa = \frac{5(1 + \nu)}{6 + 5\nu} \quad (2.24)$$

where ν is Poisson's ratio for the material. Eq. (2.24) yields $\kappa = 0.870$ for $\nu = 1/3$ and a range of $0.833 \leq \kappa \leq 0.882$ for $0 \leq \nu \leq 1/2$. Kaneko [11] also states that the study by Higuchi *et al.* [8] on the flexural vibration of a thick beam leads to Eq. (2.24) through a two-dimensional analysis of the equation of flexural motion for a beam. Cowper [2] integrates the elasticity equations for a beam with the assumption of plane stress made to obtain

$$\kappa = \frac{10(1 + \nu)}{12 + 11\nu} \quad (2.25)$$

for a rectangular cross-section. Based on his experimental results, Kaneko [11] determines Eq. (2.24) to be the best theoretical expression for the shear correction coefficient for the Timoshenko beam.

Alternate values are obtained for the shear coefficient when studying plates directly. Reissner [25] assumes a linear distribution of bending stresses through the thickness of the plate that results in $\kappa = 5/6$. Mindlin [17] investigates flexural and thickness-shear waves in a plate. He compares his results to that obtained from the three-dimensional equations of elasticity for straight-crested flexural waves in an infinite plate. To bring his results into agreement with Rayleigh surface waves at very short wavelengths he found the following expression for κ for flexural waves

$$4\sqrt{(1 - \alpha\kappa)(1 - \kappa)} = (2 - \kappa)^2 \quad (2.26)$$

where

$$\alpha = \frac{1 - 2\nu}{2(1 - \nu)} \quad (2.27)$$

Equation (2.26) yields $\kappa = 0.870$ for $\nu = 1/3$ and a range of $0.764 \leq \kappa \leq 0.913$ for $0 \leq \nu \leq 1/2$. For thickness-shear waves a value of $\kappa = \pi^2/12$ is found.

In more recent work, Stephen [29] uses a second order truncation approximation to match the lowest flexural mode of vibration of the Mindlin plate to the lowest flexural branch of the Rayleigh-Lamb frequency spectrum for the infinite plate. He found the shear coefficient that leads to the best matching of the flexural vibration frequencies to be

$$\kappa = \frac{5}{6 - \nu} \quad (2.28)$$

Equation (2.28) yields $\kappa = 0.882$ for $\nu = 1/3$ and a range of $0.833 \leq \kappa \leq 0.909$ for $0 \leq \nu \leq 1/2$. Further inspection of Eq. (2.28) shows that it is the plane strain analog of

the plane stress coefficient given in Eq. (2.24) if we replace ν in that equation by $\nu/(1-\nu)$. Stephen also comments that the value $\kappa = \pi^2/12$ from Mindlin [17], gives exact agreement with the horizontal shear vibrational frequencies of the elastodynamic infinite plate. In his study of thick circular plates, Hutchinson [10] also determined that Eq. (2.28) and $\kappa = \pi^2/12$ are the best values of the shear coefficient for matching flexural and horizontal shear vibrational frequencies in a plate, respectively.

Before proceeding, we note that the shear correction coefficient given in Eq. (2.24) for the Timoshenko beam and Eq. (2.28) for the Mindlin plate both reduce to $\kappa = 5/6$ for $\nu = 0$, which is the value that results when making the assumptions in Reissner [25]. This implies the results of Reissner would be most accurate when Poisson's ratio is near zero and would lose accuracy as Poisson's ratio gets larger.

2.3 Mindlin Plate Theory

In this section, we present the force formulation for the equations of motion that govern the isotropic, elastic Mindlin plate as derived in Bottega [1]. For this development, we consider only geometrically linear plate theory, which results in the decoupling of the in-plane motion and the out-of-plane transverse motion. As a result, the in-plane equations of motion will not be presented.

We consider a plate subjected to a distributed transverse load, $q(x, y, t)$, and distributed body couples, $b_x(x, y, t)$ and $b_y(x, y, t)$. Summing the forces acting on a differential plate element in the transverse, z , direction, while only including geometrically linear terms, gives the linear equation of transverse motion.

$$\frac{\partial Q_x}{\partial x} + \frac{\partial Q_y}{\partial y} + q(x, y, t) = m \frac{\partial^2 w}{\partial t^2} \quad (2.29)$$

Here, m is the mass per unit area of the plate.

We next consider the equations of rotational motion of the Mindlin plate. Taking the moments about the y -axis and then the moments about the x -axis of the differential element of the plate results in the equations that govern rotational motion of the plate. Hence,

$$Q_x - \frac{\partial M_{xx}}{\partial x} - \frac{\partial M_{yx}}{\partial y} = I_\rho \frac{\partial^2 \varphi_x}{\partial t^2} - b_x(x, y, t) \quad (2.30)$$

$$Q_y - \frac{\partial M_{xy}}{\partial x} - \frac{\partial M_{yy}}{\partial y} = I_\rho \frac{\partial^2 \varphi_y}{\partial t^2} - b_y(x, y, t) \quad (2.31)$$

Here, I_ρ is the rotatory inertia, or mass moment of inertia per unit area, of the plate. It is the resistance to rotation of the plate due to its mass and is the same in both the x and y -directions since we are considering isotropic plates. Eqs. (2.29)-(2.31) represent the force formulation for the out-of-plane motion of the Mindlin plate.

When solving the equations of motion in Chapter 4, it will be desirable to represent Eqs. (2.29)-(2.31) in terms of a displacement formulation. To convert to a displacement formulation, we substitute Eqs. (2.18), (2.23a), and (2.23b) into Eqs. (2.29)-(2.31). The equations of transverse and rotational motion are presented with the transverse displacement, w , and the rotations due to bending, φ_x and φ_y , as the measures of the motion of the plate. Hence,

$$m \frac{\partial^2 w}{\partial t^2} - k \left\{ \frac{\partial^2 w}{\partial x^2} + \frac{\partial^2 w}{\partial y^2} \right\} + k \frac{\partial \varphi_x}{\partial x} + k \frac{\partial \varphi_y}{\partial y} = q(x, y, t) \quad (2.32)$$

$$I_\rho \frac{\partial^2 \varphi_x}{\partial t^2} - k \frac{\partial w}{\partial x} + k \varphi_x - D \left\{ \frac{\partial^2 \varphi_x}{\partial x^2} + \frac{(1-\nu)}{2} \frac{\partial^2 \varphi_x}{\partial y^2} \right\} - D \frac{(1+\nu)}{2} \frac{\partial^2 \varphi_y}{\partial x \partial y} = b_x(x, y, t) \quad (2.33)$$

$$I_\rho \frac{\partial^2 \varphi_y}{\partial t^2} - k \frac{\partial w}{\partial y} - D \frac{(1+\nu)}{2} \frac{\partial^2 \varphi_x}{\partial x \partial y} + k \varphi_y - D \left\{ \frac{\partial^2 \varphi_y}{\partial y^2} + \frac{(1-\nu)}{2} \frac{\partial^2 \varphi_y}{\partial x^2} \right\} = b_y(x, y, t) \quad (2.34)$$

Since Eqs. (2.32)-(2.34) are coupled in terms of the variables w , φ_x , and φ_y , we will write the equations of motion in matrix operator form as developed in Bottega [1]. Hence,

$$\mathbf{m} \frac{\partial^2 \mathbf{u}}{\partial t^2} + \mathbf{k} \mathbf{u} = \mathbf{F} \quad (2.35)$$

where

$$\mathbf{m} = \begin{bmatrix} m & 0 & 0 \\ 0 & I_\rho & 0 \\ 0 & 0 & I_\rho \end{bmatrix} = m \begin{bmatrix} 1 & 0 & 0 \\ 0 & r_{gyr}^2 & 0 \\ 0 & 0 & r_{gyr}^2 \end{bmatrix} \quad (2.36)$$

is the mass matrix and r_{gyr} is the radius of gyration per unit width of a cross section of the plate. In addition, the stiffness matrix is given by

$$\mathbf{k} = \begin{bmatrix} -k \left\{ \frac{\partial^2}{\partial x^2} + \frac{\partial^2}{\partial y^2} \right\} & k \frac{\partial}{\partial x} & k \frac{\partial}{\partial y} \\ -k \frac{\partial}{\partial x} & \left\{ k - D \left(\frac{\partial^2}{\partial x^2} + \frac{(1-\nu)}{2} \frac{\partial^2}{\partial y^2} \right) \right\} & -D \frac{(1+\nu)}{2} \frac{\partial^2}{\partial x \partial y} \\ -k \frac{\partial}{\partial y} & -D \frac{(1+\nu)}{2} \frac{\partial^2}{\partial x \partial y} & \left\{ k - D \left(\frac{\partial^2}{\partial y^2} + \frac{(1-\nu)}{2} \frac{\partial^2}{\partial x^2} \right) \right\} \end{bmatrix} \quad (2.37)$$

the displacement matrix is

$$\mathbf{u} = \begin{Bmatrix} w(x, y, t) \\ \varphi_x(x, y, t) \\ \varphi_y(x, y, t) \end{Bmatrix} \quad (2.38)$$

and the force matrix is

$$\mathbf{F} = \begin{Bmatrix} q(x, y, t) \\ b_x(x, y, t) \\ b_y(x, y, t) \end{Bmatrix} \quad (2.39)$$

The stiffness matrix given in Eq. (2.37) appears to be non-symmetric because of the sign convention and coordinate system chosen in the derivation. If the first row of the matrix Eq. (2.35) is multiplied by a negative sign, the stiffness matrix would appear symmetric as expected. Equations (2.35)-(2.38) will be used to find a solution to the free vibration of Mindlin plates in Chapter 4 in conjunction with the appropriate boundary and initial conditions.

2.3.1 Boundary and Initial Conditions

Since the Mindlin plate has three unknown variables, it will be necessary to specify three boundary conditions on a given bounding edge, S , of the plate. To satisfy the three degrees of freedom one term in each of the expressions for the work of the transverse load $Q_n w$, the bending moment $M_{nn} \varphi_n$, and the twisting moment $M_{ns} \varphi_s$ must be specified on each edge of the plate as stated in Bottega [1]. Hence, we have

$$Q_n|_S = k \left[\frac{\partial w}{\partial n} - \varphi_n \right]_S \quad \text{or} \quad w|_S \quad \text{prescribed} \quad (2.40)$$

$$M_{nn}|_S = -D \left[\frac{\partial \varphi_n}{\partial n} + \nu \frac{\partial \varphi_s}{\partial s} \right]_S \quad \text{or} \quad \varphi_n|_S \quad \text{prescribed} \quad (2.41)$$

$$M_{ns}|_S = -D \frac{(1-\nu)}{2} \left[\frac{\partial \varphi_s}{\partial n} + \frac{\partial \varphi_n}{\partial s} \right]_S \quad \text{or} \quad \varphi_s|_S \quad \text{prescribed} \quad (2.42)$$

In the above relations, n represents the normal direction to the edge and s represents the tangential direction to the edge.

Specification of the initial velocity and position of the plate is necessary to complete the statement of the free vibration problem of the Mindlin plate. Hence,

$$w(x, y, 0) = w_0(x, y) \quad \text{and} \quad \left. \frac{\partial w}{\partial t} \right|_{t=0} = v_0(x, y) \quad (2.43)$$

$$\varphi_x(x, y, 0) = \varphi_{x_0}(x, y) \quad \text{and} \quad \left. \frac{\partial \varphi_x}{\partial t} \right|_{t=0} = \dot{\varphi}_{x_0}(x, y) \quad (2.44)$$

$$\varphi_y(x, y, 0) = \varphi_{y_0}(x, y) \quad \text{and} \quad \left. \frac{\partial \varphi_y}{\partial t} \right|_{t=0} = \dot{\varphi}_{y_0}(x, y) \quad (2.45)$$

Equation (2.35), along with the appropriate boundary and initial conditions, constitutes the formulation of the problem for the vibration of the Mindlin plate.

2.4 Kirchhoff Plate Theory

In this section, we present the equations of motion that govern the isotropic, elastic Kirchhoff plate. As stated previously, this theory neglects transverse shear deformation so Eqs. (2.5) and (2.6) are taken to be zero. When these transverse shear strains are taken to be zero in Eqs. (2.10) and (2.11) we find

$$\varphi_x = \frac{\partial w}{\partial x} \quad (2.46)$$

and

$$\varphi_y = \frac{\partial w}{\partial y} \quad (2.47)$$

Summing the forces in the transverse, z , direction and the moments acting on a differential plate element for the geometrically linear Kirchhoff plate gives the equations of transverse and rotational motion identical to Eqs. (2.29)-(2.31) with $I_\rho = 0$ since rotatory inertia is also neglected. Eliminating Q_x and Q_y from the equations gives a single equation for the transverse motion of the plate. Hence,

$$\frac{\partial^2 M_{xx}}{\partial x^2} + 2 \frac{\partial^2 M_{xy}}{\partial x \partial y} + \frac{\partial^2 M_{yy}}{\partial y^2} + q(x, y, t) - \left[\frac{\partial b_x}{\partial x} + \frac{\partial b_y}{\partial y} \right] = m \frac{\partial^2 w}{\partial t^2} \quad (2.48)$$

Further, substitution of Eqs. (2.18) with Eqs. (2.46) and (2.47) into Eq. (2.48) gives the equation of motion as

$$m \frac{\partial^2 w}{\partial t^2} + D \left\{ \frac{\partial^4 w}{\partial x^4} + 2 \frac{\partial^4 w}{\partial x^2 \partial y^2} + \frac{\partial^4 w}{\partial y^4} \right\} = q(x, y, t) - \left[\frac{\partial b_x}{\partial x} + \frac{\partial b_y}{\partial y} \right] \quad (2.49)$$

which governs the transverse displacement, w , for the Kirchhoff plate.

2.4.1 Boundary and Initial Conditions

Kirchhoff plate theory requires the specification of two boundary conditions on a given bounding edge, S , of the plate. Hence, we have

$$\left[Q_n + \frac{\partial M_{ns}}{\partial s} \right]_S \quad \text{or} \quad w|_S \quad \text{prescribed} \quad (2.50)$$

$$M_{nn}|_S \quad \text{or} \quad \frac{\partial w}{\partial n} \Big|_S \quad \text{prescribed} \quad (2.51)$$

In the above relations, n represents the normal direction to the edge and s represents the tangential direction to the edge. The term on the left side of Eq. (2.50) represents the Kirchhoff effective transverse shear force.

Specification of the initial velocity and position of the plate is necessary to complete the statement of the free vibration problem of the Kirchhoff plate. Hence,

$$w(x, y, 0) = w_0(x, y) \quad \text{and} \quad \frac{\partial w}{\partial t} \Big|_{t=0} = v_0(x, y) \quad (2.52)$$

Equation (2.49), along with the appropriate boundary and initial conditions, constitutes the formulation of the problem for the vibration of the Kirchhoff plate.

Chapter 3

The Infinite Elastodynamic Plate

Here we consider the frequency spectrum for the infinite elastodynamic plate under the theory of elasticity. This will later be used to assess the accuracy of the frequency spectrum for the Mindlin plate. We present a review of the work done by Meeker and Meitzler [16] which was later expanded upon in Graff [6]. Navier's equation is the vector equation of motion for an isotropic elastic medium without consideration of body forces. It is given as

$$\mu \nabla^2 \vec{u} + (\lambda + \mu) \nabla (\nabla \cdot \vec{u}) = \rho \frac{\partial^2 \vec{u}}{\partial t^2} \quad (3.1)$$

where ρ is the density, and λ and μ are the Lamé constants of elasticity. The displacement vector, \vec{u} , for the elastodynamic plate is given by

$$\vec{u} = u_x(x, y, z, t) \hat{i} + u_y(x, y, z, t) \hat{j} + u_z(x, y, z, t) \hat{k} \quad (3.2)$$

The Lamé constants are related to the Young's modulus and Poisson's ratio by

$$\mu = G = \frac{E}{2(1 + \nu)} \quad (3.3)$$

and

$$\lambda = \frac{2G\nu}{1 - 2\nu} = \frac{E\nu}{(1 + \nu)(1 - 2\nu)} \quad (3.4)$$

Before proceeding, we introduce a non-dimensionalization of the given parameters with respect to the thickness of the plate, h . Hence,

$$\vec{\bar{u}} = \vec{u}/h, \quad \bar{x} = x/h, \quad \bar{y} = y/h, \quad \bar{z} = z/h, \quad \bar{h} = 1 \quad (3.5)$$

The non-dimensional Navier equation takes the form

$$\frac{\mu}{\rho h^2 \omega_0^2} \bar{\nabla}^2 \vec{\bar{u}} + \frac{\lambda + \mu}{\rho h^2 \omega_0^2} \bar{\nabla} (\bar{\nabla} \cdot \vec{\bar{u}}) = \frac{\partial^2 \vec{\bar{u}}}{\partial \bar{t}^2} \quad (3.6)$$

where

$$\bar{t} = \omega_0 t \quad \text{and} \quad \omega_0 = \sqrt{\frac{D}{mh^4}} \quad (3.7)$$

The non-dimensional time has been scaled by ω_0 to facilitate comparison with Mindlin plate theory in the next chapter.

A solution to Eq. (3.6) for an infinite plate is formed by Helmholtz decomposition into the combination of a vector potential function, $\vec{\psi}$, and a scalar potential function, ϕ , related by

$$\vec{u} = \bar{\nabla}\phi + \bar{\nabla} \times \vec{\psi} \quad (3.8)$$

where $\vec{\psi}$ and ϕ are solutions to the equations

$$\bar{\nabla}^2 \phi = \frac{1}{\bar{c}_d^2} \frac{\partial^2 \phi}{\partial \bar{t}^2} \quad (3.9)$$

and

$$\bar{\nabla}^2 \vec{\psi} = \frac{1}{\bar{c}_s^2} \frac{\partial^2 \vec{\psi}}{\partial \bar{t}^2} \quad (3.10)$$

with

$$\bar{\nabla} \cdot \vec{\psi} = 0 \quad (3.11)$$

In Eqs. (3.9) and (3.10), \bar{c}_d is the non-dimensional dilatational wave velocity and \bar{c}_s is the non-dimensional shear wave velocity. They are, respectively, given by

$$\bar{c}_d = \frac{c_d}{h\omega_0} = \sqrt{\frac{12(1-\nu)^2}{1-2\nu}} \quad (3.12)$$

and

$$\bar{c}_s = \frac{c_s}{h\omega_0} = \sqrt{6(1-\nu)} \quad (3.13)$$

where their dimensional forms are

$$c_d = \sqrt{\frac{\lambda + 2\mu}{\rho}} \quad (3.14)$$

and

$$c_s = \sqrt{\frac{\mu}{\rho}} \quad (3.15)$$

We consider a plate bounded by traction free surfaces at $\bar{z} = \pm \bar{h}/2$ and infinite in extent in the \bar{x} and \bar{y} -directions. A solution to the wave equation in Eq. (3.9) follows as

$$\phi = (A \cos \bar{\alpha} \bar{z} + B \sin \bar{\alpha} \bar{z}) e^{i(\bar{\xi} \bar{x} - \bar{\omega} \bar{t})} \quad (3.16)$$

where $\bar{\omega}$ is the non-dimensional natural frequency, $\bar{\alpha}$ and $\bar{\xi}$ are non-dimensional wave numbers, and A and B are integration constants. The non-dimensional wave numbers and natural frequency are related by

$$\bar{\alpha}^2 + \bar{\xi}^2 = \bar{\omega}^2 / c_d^2 \quad (3.17)$$

The non-dimensional parameters $\bar{\omega}$, $\bar{\alpha}$, and $\bar{\xi}$ are related to their dimensional counterparts by

$$\bar{\omega} = \omega / \omega_0, \quad \bar{\alpha} = \alpha h, \quad \bar{\xi} = \xi h \quad (3.18)$$

The vector components of Eq. (3.10) yield solutions of similar form for the components of $\vec{\psi}$. Hence,

$$\psi_x = (C \cos \bar{\beta} \bar{z} + D \sin \bar{\beta} \bar{z}) e^{i(\bar{\xi} \bar{x} - \bar{\omega} \bar{t})} \quad (3.19)$$

$$\psi_y = (E \cos \bar{\beta} \bar{z} + F \sin \bar{\beta} \bar{z}) e^{i(\bar{\xi} \bar{x} - \bar{\omega} \bar{t})} \quad (3.20)$$

$$\psi_z = (G \cos \bar{\beta} \bar{z} + H \sin \bar{\beta} \bar{z}) e^{i(\bar{\xi} \bar{x} - \bar{\omega} \bar{t})} \quad (3.21)$$

where $\bar{\beta}$ is a non-dimensional wave number and C - H are integration constants. The non-dimensional wave numbers and natural frequency are related by

$$\bar{\beta}^2 + \bar{\xi}^2 = \bar{\omega}^2 / c_s^2 \quad (3.22)$$

The non-dimensional parameter $\bar{\beta}$ is related to its dimensional counterpart by

$$\bar{\beta} = \beta h \quad (3.23)$$

The solutions given in Eq. (3.16) and Eqs. (3.19)-(3.21) propagate independently of the \bar{y} -direction. This is because the infinite isotropic plate does not have a preferred direction for the waves to travel, so we take the \bar{x} -direction as the direction of wave propagation for mathematical simplicity. The general solution for propagation in any arbitrary in-plane coordinate system rotated by an angle θ about the \bar{z} -axis is obtained by replacing $\bar{\xi} \bar{x}$ with $\vec{\xi} \cdot \vec{x}$, where $\vec{\xi} = \bar{\xi}(\cos \theta \hat{i} + \sin \theta \hat{j})$ and $\vec{x} = \bar{x} \hat{i} + \bar{y} \hat{j}$.

From Eq. (3.8), the components of \vec{u} are given by

$$\bar{u}_x = \frac{\partial \phi}{\partial \bar{x}} + \frac{\partial \psi_z}{\partial \bar{y}} - \frac{\partial \psi_y}{\partial \bar{z}} \quad (3.24)$$

$$\bar{u}_y = \frac{\partial \phi}{\partial \bar{y}} - \frac{\partial \psi_z}{\partial \bar{x}} + \frac{\partial \psi_x}{\partial \bar{z}} \quad (3.25)$$

$$\bar{u}_z = \frac{\partial \phi}{\partial \bar{z}} + \frac{\partial \psi_y}{\partial \bar{x}} - \frac{\partial \psi_x}{\partial \bar{y}} \quad (3.26)$$

In addition, from Eq. (3.11), we have

$$\frac{\partial \psi_x}{\partial \bar{x}} + \frac{\partial \psi_y}{\partial \bar{y}} + \frac{\partial \psi_z}{\partial \bar{z}} = 0 \quad (3.27)$$

Substitution of Eq. (3.16) and Eqs. (3.19)-(3.21) into Eqs. (3.24)-(3.26), gives the components of \vec{u} in terms of the integration constants $A-H$ as

$$\bar{u}_x = \{i\bar{\xi} (A \cos \bar{\alpha}\bar{z} + B \sin \bar{\alpha}\bar{z}) + \bar{\beta} (E \sin \bar{\beta}\bar{z} - F \cos \bar{\beta}\bar{z})\} e^{i(\bar{\xi}\bar{x} - \bar{\omega}\bar{t})} \quad (3.28)$$

$$\bar{u}_y = \{\bar{\beta} (-C \sin \bar{\beta}\bar{z} + D \cos \bar{\beta}\bar{z}) - i\bar{\xi} (G \cos \bar{\beta}\bar{z} + H \sin \bar{\beta}\bar{z})\} e^{i(\bar{\xi}\bar{x} - \bar{\omega}\bar{t})} \quad (3.29)$$

$$\bar{u}_z = \{\bar{\alpha} (-A \sin \bar{\alpha}\bar{z} + B \cos \bar{\alpha}\bar{z}) + i\bar{\xi} (E \cos \bar{\beta}\bar{z} + F \sin \bar{\beta}\bar{z})\} e^{i(\bar{\xi}\bar{x} - \bar{\omega}\bar{t})} \quad (3.30)$$

For the infinite elastic plate with traction free surfaces, the boundary conditions on the planar faces of the plate are

$$\bar{\sigma}_{zz}|_{\pm\bar{h}/2} = \frac{1}{(1+\nu)(1-2\nu)} \left[(1-\nu) \frac{\partial \bar{u}_z}{\partial \bar{z}} + \nu \left(\frac{\partial \bar{u}_x}{\partial \bar{x}} + \frac{\partial \bar{u}_y}{\partial \bar{y}} \right) \right]_{\pm\bar{h}/2} = 0 \quad (3.31)$$

$$\bar{\sigma}_{zx}|_{\pm\bar{h}/2} = \frac{1}{2(1+\nu)} \left[\frac{\partial \bar{u}_x}{\partial \bar{z}} + \frac{\partial \bar{u}_z}{\partial \bar{x}} \right]_{\pm\bar{h}/2} = 0 \quad (3.32)$$

$$\bar{\sigma}_{zy}|_{\pm\bar{h}/2} = \frac{1}{2(1+\nu)} \left[\frac{\partial \bar{u}_y}{\partial \bar{z}} + \frac{\partial \bar{u}_z}{\partial \bar{y}} \right]_{\pm\bar{h}/2} = 0 \quad (3.33)$$

where

$$\bar{\sigma}_{zz} = \sigma_{zz}/E \quad \bar{\sigma}_{zx} = \sigma_{zx}/E \quad \bar{\sigma}_{zy} = \sigma_{zy}/E \quad (3.34)$$

Imposing the boundary conditions given in Eqs. (3.31)-(3.33) on the displacement field given by Eqs. (3.28)-(3.30) at $\bar{z} = \pm\bar{h}/2$ results in the following expressions

$$\begin{aligned} & \{(1-\nu)\bar{\alpha}^2 + \nu\bar{\xi}^2\} (A \cos \bar{\alpha}\bar{h}/2 + B \sin \bar{\alpha}\bar{h}/2) \\ & + \{(1-2\nu)i\bar{\beta}\bar{\xi}\} (E \sin \bar{\beta}\bar{h}/2 - F \cos \bar{\beta}\bar{h}/2) = 0 \end{aligned} \quad (3.35)$$

$$\begin{aligned} & \{(1-\nu)\bar{\alpha}^2 + \nu\bar{\xi}^2\} (A \cos \bar{\alpha}\bar{h}/2 - B \sin \bar{\alpha}\bar{h}/2) \\ & - \{(1-2\nu)i\bar{\beta}\bar{\xi}\} (E \sin \bar{\beta}\bar{h}/2 + F \cos \bar{\beta}\bar{h}/2) = 0 \end{aligned} \quad (3.36)$$

$$2i\bar{\alpha}\bar{\xi} (-A \sin \bar{\alpha}\bar{h}/2 + B \cos \bar{\alpha}\bar{h}/2) + \{\bar{\beta}^2 - \bar{\xi}^2\} (E \cos \bar{\beta}\bar{h}/2 + F \sin \bar{\beta}\bar{h}/2) = 0 \quad (3.37)$$

$$2i\bar{\alpha}\bar{\xi} (A \sin \bar{\alpha}\bar{h}/2 + B \cos \bar{\alpha}\bar{h}/2) + \{\bar{\beta}^2 - \bar{\xi}^2\} (E \cos \bar{\beta}\bar{h}/2 - F \sin \bar{\beta}\bar{h}/2) = 0 \quad (3.38)$$

$$\bar{\beta}^2 (C \cos \bar{\beta}\bar{h}/2 + D \sin \bar{\beta}\bar{h}/2) + i\bar{\beta}\bar{\xi} (-G \sin \bar{\beta}\bar{h}/2 + H \cos \bar{\beta}\bar{h}/2) = 0 \quad (3.39)$$

$$\bar{\beta}^2 (C \cos \bar{\beta}\bar{h}/2 - D \sin \bar{\beta}\bar{h}/2) + i\bar{\beta}\bar{\xi} (G \sin \bar{\beta}\bar{h}/2 + H \cos \bar{\beta}\bar{h}/2) = 0 \quad (3.40)$$

In addition, Eq. (3.27) must be satisfied at $\bar{z} = \pm\bar{h}/2$, which results in

$$i\bar{\xi} (C \cos \bar{\beta}\bar{h}/2 + D \sin \bar{\beta}\bar{h}/2) + \bar{\beta} (-G \sin \bar{\beta}\bar{h}/2 + H \cos \bar{\beta}\bar{h}/2) = 0 \quad (3.41)$$

$$i\bar{\xi} (C \cos \bar{\beta}\bar{h}/2 - D \sin \bar{\beta}\bar{h}/2) + \bar{\beta} (G \sin \bar{\beta}\bar{h}/2 + H \cos \bar{\beta}\bar{h}/2) = 0 \quad (3.42)$$

Equations (3.35)-(3.42) can be written in the form of an eight by eight matrix. Hence, this is done in Eq. (3.43), which appears on the next page, where

$$f_1 = (1 - \nu)\bar{\alpha}^2 + \nu\bar{\xi}^2 \quad (3.44)$$

$$f_2 = (1 - 2\nu)i\bar{\beta}\bar{\xi} \quad (3.45)$$

$$f_3 = \bar{\beta}^2 - \bar{\xi}^2 \quad (3.46)$$

In order to obtain non-trivial solutions the determinant of the matrix given in Eq. (3.43) must vanish. In finding the determinant of the matrix, we first simplify the matrix by row reduction to obtain Eq. (3.47), which also appears on the next page. The determinant of the matrix can now be found from the product of four submatrices. We will now consider the determinant of each of the submatrices in Eq. (3.47) separately to determine the frequency response of the infinite elastodynamic plate.

Case 1:

Here, we take the integration constants C and H to be non-zero while the other six integration constants are zero. This leaves the submatrix

$$\begin{bmatrix} \bar{\beta}^2 \cos \bar{\beta}\bar{h}/2 & i\bar{\beta}\bar{\xi} \cos \bar{\beta}\bar{h}/2 \\ i\bar{\xi} \cos \bar{\beta}\bar{h}/2 & \bar{\beta} \cos \bar{\beta}\bar{h}/2 \end{bmatrix} \begin{Bmatrix} C \\ H \end{Bmatrix} = 0 \quad (3.48)$$

and the displacement field

$$\bar{u}_x = 0 \quad (3.49a)$$

$$\bar{u}_y = - (C\bar{\beta} + iH\bar{\xi}) e^{i(\bar{\xi}\bar{x} - \bar{\omega}\bar{t})} \sin \bar{\beta}\bar{z} \quad (3.49b)$$

$$\bar{u}_z = 0 \quad (3.49c)$$

$$\begin{bmatrix}
f_1 \cos \bar{\alpha} \bar{h}/2 & f_1 \sin \bar{\alpha} \bar{h}/2 & 0 & f_2 \sin \bar{\beta} \bar{h}/2 & -f_2 \cos \bar{\beta} \bar{h}/2 & 0 & 0 \\
f_1 \cos \bar{\alpha} \bar{h}/2 & -f_1 \sin \bar{\alpha} \bar{h}/2 & 0 & -f_2 \sin \bar{\beta} \bar{h}/2 & -f_2 \cos \bar{\beta} \bar{h}/2 & 0 & 0 \\
-2i\bar{\alpha}\bar{\xi} \sin \bar{\alpha} \bar{h}/2 & 2i\bar{\alpha}\bar{\xi} \cos \bar{\alpha} \bar{h}/2 & 0 & f_3 \cos \bar{\beta} \bar{h}/2 & f_3 \sin \bar{\beta} \bar{h}/2 & 0 & 0 \\
2i\bar{\alpha}\bar{\xi} \sin \bar{\alpha} \bar{h}/2 & 2i\bar{\alpha}\bar{\xi} \cos \bar{\alpha} \bar{h}/2 & 0 & f_3 \cos \bar{\beta} \bar{h}/2 & -f_3 \sin \bar{\beta} \bar{h}/2 & 0 & 0 \\
0 & 0 & \bar{\beta}^2 \cos \bar{\beta} \bar{h}/2 & 0 & 0 & -i\bar{\beta}\bar{\xi} \sin \bar{\beta} \bar{h}/2 & i\bar{\beta}\bar{\xi} \cos \bar{\beta} \bar{h}/2 \\
0 & 0 & \bar{\beta}^2 \cos \bar{\beta} \bar{h}/2 & \bar{\beta}^2 \sin \bar{\beta} \bar{h}/2 & 0 & i\bar{\beta}\bar{\xi} \sin \bar{\beta} \bar{h}/2 & i\bar{\beta}\bar{\xi} \cos \bar{\beta} \bar{h}/2 \\
0 & 0 & i\bar{\xi} \cos \bar{\beta} \bar{h}/2 & -\beta^2 \sin \bar{\beta} \bar{h}/2 & 0 & -\beta \sin \bar{\beta} \bar{h}/2 & \bar{\beta} \cos \bar{\beta} \bar{h}/2 \\
0 & 0 & i\bar{\xi} \cos \bar{\beta} \bar{h}/2 & -i\bar{\xi} \sin \bar{\beta} \bar{h}/2 & 0 & \bar{\beta} \sin \bar{\beta} \bar{h}/2 & \bar{\beta} \cos \bar{\beta} \bar{h}/2
\end{bmatrix}
\begin{bmatrix}
A \\
B \\
C \\
D \\
E \\
F \\
G \\
H
\end{bmatrix}
= 0$$

Equation (3.43)

$$\begin{bmatrix}
f_1 \sin \bar{\alpha} \bar{h}/2 & f_2 \sin \bar{\beta} \bar{h}/2 & 0 & 0 & 0 & 0 & 0 \\
2i\bar{\alpha}\bar{\xi} \cos \bar{\alpha} \bar{h}/2 & f_3 \cos \bar{\beta} \bar{h}/2 & 0 & 0 & 0 & 0 & 0 \\
0 & 0 & f_1 \cos \bar{\alpha} \bar{h}/2 & -f_2 \cos \bar{\beta} \bar{h}/2 & 0 & 0 & 0 \\
0 & 0 & -2i\bar{\alpha}\bar{\xi} \sin \bar{\alpha} \bar{h}/2 & f_3 \sin \bar{\beta} \bar{h}/2 & 0 & 0 & 0 \\
0 & 0 & 0 & 0 & -i\bar{\beta}\bar{\xi} \sin \bar{\beta} \bar{h}/2 & 0 & 0 \\
0 & 0 & 0 & 0 & -\beta \sin \bar{\beta} \bar{h}/2 & 0 & 0 \\
0 & 0 & 0 & 0 & 0 & \bar{\beta}^2 \cos \bar{\beta} \bar{h}/2 & i\bar{\beta}\bar{\xi} \cos \bar{\beta} \bar{h}/2 \\
0 & 0 & 0 & 0 & 0 & i\bar{\xi} \cos \bar{\beta} \bar{h}/2 & \bar{\beta} \cos \bar{\beta} \bar{h}/2
\end{bmatrix}
\begin{bmatrix}
B \\
E \\
A \\
F \\
G \\
D \\
C \\
H
\end{bmatrix}
= 0$$

Equation (3.47)

The displacement field has been included to identify the motion of the wave resulting from this solution type. The resulting motion is a wave propagating in the \bar{x} -direction causing displacement solely in the \bar{y} -direction. We also see from Eq. (3.49b), that the displacement is anti-symmetric through the thickness of the plate. Hence, waves of this nature are classified as *anti-symmetric horizontal shear* waves since they result in in-plane motion perpendicular to the direction of propagation. The frequency equation for waves of this type is found when the determinant of Eq. (3.48) vanishes. Hence,

$$\bar{\beta} (\bar{\beta}^2 + \bar{\xi}^2) \cos^2 \bar{\beta} \bar{h}/2 = 0 \quad (3.50)$$

The roots of Eq. (3.50) will be used to plot the frequency spectrum of the infinite plate.

Case 2:

When the constants D and G are non-zero and all other constants are zero, we get similar results to the previous case. The reduced submatrix for this case is

$$\begin{bmatrix} -i\bar{\beta}\bar{\xi} \sin \bar{\beta} \bar{h}/2 & \bar{\beta}^2 \sin \bar{\beta} \bar{h}/2 \\ -\bar{\beta} \sin \bar{\beta} \bar{h}/2 & i\bar{\xi} \sin \bar{\beta} \bar{h}/2 \end{bmatrix} \begin{Bmatrix} G \\ D \end{Bmatrix} = 0 \quad (3.51)$$

and the displacement field is

$$\bar{u}_x = 0 \quad (3.52a)$$

$$\bar{u}_y = (D\bar{\beta} - iG\bar{\xi}) e^{i(\bar{\xi}\bar{x} - \bar{\omega}t)} \cos \bar{\beta} \bar{z} \quad (3.52b)$$

$$\bar{u}_z = 0 \quad (3.52c)$$

Here, we have a wave propagating in the \bar{x} -direction causing displacement solely in the \bar{y} -direction that is symmetric through the thickness of the plate. Waves of this nature are classified as *symmetric horizontal shear* waves. The frequency equation is found when the determinant of Eq. (3.51) vanishes. Hence,

$$\bar{\beta} (\bar{\beta}^2 + \bar{\xi}^2) \sin^2 \bar{\beta} \bar{h}/2 = 0 \quad (3.53)$$

The roots of Eq. (3.53) will also be used to plot the frequency spectrum of the infinite plate.

Case 3:

We next consider the case when the constants A and F are non-zero while the other constants are zero. This leaves us with the submatrix

$$\begin{bmatrix} f_1 \cos \bar{\alpha} \bar{h}/2 & -f_2 \cos \bar{\beta} \bar{h}/2 \\ -2i\bar{\alpha} \bar{\xi} \sin \bar{\alpha} \bar{h}/2 & f_3 \sin \bar{\beta} \bar{h}/2 \end{bmatrix} \begin{Bmatrix} A \\ F \end{Bmatrix} = 0 \quad (3.54)$$

and the displacement field

$$\bar{u}_x = \{iA\bar{\xi} \cos \bar{\alpha} \bar{z} - F\bar{\beta} \cos \bar{\beta} \bar{z}\} e^{i(\bar{\xi} \bar{x} - \bar{\omega} \bar{t})} \quad (3.55a)$$

$$\bar{u}_y = 0 \quad (3.55b)$$

$$\bar{u}_z = \{-A\bar{\alpha} \sin \bar{\alpha} \bar{z} + iF\bar{\xi} \sin \bar{\beta} \bar{z}\} e^{i(\bar{\xi} \bar{x} - \bar{\omega} \bar{t})} \quad (3.55c)$$

This wave propagating in the \bar{x} -direction creates motion in both the \bar{x} and \bar{z} -directions. The in-plane motion in the \bar{x} -direction and the out-of-plane motion in the \bar{z} -direction are the result of a dilatational wave coupled with a vertical shear wave. For this case, the effects of the dilatational wave cannot be separated from the effects of the vertical shear wave. The displacement field for this case is *symmetric* with respect to the mid-plane of the plate. Solutions of this type result in motion classified as *longitudinal* waves. The frequency equation is found when the determinant of Eq. (3.54) vanishes. Hence,

$$f_1 f_3 \cos \bar{\alpha} \bar{h}/2 \sin \bar{\beta} \bar{h}/2 - 2i f_2 \bar{\alpha} \bar{\xi} \sin \bar{\alpha} \bar{h}/2 \cos \bar{\beta} \bar{h}/2 = 0 \quad (3.56)$$

The frequency equation given above is then simplified to the following form

$$\frac{\tan \bar{\beta} \bar{h}/2}{\tan \bar{\alpha} \bar{h}/2} = -\frac{4\bar{\alpha} \bar{\beta} \bar{\xi}^2}{(\bar{\xi}^2 - \bar{\beta}^2)^2} \quad (3.57)$$

Equation (3.57) is well-known as the symmetric Rayleigh-Lamb frequency equation. The equation does not yield analytical results and must be solved numerically to obtain a relationship between the natural frequency and the wave number for propagation in the \bar{x} -direction. The intricacies that must be considered when finding the roots of the equation will be discussed when plotting the frequency spectrum.

Case 4:

The final case to consider is when the constants B and E are non-zero while the other constants are zero. This results in the submatrix

$$\begin{bmatrix} f_1 \sin \bar{\alpha} \bar{h}/2 & f_2 \sin \bar{\beta} \bar{h}/2 \\ 2i\bar{\alpha} \bar{\xi} \cos \bar{\alpha} \bar{h}/2 & f_3 \cos \bar{\beta} \bar{h}/2 \end{bmatrix} \begin{Bmatrix} B \\ E \end{Bmatrix} = 0 \quad (3.58)$$

and the displacement field

$$\bar{u}_x = \{iB\bar{\xi} \sin \bar{\alpha}\bar{z} + E\bar{\beta} \sin \bar{\beta}\bar{z}\} e^{i(\bar{\xi}\bar{x} - \bar{\omega}\bar{t})} \quad (3.59a)$$

$$\bar{u}_y = 0 \quad (3.59b)$$

$$\bar{u}_z = \{B\bar{\alpha} \cos \bar{\alpha}\bar{z} + iE\bar{\xi} \cos \bar{\beta}\bar{z}\} e^{i(\bar{\xi}\bar{x} - \bar{\omega}\bar{t})} \quad (3.59c)$$

The wave motion for this case is similar to the motion found in Case 3. The in-plane motion in the \bar{x} -direction and the out-of-plane motion in the \bar{z} -direction are again the unseparable result of a dilatational wave coupled with a vertical shear wave. The displacement field for this case is, however, *anti-symmetric* with respect to the mid-plane of the plate. Solutions of this type result in motion classified as *flexural* waves. The frequency equation is found when the determinant of Eq. (3.58) vanishes. Hence,

$$f_1 f_3 \sin \bar{\alpha}\bar{h}/2 \cos \bar{\beta}\bar{h}/2 - 2i f_2 \bar{\alpha}\bar{\xi} \cos \bar{\alpha}\bar{h}/2 \sin \bar{\beta}\bar{h}/2 = 0 \quad (3.60)$$

The frequency equation given above is then simplified to the following form

$$\frac{\tan \bar{\beta}\bar{h}/2}{\tan \bar{\alpha}\bar{h}/2} = -\frac{(\bar{\xi}^2 - \bar{\beta}^2)^2}{4\bar{\alpha}\bar{\beta}\bar{\xi}^2} \quad (3.61)$$

Equation (3.61) is well-known as the anti-symmetric Rayleigh-Lamb frequency equation. As with the symmetric equation, the anti-symmetric equation does not yield analytical results and must be solved numerically, which will be discussed when plotting the frequency spectrum.

3.1 The Frequency Spectrum

We now have all of the requisite frequency equations established in order to plot the frequency spectrum for the infinite elastodynamic plate. The frequency spectrum is presented as a plot of the non-dimensional natural frequency of the plate, $\bar{\omega}$, against the wave number governing propagation in the \bar{x} -direction, $\bar{\xi}$. Each of the frequency equations described in the previous section, Eqs. (3.50), (3.53), (3.57), and (3.61), corresponds to a branch of the frequency spectrum.

We first consider the horizontal shear branches as governed by Eqs. (3.50) and (3.53). The roots of Eq. (3.53) are the *symmetric horizontal shear* branches of the frequency spectrum. Hence, the roots are found to be

$$\frac{\bar{\beta}\bar{h}}{2} = \frac{n\pi}{2} \quad \text{for } n = 0, 2, 4, \dots \quad (3.62)$$

The roots of Eq. (3.50) are the *anti-symmetric horizontal shear* branches of the frequency spectrum and are found to be

$$\frac{\bar{\beta}\bar{h}}{2} = \frac{n\pi}{2} \quad \text{for } n = 1, 3, 5, \dots \quad (3.63)$$

For both branches, the natural frequency is related to the wave number through Eq. (3.22), with the non-dimensional shear wave velocity given in Eq. (3.13). Hence,

$$\bar{\omega} = \sqrt{6(1-\nu)(n^2\pi^2 + \bar{\xi}^2)} \quad \begin{cases} \text{symmetric for } n = 0, 2, 4, \dots \\ \text{anti-symmetric for } n = 1, 3, 5, \dots \end{cases} \quad (3.64)$$

The branches of the horizontal shear spectrum given in Eq. (3.64) are plotted in Figure 3.1. In the figure, the lowest branches for both the symmetric and anti-symmetric branches are

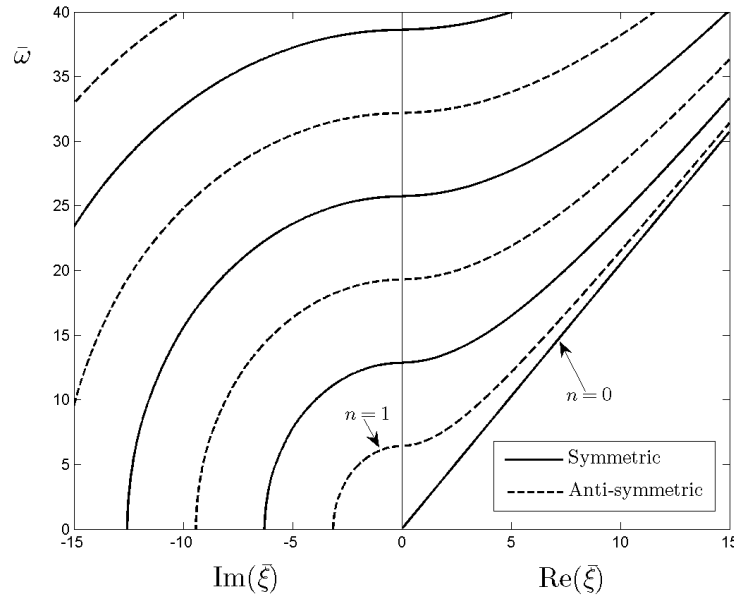


Figure 3.1: The horizontal shear frequency spectrum for the infinite elastodynamic plate with $\nu = 0.3$.

labeled. When proceeding with the remainder of this thesis, the horizontal shear branches will be referenced solely as the *symmetric shear* and the *anti-symmetric shear* branches.

We next consider the Rayleigh-Lamb branches of the frequency spectrum, which are governed by Eqs. (3.57) and (3.61). The frequency equations are solved numerically to obtain the branches of the frequency spectrum. In doing so, Eqs. (3.17) and (3.22) are used to express $\bar{\alpha}$ and $\bar{\beta}$ in terms of $\bar{\xi}$ and $\bar{\omega}$. Hence,

$$\bar{\alpha} = \sqrt{\bar{\omega}^2/\bar{c}_d^2 - \bar{\xi}^2} \quad (3.65)$$

and

$$\bar{\beta} = \sqrt{\bar{\omega}^2/\bar{c}_s^2 - \bar{\xi}^2} \quad (3.66)$$

Using these relations, the roots of Eqs. (3.57) and (3.61) are numerically found for a given value of $\bar{\xi}$. These roots comprise the branches of the frequency spectrum appearing in Figure 3.2.

When root solving, attention must be paid to the changing behavior of the branches in relation to the dilatational wave frequency and the shear wave frequency which appear as lines labeled in Figure 3.2. The relationships for $\bar{\alpha}$ and $\bar{\beta}$ appearing in Eqs. (3.65) and

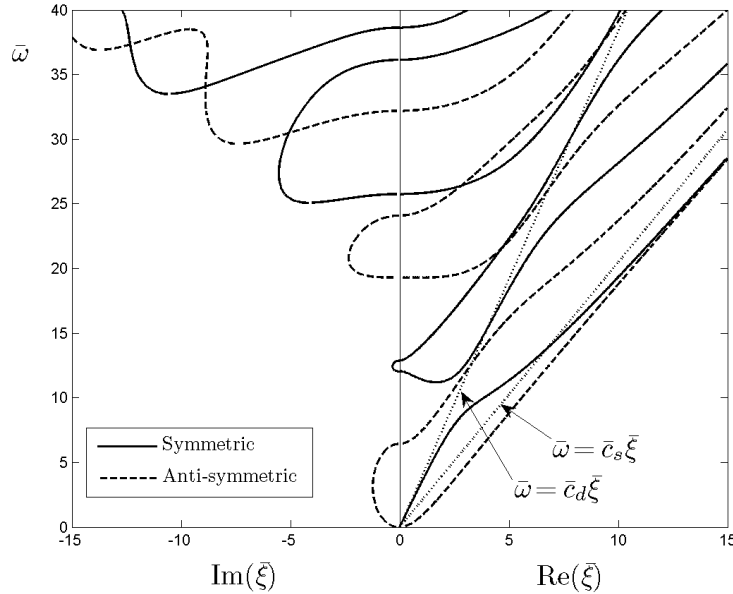


Figure 3.2: The Rayleigh-Lamb frequency spectrum for the infinite elastodynamic plate with $\nu = 0.3$.

(3.66) respectively are in fact only valid when $\bar{\omega} > \bar{c}_d \bar{\xi}$.

When $\bar{c}_s \bar{\xi} < \bar{\omega} < \bar{c}_d \bar{\xi}$, the term within the square root of Eq. (3.65) becomes negative and the relation that must be used for $\bar{\alpha}$ when root solving is

$$\bar{\alpha} = i\sqrt{\bar{\xi}^2 - \bar{\omega}^2/\bar{c}_d^2} \quad (3.67)$$

while the relation for $\bar{\beta}$ remains Eq. (3.66).

When $\bar{\omega} < \bar{c}_s \bar{\xi}$, the term within the square root of both Eqs. (3.65) and (3.66) becomes negative and Eq. (3.67) for $\bar{\alpha}$ must again be used when root solving. In this case, the relation for $\bar{\beta}$ in Eq. (3.66) must also be rewritten as

$$\bar{\beta} = i\sqrt{\bar{\xi}^2 - \bar{\omega}^2/\bar{c}_s^2} \quad (3.68)$$

The relations in Eqs. (3.67) and (3.68) were used where appropriate in solving for both the symmetric and the anti-symmetric branches of Figure 3.2.

In concluding this chapter, the four frequency branches found in Figures 3.1 and 3.2 have been combined in Figure 3.3 as the complete frequency spectrum for the infinite elastodynamic plate. The branches from Figure 3.1 have been identified as the *symmetric shear* and *anti-symmetric shear* branches. The anti-symmetric branches of Figure 3.2 have been

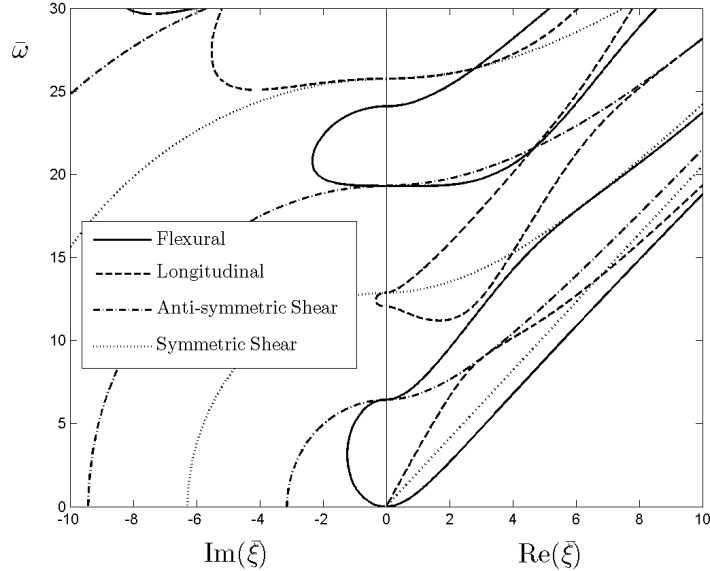


Figure 3.3: The complete frequency spectrum for the infinite elastodynamic plate with $\nu = 0.3$.

identified as the *flexural* branches while the symmetric branches have been identified as the

longitudinal branches of the frequency spectrum. We have now reviewed the developments of the frequency spectrum for the infinite elastodynamic plate that will be used to assess the accuracy of the frequency spectrum for the Mindlin plate. In the next chapter, a solution to the governing equations for the Mindlin plate presented in Section 2.3 is developed.

Chapter 4

The General Free Vibration Response for the Mindlin Plate

Here, we present the general solution for the free vibration response of the Mindlin plate theory presented in Section 2.3. The governing equation for the free vibration problem is Eq. (2.35) with the forcing matrix, \mathbf{F} , set equal to zero. We begin by non-dimensionalizing the governing equations so that the resulting frequency spectrum for the Mindlin plate can be directly compared to the frequency spectrum of the infinite elastodynamic plate as presented in Chapter 3.

4.1 The Eigenvalue Problem and Non-Dimensionalization

To solve the free vibration problem given by Eq. (2.35), we first assume a solution by separation of variables between the time and spatial variables of the plate which takes the form

$$\mathbf{u}(x, y, t) = \mathbf{U}(x, y)e^{i\omega t} \quad (4.1)$$

where

$$\mathbf{U} = \begin{Bmatrix} W(x, y) \\ \vartheta_x(x, y) \\ \vartheta_y(x, y) \end{Bmatrix} \quad (4.2)$$

and W , ϑ_x , and ϑ_y are the modal displacement and modal bending rotations in the directions indicated by the subscripts, respectively. Substitution of Eq. (4.1) into Eq. (2.35), with the external excitation given by the force matrix set equal to zero, results in an eigenvalue problem of the form

$$[\mathbf{k} - \omega^2 \mathbf{m}] \mathbf{U}(x, y) = 0 \quad (4.3)$$

We will non-dimensionalize the given parameters in order to facilitate comparison of the results with those of the previous chapter. In doing so, we will non-dimensionalize length

scales with respect to the thickness of the plate, h , which results in the non-dimensional coordinates and modal displacement

$$\bar{x} = x/h, \quad \bar{y} = y/h, \quad \bar{h} = 1, \quad \bar{W}(\bar{x}, \bar{y}) = W(x, y)/h \quad (4.4)$$

The modal bending rotations are non-dimensional in their current form. The remaining non-dimensional parameters of the plate follow as

$$\bar{k} = \frac{kh^2}{D} = 6(1 - \nu)\kappa \quad (4.5)$$

and

$$\bar{r}_{gyr} = \frac{r_{gyr}}{h} = \frac{1}{\sqrt{12}} \quad (4.6)$$

The non-dimensional natural frequency and time scale are

$$\bar{\omega} = \omega/\omega_0 \quad \text{and} \quad \bar{t} = \omega_0 t \quad (4.7)$$

where

$$\omega_0 = \sqrt{\frac{D}{mh^4}} \quad (4.8)$$

Substitution of Eqs. (4.4)-(4.8) into Eq. (4.3) results in the non-dimensional eigenvalue problem

$$[\bar{\mathbf{k}} - \bar{\omega}^2 \bar{\mathbf{m}}] \bar{\mathbf{U}}(\bar{x}, \bar{y}) = 0 \quad (4.9)$$

When expanded, the matrix in Eq. (4.9) results in

$$\left[\begin{array}{ccc} -\bar{k} \left(\frac{\partial^2}{\partial \bar{x}^2} + \frac{\partial^2}{\partial \bar{y}^2} \right) - \bar{\omega}^2 & \bar{k} \frac{\partial}{\partial \bar{x}} & \bar{k} \frac{\partial}{\partial \bar{y}} \\ -\bar{k} \frac{\partial}{\partial \bar{x}} & \bar{k} - \bar{\omega}^2 \bar{r}_{gyr}^2 - \frac{\partial^2}{\partial \bar{x}^2} - \frac{1-\nu}{2} \frac{\partial^2}{\partial \bar{y}^2} & -\frac{1+\nu}{2} \frac{\partial^2}{\partial \bar{x} \partial \bar{y}} \\ -\bar{k} \frac{\partial}{\partial \bar{y}} & -\frac{1+\nu}{2} \frac{\partial^2}{\partial \bar{x} \partial \bar{y}} & \bar{k} - \bar{\omega}^2 \bar{r}_{gyr}^2 - \frac{1-\nu}{2} \frac{\partial^2}{\partial \bar{x}^2} - \frac{\partial^2}{\partial \bar{y}^2} \end{array} \right] \quad (4.10)$$

and the non-dimensional modal matrix is

$$\bar{\mathbf{U}}(\bar{x}, \bar{y}) = \left\{ \begin{array}{l} \bar{W}(\bar{x}, \bar{y}) \\ \vartheta_x(\bar{x}, \bar{y}) \\ \vartheta_y(\bar{x}, \bar{y}) \end{array} \right\} \quad (4.11)$$

4.2 Solution Procedure

To solve the system of differential equations given by Eq. (4.9) we again assume a solution by separation of variables, but now seek to separate the spatial coordinates, \bar{x} and \bar{y} . Hence,

$$\bar{\mathbf{U}}(\bar{x}, \bar{y}) = \begin{Bmatrix} \bar{W}(\bar{x}, \bar{y}) \\ \vartheta_x(\bar{x}, \bar{y}) \\ \vartheta_y(\bar{x}, \bar{y}) \end{Bmatrix} = \begin{Bmatrix} \bar{A} \\ \bar{B} \\ \bar{C} \end{Bmatrix} e^{i\bar{\eta}_x \bar{x}} e^{i\bar{\eta}_y \bar{y}} \quad (4.12)$$

where the spatial exponents chosen represent the wave number of a vibrational wave traveling in the direction indicated by the subscript. The method is similar to that found in Bottega [1] with the exception that imaginary directional wave numbers have been chosen, as they lead to propagating wave solutions. The non-dimensional directional wave numbers are

$$\bar{\eta}_x = \eta_x h, \quad \bar{\eta}_y = \eta_y h \quad (4.13)$$

When Eq. (4.12) is substituted into Eq. (4.9), the system of differential equations becomes an algebraic system of equations. It is given by

$$\begin{bmatrix} \bar{k}(\bar{\eta}_x^2 + \bar{\eta}_y^2) - \bar{\omega}^2 & i\bar{k}\bar{\eta}_x & i\bar{k}\bar{\eta}_y \\ -i\bar{k}\bar{\eta}_x & F_{xy} & \frac{1+\nu}{2}\bar{\eta}_x\bar{\eta}_y \\ -i\bar{k}\bar{\eta}_y & \frac{1+\nu}{2}\bar{\eta}_x\bar{\eta}_y & F_{yx} \end{bmatrix} \begin{Bmatrix} \bar{A} \\ \bar{B} \\ \bar{C} \end{Bmatrix} = \begin{Bmatrix} 0 \\ 0 \\ 0 \end{Bmatrix} \quad (4.14)$$

where

$$F_{xy} = \bar{k} - \bar{\omega}^2 \bar{r}_{gyr}^2 + \bar{\eta}_x^2 + \frac{1-\nu}{2}\bar{\eta}_y^2 \quad (4.15)$$

and

$$F_{yx} = \bar{k} - \bar{\omega}^2 \bar{r}_{gyr}^2 + \frac{1-\nu}{2}\bar{\eta}_x^2 + \bar{\eta}_y^2 \quad (4.16)$$

To solve the system of equations given by Eq. (4.14) we multiply the second row of the matrix by $\bar{\eta}_y$ and subtract the third row of the matrix multiplied by $\bar{\eta}_x$ from it. This gives

$$\bar{B}\bar{\eta}_y \left[F_{xy} - \frac{1+\nu}{2}\bar{\eta}_x^2 \right] - \bar{C}\bar{\eta}_x \left[F_{yx} - \frac{1+\nu}{2}\bar{\eta}_y^2 \right] = 0 \quad (4.17)$$

Here, algebraic manipulation shows that

$$F_{xy} - \frac{1+\nu}{2}\bar{\eta}_x^2 = F_{yx} - \frac{1+\nu}{2}\bar{\eta}_y^2 = F_0^* \quad (4.18)$$

where

$$F_0^* = \bar{k} - \bar{\omega}^2 \bar{r}_{gyr}^2 + \frac{1-\nu}{2} (\bar{\eta}_x^2 + \bar{\eta}_y^2) \quad (4.19)$$

Hence, Eq. (4.17) is simplified as

$$[\bar{B}\bar{\eta}_y - \bar{C}\bar{\eta}_x] F_0^* = 0 \quad (4.20)$$

and one or both of the two terms in the above equation must be equal to zero. We first consider the case when the term in brackets is taken to be zero.

Case 1:

From Eq. (4.20) we have

$$\bar{B}\bar{\eta}_y - \bar{C}\bar{\eta}_x = 0 \quad (4.21)$$

Substitution of this relation between \bar{B} and \bar{C} back into the second and third row of Eq. (4.14) yields expressions for \bar{B} and \bar{C} , respectively, in terms of \bar{A} as

$$\bar{B} = \frac{i\bar{k}\bar{\eta}_x}{F_0} \bar{A} \quad (4.22)$$

and

$$\bar{C} = \frac{i\bar{k}\bar{\eta}_y}{F_0} \bar{A} \quad (4.23)$$

where

$$F_0 = F_{xy} + \frac{1+\nu}{2} \bar{\eta}_y^2 = F_{yx} + \frac{1+\nu}{2} \bar{\eta}_x^2 = \bar{k} - \bar{\omega}^2 \bar{r}_{gyr}^2 + \bar{\eta}_x^2 + \bar{\eta}_y^2 \quad (4.24)$$

Substitution of Eqs. (4.22) and (4.23) into the first row of Eq. (4.14) results in

$$[\{\bar{k}(\bar{\eta}_x^2 + \bar{\eta}_y^2) - \bar{\omega}^2\} F_0 - \bar{k}^2 (\bar{\eta}_x^2 + \bar{\eta}_y^2)] \bar{A} = 0 \quad (4.25)$$

For non-trivial solutions, \bar{A} must be non-zero and the term in brackets must vanish. This allows for Eqs. (4.22) and (4.23) to be rewritten in the form

$$\bar{B} = i\bar{\eta}_x g(\bar{\eta}_x, \bar{\eta}_y, \bar{\omega}) \bar{A} \quad (4.26)$$

and

$$\bar{C} = i\bar{\eta}_y g(\bar{\eta}_x, \bar{\eta}_y, \bar{\omega}) \bar{A} \quad (4.27)$$

where

$$g(\bar{\eta}_x, \bar{\eta}_y, \bar{\omega}) = \frac{\bar{k}}{F_0} = \frac{\bar{k}\bar{\eta}^2 - \bar{\omega}^2}{\bar{k}\bar{\eta}^2} \quad (4.28)$$

with

$$\bar{\eta}^2 = \bar{\eta}_x^2 + \bar{\eta}_y^2 \quad (4.29)$$

Further, substitution of the last form for F_0 appearing in Eq. (4.24) into the square bracketed term of Eq. (4.25) results in the frequency equation for the present case considered as

$$\bar{k}(\bar{\eta}^2)^2 - \bar{\omega}^2 [\bar{k}\bar{r}_{gyr}^2 + 1] (\bar{\eta}^2) + \bar{\omega}^2 [\bar{\omega}^2\bar{r}_{gyr}^2 - \bar{k}] = 0 \quad (4.30)$$

Eq. (4.30) is the characteristic frequency equation for the case when Eq. (4.21) holds. The equation is quadratic and hence will lead to two roots for $\bar{\eta}^2$. Each root relates the directional wave numbers to the natural frequencies of the plate and hence, acts as a branch of the frequency spectrum for the Mindlin plate.

We will later find that the roots of Eq. (4.30) contribute to *flexural* motion of the plate and hence, will refer to the resulting frequency branches as *flexural* branches. A detailed explanation of the *flexural* frequency branches follows. The development improves upon the solution found in Bottega [1] by identifying the physical interpretation of the wave numbers for each branch of the spectrum separately. This leads to more clearly defined relationships between the natural frequencies and wave numbers. The first *flexural* branch is given by

$$\bar{\eta}_1^2 = \bar{\omega}^2 F_1 \quad (4.31)$$

where

$$F_1 = \frac{1}{2\bar{k}_1} \left[\bar{k}_1\bar{r}_{gyr}^2 + 1 + \sqrt{(\bar{k}_1\bar{r}_{gyr}^2 - 1)^2 + 4\bar{k}_1^2\bar{\omega}^{-2}} \right] \quad (4.32)$$

Further advancing on Bottega [1], \bar{k} has been given a subscript of one in Eq. (4.32) in this study to indicate it is the non-dimensional shear stiffness associated with the first *flexural* branch of the frequency spectrum. This will later be used when selecting the best value for the shear correction coefficient.

Employing Eq. (4.31), we proceed to the determination of the form of $\bar{\eta}_x$ and $\bar{\eta}_y$ for *flexural* branch one. Inspection of Eq. (4.32) shows that F_1 will be positive for all values of $\bar{\omega}$, while $\bar{\omega}$ must always be positive as well. As a result, $\bar{\eta}_1^2$ must be strictly positive, which means it is propagating in form. In order for this requirement to be satisfied, the wave number in one coordinate direction must be strictly propagating in form. Hence, we assume the \bar{x} -direction will have a propagating wave number and take $\bar{\eta}_x$ to be real

valued as we initially assumed propagating solutions. This suggests the plate will then have simply-supported boundary conditions at each edge of the plate in the \bar{x} -direction. This leads to

$$\bar{\eta}_x = \pm\bar{\alpha} = \pm\alpha h \quad (4.33)$$

For this branch, we will also assume $\bar{\eta}_y$ to be real valued which leads to

$$\bar{\eta}_{y1} = \pm\bar{\gamma} = \pm\gamma h \quad (4.34)$$

For some boundary conditions, it is possible for $\bar{\eta}_{y1}$ to be imaginary valued at low frequencies. For this possibility, $\bar{\eta}_{y1} = \pm i\hat{\gamma} = \pm i\gamma h$ in Eq. (4.34), which must be considered when applying boundary conditions but will not always lead to real valued solutions for the natural frequency. Hence, the real valued wave number represents the more robust form of the solution.

For the first *flexural* branch, Eq. (4.33) and the real or imaginary form of Eq. (4.34) are the components of $\bar{\eta}_1$ which are related through Eq. (4.31) as

$$\bar{\alpha}^2 - \hat{\gamma}^2 = \bar{\omega}^2 F_1 \text{ for } (\bar{\alpha}^2 > \hat{\gamma}^2), \quad \text{or} \quad \bar{\alpha}^2 + \bar{\gamma}^2 = \bar{\omega}^2 F_1 \quad (4.35)$$

For most geometries and magnitudes of the natural frequency, the expression on the right in Eq. (4.35) will represent the relationship between the directional wave numbers and the natural frequencies for this branch. When the expression on the left is a possible solution, the magnitude of $\bar{\omega}$ will reach a value where $\bar{\alpha}^2$ is no longer greater than $\hat{\gamma}^2$. Here, $i\hat{\gamma} \rightarrow \bar{\gamma}$ and the term on the right in Eq. (4.35) will govern the relationship between the directional wave numbers and the natural frequencies for all subsequent values of $\bar{\omega}$.

The second *flexural* branch is given by

$$\bar{\eta}_2^2 = \bar{\omega}^2 F_2 \quad (4.36)$$

where

$$F_2 = \frac{1}{2k_2} \left[\bar{k}_2 \bar{r}_{gyr}^2 + 1 - \sqrt{(\bar{k}_2 \bar{r}_{gyr}^2 - 1)^2 + 4\bar{k}_2^2 \bar{\omega}^{-2}} \right] \quad (4.37)$$

This time, \bar{k} has been given a subscript of two in Eq. (4.37) to indicate it is the non-dimensional shear stiffness associated with the second *flexural* branch of the frequency spectrum. In order to relate this branch of the spectrum to the first *flexural* branch we take

the directional wave number in the \bar{x} -direction for this branch to be given by Eq. (4.33). Now, we see that $F_2 < 0$ for low values of $\bar{\omega}$. As a result, we consider an imaginary wave number in the \bar{y} -direction

$$\bar{\eta}_{y_2} = \pm i\hat{\mu} = \pm i\mu h \quad (4.38)$$

where $\hat{\mu}$ is real valued and a hat has been used to signify that the directional wave number corresponds to a non-propagating wave solution. When $\bar{\omega} > \sqrt{\bar{k}_2/\bar{r}_{gyr}^2}$, we see that $F_2 > 0$ and it is possible for $\pm i\hat{\mu} \rightarrow \pm\bar{\mu}$ in the above relation. For this branch, the magnitude of $\bar{\omega}$ determines how the directional wave numbers given by Eqs. (4.33) and (4.38) are related to the natural frequencies through Eq. (4.36).

When $\bar{\omega} < \sqrt{\bar{k}_2/\bar{r}_{gyr}^2} \rightarrow F_2 < 0$:

$$\bar{\alpha}^2 - \hat{\mu}^2 = \bar{\omega}^2 F_2 \quad \text{for } (\hat{\mu}^2 > \bar{\alpha}^2) \quad (4.39)$$

When $\bar{\omega} > \sqrt{\bar{k}_2/\bar{r}_{gyr}^2} \rightarrow F_2 > 0$:

$$\bar{\alpha}^2 - \hat{\mu}^2 = \bar{\omega}^2 F_2 \quad \text{for } (\bar{\alpha}^2 > \hat{\mu}^2), \quad \text{or} \quad \bar{\alpha}^2 + \bar{\mu}^2 = \bar{\omega}^2 F_2 \quad (4.40)$$

As $\bar{\omega}$ increases beyond $\sqrt{\bar{k}_2/\bar{r}_{gyr}^2}$, Eq. (4.39) will transition to the term on the left in Eq. (4.40). Then, as $\bar{\omega}$ continues to increase there will reach a point when $\bar{\alpha}^2$ is no longer greater than $\hat{\mu}^2$. Here, $i\hat{\mu} \rightarrow \bar{\mu}$ and the term on the right in Eq. (4.40) will govern the relationship between the directional wave numbers and the natural frequencies for all subsequent values of $\bar{\omega}$. We now proceed back to Eq. (4.20) to determine the behavior of the remaining frequency branch.

Case 2:

When considering the latter term of Eq. (4.20) we have

$$F_0^* = 0 \quad (4.41)$$

Letting $F_0^* = 0$ in Eq. (4.18) gives new relations for F_{xy} and F_{yx} that can be substituted into Eq. (4.14) to obtain the alternate form

$$\begin{bmatrix} \bar{k}\bar{\eta}^2 - \bar{\omega}^2 & i\bar{k}\bar{\eta}_x & i\bar{k}\bar{\eta}_y \\ -i\bar{k}\bar{\eta}_x & \frac{1+\nu}{2}\bar{\eta}_x^2 & \frac{1+\nu}{2}\bar{\eta}_x\bar{\eta}_y \\ -i\bar{k}\bar{\eta}_y & \frac{1+\nu}{2}\bar{\eta}_x\bar{\eta}_y & \frac{1+\nu}{2}\bar{\eta}_y^2 \end{bmatrix} \begin{Bmatrix} \bar{A} \\ \bar{B} \\ \bar{C} \end{Bmatrix} = \begin{Bmatrix} 0 \\ 0 \\ 0 \end{Bmatrix} \quad (4.42)$$

The second and third row of the above matrix are now linearly dependent. Hence, we multiply the first row of the matrix by $i\bar{k}\bar{\eta}_x$ and add the second row of the matrix multiplied by $(\bar{k}\bar{\eta}^2 - \bar{\omega}^2)$ to it. This results in the relation

$$\bar{C} = -\frac{\bar{\eta}_x}{\bar{\eta}_y} \bar{B} \quad (4.43)$$

Substitution of Eq. (4.43) into any row of Eq. (4.42) results in

$$\bar{A} = 0 \quad (4.44)$$

Hence, the solutions corresponding to the present case (Case 2) will not appear in the modal displacement function. The integration constants of the modal bending rotation functions for Case 2 are related through Eq. (4.43).

We will find that motion associated with Case 2 will correspond to shear motion and hence, we will call this the *anti-symmetric shear* branch of the frequency spectrum or the *shear* branch for short. Now, Eq. (4.41) is the frequency equation for Case 2 and setting Eq. (4.19) equal to zero results in

$$\bar{\eta}_s^2 = S \quad (4.45)$$

where

$$S = -\frac{2}{(1-\nu)} [\bar{k}_s - \bar{\omega}^2 \bar{r}_{gyr}^2] \quad (4.46)$$

Here, \bar{k} has been given a subscript of s in Eq. (4.46) to indicate it is the non-dimensional shear stiffness associated with the *shear* branch of the frequency spectrum. As with the *flexural* branches, the directional wave number in the \bar{x} -direction is given by Eq. (4.33). Similar to the second *flexural* branch, we see that $S < 0$ for low values of $\bar{\omega}$ and therefore also consider an imaginary wave number in the \bar{y} -direction for this branch. This gives

$$\bar{\eta}_{y_s} = \pm i\hat{\beta} = \pm i\beta h \quad (4.47)$$

where $\hat{\beta}$ is real valued. When $\bar{\omega} > \sqrt{\bar{k}_s/\bar{r}_{gyr}^2}$, we see that $S > 0$ and it is possible for $\pm i\hat{\beta} \rightarrow \pm\bar{\beta}$ in the above relation. In the same manner as with *flexural* branch two, the magnitude of $\bar{\omega}$ determines how the directional wave numbers given by Eqs. (4.33) and (4.47) are related to the natural frequencies through Eq. (4.45). Considering both real and imaginary values for $\bar{\eta}_{y_s}$ in Eq. (4.47) results in the admissible relations between the natural

frequencies and the directional wave numbers.

When $\bar{\omega} < \sqrt{\bar{k}_s/\bar{r}_{gyr}^2} \rightarrow S < 0$:

$$\bar{\alpha}^2 - \hat{\beta}^2 = S \text{ for } (\hat{\beta}^2 > \bar{\alpha}^2) \quad (4.48)$$

When $\bar{\omega} > \sqrt{\bar{k}_s/\bar{r}_{gyr}^2} \rightarrow S > 0$:

$$\bar{\alpha}^2 - \hat{\beta}^2 = S \text{ for } (\bar{\alpha}^2 > \hat{\beta}^2), \quad \text{or} \quad \bar{\alpha}^2 + \bar{\beta}^2 = S \quad (4.49)$$

As $\bar{\omega}$ increases, Eqs. (4.48) and (4.49) will follow the same behavior as Eqs. (4.39) and (4.40) did for the second *flexural* branch. In general, the natural frequency for which $i\hat{\beta} \rightarrow \bar{\beta}$ will not be the same as the frequency for which $i\hat{\mu} \rightarrow \bar{\mu}$.

With the relations between the integration constants of the modal functions and the natural frequency-wave number relations for all three branches of the frequency spectrum established, we proceed to obtain the general expressions for the modal functions.

4.3 The Modal Functions

The general solution for the modal functions is found by taking the linear combination of all possible solutions obtained when substituting the admissible wave numbers into Eq. (4.12). For the first *flexural* branch, the admissible wave numbers given by Eqs. (4.33) and (4.34), which are related through Eq. (4.35), contribute to the modal displacement and bending rotations as follows

$$\bar{W}_1(\bar{x}, \bar{y}) = \bar{A}_1 e^{i\bar{\alpha}\bar{x}} e^{i\bar{\gamma}\bar{y}} + \bar{A}_2 e^{-i\bar{\alpha}\bar{x}} e^{i\bar{\gamma}\bar{y}} + \bar{A}_3 e^{i\bar{\alpha}\bar{x}} e^{-i\bar{\gamma}\bar{y}} + \bar{A}_4 e^{-i\bar{\alpha}\bar{x}} e^{-i\bar{\gamma}\bar{y}} \quad (4.50)$$

$$\vartheta_{x_1}(\bar{x}, \bar{y}) = \bar{B}_1 e^{i\bar{\alpha}\bar{x}} e^{i\bar{\gamma}\bar{y}} + \bar{B}_2 e^{-i\bar{\alpha}\bar{x}} e^{i\bar{\gamma}\bar{y}} + \bar{B}_3 e^{i\bar{\alpha}\bar{x}} e^{-i\bar{\gamma}\bar{y}} + \bar{B}_4 e^{-i\bar{\alpha}\bar{x}} e^{-i\bar{\gamma}\bar{y}} \quad (4.51)$$

$$\vartheta_{y_1}(\bar{x}, \bar{y}) = \bar{C}_1 e^{i\bar{\alpha}\bar{x}} e^{i\bar{\gamma}\bar{y}} + \bar{C}_2 e^{-i\bar{\alpha}\bar{x}} e^{i\bar{\gamma}\bar{y}} + \bar{C}_3 e^{i\bar{\alpha}\bar{x}} e^{-i\bar{\gamma}\bar{y}} + \bar{C}_4 e^{-i\bar{\alpha}\bar{x}} e^{-i\bar{\gamma}\bar{y}} \quad (4.52)$$

When applying boundary conditions and interpreting results, it is advantageous to work with the above equations in the form of trigonometric functions. The transverse modal displacement for the first *flexural* branch, \bar{W}_1 , given by Eq. (4.50) is rewritten as

$$\bar{W}_1(\bar{x}, \bar{y}) = [A_1 \cos \bar{\alpha}\bar{x} + A_2 \sin \bar{\alpha}\bar{x}] \times [A_3 \cos \bar{\gamma}\bar{y} + A_4 \sin \bar{\gamma}\bar{y}] \quad (4.53)$$

where

$$\begin{aligned} A_1 A_3 &= \bar{A}_1 + \bar{A}_2 + \bar{A}_3 + \bar{A}_4 & A_1 A_4 &= i \{ \bar{A}_1 + \bar{A}_2 - \bar{A}_3 - \bar{A}_4 \} \\ A_2 A_3 &= i \{ \bar{A}_1 - \bar{A}_2 + \bar{A}_3 - \bar{A}_4 \} & A_2 A_4 &= - \{ \bar{A}_1 - \bar{A}_2 - \bar{A}_3 + \bar{A}_4 \} \end{aligned} \quad (4.54)$$

When rewriting the modal bending rotation ϑ_{x_1} given by Eq. (4.51) in a form similar to that of Eq. (4.53), we will also express the constants \bar{B}_1 - \bar{B}_4 in terms of the constants \bar{A}_1 - \bar{A}_4 as related by Eq. (4.26). Hence,

$$\begin{aligned} \bar{B}_1 &= i\bar{\alpha}g_1\bar{A}_1 \\ \bar{B}_2 &= -i\bar{\alpha}g_1\bar{A}_2 \\ \bar{B}_3 &= i\bar{\alpha}g_1\bar{A}_3 \\ \bar{B}_4 &= -i\bar{\alpha}g_1\bar{A}_4 \end{aligned} \quad (4.55)$$

where, from Eqs. (4.28) and (4.35)

$$g_1 = g(\bar{\alpha}, \bar{\gamma}, \bar{\omega}) = \frac{\bar{k}_1 F_1 - 1}{\bar{k}_1 F_1} \quad (4.56)$$

Using Eqs. (4.54) and (4.55), we rewrite ϑ_{x_1} as

$$\vartheta_{x_1}(\bar{x}, \bar{y}) = -\bar{\alpha}g_1 [A_1 \sin \bar{\alpha}\bar{x} - A_2 \cos \bar{\alpha}\bar{x}] \times [A_3 \cos \bar{\gamma}\bar{y} + A_4 \sin \bar{\gamma}\bar{y}] \quad (4.57)$$

When rewriting the modal bending rotation ϑ_{y_1} given by Eq. (4.52) in a form similar to that of Eq. (4.53), we will also express the constants \bar{C}_1 - \bar{C}_4 in terms of the constants \bar{A}_1 - \bar{A}_4 as related by Eq. (4.27). Hence,

$$\begin{aligned} \bar{C}_1 &= i\bar{\gamma}g_1\bar{A}_1 \\ \bar{C}_2 &= i\bar{\gamma}g_1\bar{A}_2 \\ \bar{C}_3 &= -i\bar{\gamma}g_1\bar{A}_3 \\ \bar{C}_4 &= -i\bar{\gamma}g_1\bar{A}_4 \end{aligned} \quad (4.58)$$

Using Eqs. (4.54) and (4.58), we rewrite ϑ_{y_1} as

$$\vartheta_{y_1}(\bar{x}, \bar{y}) = -\bar{\gamma}g_1 [A_1 \cos \bar{\alpha}\bar{x} + A_2 \sin \bar{\alpha}\bar{x}] \times [A_3 \sin \bar{\gamma}\bar{y} - A_4 \cos \bar{\gamma}\bar{y}] \quad (4.59)$$

The modal displacement and bending rotations for the first *flexural* branch are given by Eqs. (4.53), (4.57), and (4.59).

If for low values of $\bar{\omega}$, there exists solutions such that $\bar{\gamma} \rightarrow i\hat{\gamma}$, the modal displacement and bending rotations for the first *flexural* branch then take the form

$$\bar{W}_1(\bar{x}, \bar{y}) = [A_1 \cos \bar{\alpha}\bar{x} + A_2 \sin \bar{\alpha}\bar{x}] \times [A_3 \cosh \hat{\gamma}\bar{y} + A_4 \sinh \hat{\gamma}\bar{y}] \quad (4.60)$$

$$\vartheta_{x_1}(\bar{x}, \bar{y}) = -\bar{\alpha}g_1 [A_1 \sin \bar{\alpha}\bar{x} - A_2 \cos \bar{\alpha}\bar{x}] \times [A_3 \cosh \hat{\gamma}\bar{y} + A_4 \sinh \hat{\gamma}\bar{y}] \quad (4.61)$$

$$\vartheta_{y_1}(\bar{x}, \bar{y}) = \hat{\gamma}g_1 [A_1 \cos \bar{\alpha}\bar{x} + A_2 \sin \bar{\alpha}\bar{x}] \times [A_3 \sinh \hat{\gamma}\bar{y} + A_4 \cosh \hat{\gamma}\bar{y}] \quad (4.62)$$

The multiplicative combinations of the constants A_1 and A_2 with A_3 and A_4 are then related to the constants \bar{A}_1 - \bar{A}_4 , \bar{B}_1 - \bar{B}_4 , and \bar{C}_1 - \bar{C}_4 by relations similar to those that will be seen for *flexural* branch two with the subscripts changed accordingly. The parameter g_1 remains defined by Eq. (4.56).

The admissible wave numbers for the second *flexural* branch are given by Eqs. (4.33) and (4.38) and are related through Eq. (4.39) or Eq. (4.40) depending on the magnitude of $\bar{\omega}$. In this development, we use Eq. (4.39) since it corresponds to lower values of $\bar{\omega}$. The modal displacement and bending rotations follow as

$$\bar{W}_2(\bar{x}, \bar{y}) = \bar{A}_5 e^{i\bar{\alpha}\bar{x}} e^{-\hat{\mu}\bar{y}} + \bar{A}_6 e^{-i\bar{\alpha}\bar{x}} e^{-\hat{\mu}\bar{y}} + \bar{A}_7 e^{i\bar{\alpha}\bar{x}} e^{\hat{\mu}\bar{y}} + \bar{A}_8 e^{-i\bar{\alpha}\bar{x}} e^{\hat{\mu}\bar{y}} \quad (4.63)$$

$$\vartheta_{x_2}(\bar{x}, \bar{y}) = \bar{B}_5 e^{i\bar{\alpha}\bar{x}} e^{-\hat{\mu}\bar{y}} + \bar{B}_6 e^{-i\bar{\alpha}\bar{x}} e^{-\hat{\mu}\bar{y}} + \bar{B}_7 e^{i\bar{\alpha}\bar{x}} e^{\hat{\mu}\bar{y}} + \bar{B}_8 e^{-i\bar{\alpha}\bar{x}} e^{\hat{\mu}\bar{y}} \quad (4.64)$$

$$\vartheta_{y_2}(\bar{x}, \bar{y}) = \bar{C}_5 e^{i\bar{\alpha}\bar{x}} e^{-\hat{\mu}\bar{y}} + \bar{C}_6 e^{-i\bar{\alpha}\bar{x}} e^{-\hat{\mu}\bar{y}} + \bar{C}_7 e^{i\bar{\alpha}\bar{x}} e^{\hat{\mu}\bar{y}} + \bar{C}_8 e^{-i\bar{\alpha}\bar{x}} e^{\hat{\mu}\bar{y}} \quad (4.65)$$

Rewriting the modal functions of the second *flexural* branch in terms of trigonometric and hyperbolic functions is done in a similar procedure to that of the first *flexural* branch. The transverse modal displacement for the second *flexural* branch, \bar{W}_2 , given by Eq. (4.63) is rewritten as

$$\bar{W}_2(\bar{x}, \bar{y}) = [A_1 \cos \bar{\alpha}\bar{x} + A_2 \sin \bar{\alpha}\bar{x}] \times [A_5 \cosh \hat{\mu}\bar{y} + A_6 \sinh \hat{\mu}\bar{y}] \quad (4.66)$$

where

$$\begin{aligned} A_1 A_5 &= \bar{A}_5 + \bar{A}_6 + \bar{A}_7 + \bar{A}_8 & A_1 A_6 &= -\{\bar{A}_5 + \bar{A}_6 - \bar{A}_7 - \bar{A}_8\} \\ A_2 A_5 &= i\{\bar{A}_5 - \bar{A}_6 + \bar{A}_7 - \bar{A}_8\} & A_2 A_6 &= -i\{\bar{A}_5 - \bar{A}_6 - \bar{A}_7 + \bar{A}_8\} \end{aligned} \quad (4.67)$$

When rewriting the bending rotation ϑ_{x_2} given by Eq. (4.64), the constants \bar{B}_5 - \bar{B}_8 are related to the constants \bar{A}_5 - \bar{A}_8 by Eq. (4.26). Hence,

$$\begin{aligned} \bar{B}_5 &= i\bar{\alpha}g_2 \bar{A}_5 \\ \bar{B}_6 &= -i\bar{\alpha}g_2 \bar{A}_6 \\ \bar{B}_7 &= i\bar{\alpha}g_2 \bar{A}_7 \\ \bar{B}_8 &= -i\bar{\alpha}g_2 \bar{A}_8 \end{aligned} \quad (4.68)$$

where, from Eqs. (4.28) and (4.39)

$$g_2 = g(\bar{\alpha}, i\hat{\mu}, \bar{\omega}) = \frac{\bar{k}_2 F_2 - 1}{\bar{k}_2 F_2} \quad (4.69)$$

Using Eqs. (4.67) and (4.68), we rewrite ϑ_{x_2} as

$$\vartheta_{x_2}(\bar{x}, \bar{y}) = -\bar{\alpha}g_2 [A_1 \sin \bar{\alpha}\bar{x} - A_2 \cos \bar{\alpha}\bar{x}] \times [A_5 \cosh \hat{\mu}\bar{y} + A_6 \sinh \hat{\mu}\bar{y}] \quad (4.70)$$

When rewriting the bending rotation ϑ_{y_2} given by Eq. (4.65), the constants \bar{C}_5 - \bar{C}_8 are related to the constants \bar{A}_5 - \bar{A}_8 by Eq. (4.27). Hence,

$$\begin{aligned} \bar{C}_5 &= -\hat{\mu}g_2\bar{A}_5 \\ \bar{C}_6 &= -\hat{\mu}g_2\bar{A}_6 \\ \bar{C}_7 &= \hat{\mu}g_2\bar{A}_7 \\ \bar{C}_8 &= \hat{\mu}g_2\bar{A}_8 \end{aligned} \quad (4.71)$$

Using Eqs. (4.67) and (4.71), we rewrite ϑ_{y_2} as

$$\vartheta_{y_2}(\bar{x}, \bar{y}) = \hat{\mu}g_2 [A_1 \cos \bar{\alpha}\bar{x} + A_2 \sin \bar{\alpha}\bar{x}] \times [A_5 \sinh \hat{\mu}\bar{y} + A_6 \cosh \hat{\mu}\bar{y}] \quad (4.72)$$

The modal displacement and bending rotations for the second *flexural* branch for low natural frequencies are given by Eqs. (4.66), (4.70), and (4.72).

If $\bar{\omega}$ reaches sufficient magnitude such that $i\hat{\mu} \rightarrow \bar{\mu}$, the modal displacement and bending rotations for the second *flexural* branch then take the form

$$\bar{W}_2(\bar{x}, \bar{y}) = [A_1 \cos \bar{\alpha}\bar{x} + A_2 \sin \bar{\alpha}\bar{x}] \times [A_5 \cos \bar{\mu}\bar{y} + A_6 \sin \bar{\mu}\bar{y}] \quad (4.73)$$

$$\vartheta_{x_2}(\bar{x}, \bar{y}) = -\bar{\alpha}g_2 [A_1 \sin \bar{\alpha}\bar{x} - A_2 \cos \bar{\alpha}\bar{x}] \times [A_5 \cos \bar{\mu}\bar{y} + A_6 \sin \bar{\mu}\bar{y}] \quad (4.74)$$

$$\vartheta_{y_2}(\bar{x}, \bar{y}) = -\bar{\mu}g_2 [A_1 \cos \bar{\alpha}\bar{x} + A_2 \sin \bar{\alpha}\bar{x}] \times [A_5 \sin \bar{\mu}\bar{y} - A_6 \cos \bar{\mu}\bar{y}] \quad (4.75)$$

The multiplicative combinations of the constants A_1 and A_2 with A_5 and A_6 are then related to the constants \bar{A}_5 - \bar{A}_8 , \bar{B}_5 - \bar{B}_8 , and \bar{C}_5 - \bar{C}_8 by relations similar to those of *flexural* branch one with the subscripts changed accordingly. The parameter g_2 remains defined by Eq. (4.69).

From Eq. (4.44), we see that the *shear* frequency branch will not contribute to the transverse modal displacement function. It does however, contribute to the modal bending

rotations. The admissible wave numbers for the *shear* branch are given by Eqs. (4.33) and (4.47) and are related through Eq. (4.48) or Eq. (4.49) depending on the magnitude of $\bar{\omega}$. In this development we use Eq. (4.48) since it corresponds to lower values of $\bar{\omega}$. The modal bending rotations follow as

$$\vartheta_{x_s}(\bar{x}, \bar{y}) = \bar{B}_9 e^{i\bar{\alpha}\bar{x}} e^{-\hat{\beta}\bar{y}} + \bar{B}_{10} e^{-i\bar{\alpha}\bar{x}} e^{-\hat{\beta}\bar{y}} + \bar{B}_{11} e^{i\bar{\alpha}\bar{x}} e^{\hat{\beta}\bar{y}} + \bar{B}_{12} e^{-i\bar{\alpha}\bar{x}} e^{\hat{\beta}\bar{y}} \quad (4.76)$$

$$\vartheta_{y_s}(\bar{x}, \bar{y}) = \bar{C}_9 e^{i\bar{\alpha}\bar{x}} e^{-\hat{\beta}\bar{y}} + \bar{C}_{10} e^{-i\bar{\alpha}\bar{x}} e^{-\hat{\beta}\bar{y}} + \bar{C}_{11} e^{i\bar{\alpha}\bar{x}} e^{\hat{\beta}\bar{y}} + \bar{C}_{12} e^{-i\bar{\alpha}\bar{x}} e^{\hat{\beta}\bar{y}} \quad (4.77)$$

In this case, we rewrite the modal bending rotation ϑ_{x_s} in terms of trigonometric and hyperbolic functions. Hence, Eq. (4.76) becomes

$$\vartheta_{x_s}(\bar{x}, \bar{y}) = [B_7 \cos \bar{\alpha}\bar{x} + B_8 \sin \bar{\alpha}\bar{x}] \times [B_9 \cosh \hat{\beta}\bar{y} + B_{10} \sinh \hat{\beta}\bar{y}] \quad (4.78)$$

where

$$\begin{aligned} B_7 B_9 &= \bar{B}_9 + \bar{B}_{10} + \bar{B}_{11} + \bar{B}_{12} & B_7 B_{10} &= -\{\bar{B}_9 + \bar{B}_{10} - \bar{B}_{11} - \bar{B}_{12}\} \\ B_8 B_9 &= i\{\bar{B}_9 - \bar{B}_{10} + \bar{B}_{11} - \bar{B}_{12}\} & B_8 B_{10} &= -i\{\bar{B}_9 - \bar{B}_{10} - \bar{B}_{11} + \bar{B}_{12}\} \end{aligned} \quad (4.79)$$

When rewriting the bending rotation ϑ_{y_s} given by Eq. (4.77), the constants \bar{C}_9 - \bar{C}_{12} are related to the constants \bar{B}_9 - \bar{B}_{12} by Eq. (4.43). Hence,

$$\begin{aligned} \bar{C}_9 &= i\frac{\bar{\alpha}}{\hat{\beta}}\bar{B}_9 \\ \bar{C}_{10} &= -i\frac{\bar{\alpha}}{\hat{\beta}}\bar{B}_{10} \\ \bar{C}_{11} &= -i\frac{\bar{\alpha}}{\hat{\beta}}\bar{B}_{11} \\ \bar{C}_{12} &= i\frac{\bar{\alpha}}{\hat{\beta}}\bar{B}_{12} \end{aligned} \quad (4.80)$$

Using Eqs. (4.79) and (4.80), we rewrite ϑ_{y_s} as

$$\vartheta_{y_s}(\bar{x}, \bar{y}) = \frac{\bar{\alpha}}{\hat{\beta}} [B_7 \sin \bar{\alpha}\bar{x} - B_8 \cos \bar{\alpha}\bar{x}] \times [B_9 \sinh \hat{\beta}\bar{y} + B_{10} \cosh \hat{\beta}\bar{y}] \quad (4.81)$$

The modal bending rotations for the *shear* branch for low natural frequencies are given by Eqs. (4.78) and (4.81).

If $\bar{\omega}$ reaches sufficient magnitude such that $i\hat{\beta} \rightarrow \bar{\beta}$, the modal bending rotations for the *shear* branch then take the form

$$\vartheta_{x_s}(\bar{x}, \bar{y}) = [B_7 \cos \bar{\alpha}\bar{x} + B_8 \sin \bar{\alpha}\bar{x}] \times [B_9 \cos \bar{\beta}\bar{y} + B_{10} \sin \bar{\beta}\bar{y}] \quad (4.82)$$

$$\vartheta_{y_s}(\bar{x}, \bar{y}) = \frac{\bar{\alpha}}{\bar{\beta}} [B_7 \sin \bar{\alpha}\bar{x} - B_8 \cos \bar{\alpha}\bar{x}] \times [B_9 \sin \bar{\beta}\bar{y} - B_{10} \cos \bar{\beta}\bar{y}] \quad (4.83)$$

In this development, Eqs. (4.79) and (4.80) would have different definitions for the relationships between the integration constants B_7 - B_{10} .

The total solution for the modal displacement and bending rotations for the free vibration of the Mindlin plate is obtained from the linear combination of the individual solutions for each of the three branches of the frequency spectrum. The solution includes twelve independent integration constants as shown in Eqs. (4.54), (4.67), and (4.79). It was seen in Section 2.3 that Mindlin plate theory requires the specification of three independent boundary conditions on a given edge of a structure and hence twelve independent conditions on the boundaries of a square or rectangular plate to solve for the twelve integration constants.

The general form of the modal functions for a Mindlin plate are shown here

$$\begin{aligned} \bar{W}(\bar{x}, \bar{y}) &= \bar{W}_1 + \bar{W}_2 \\ &= [A_1 \cos \bar{\alpha}\bar{x} + A_2 \sin \bar{\alpha}\bar{x}] \\ &\quad \times [A_3 \cos \bar{\gamma}\bar{y} + A_4 \sin \bar{\gamma}\bar{y} + A_5 \cosh \hat{\mu}\bar{y} + A_6 \sinh \hat{\mu}\bar{y}] \end{aligned} \quad (4.84)$$

$$\begin{aligned} \vartheta_x(\bar{x}, \bar{y}) &= \vartheta_{x_1} + \vartheta_{x_2} + \vartheta_{x_s} \\ &= -\bar{\alpha} [A_1 \sin \bar{\alpha}\bar{x} - A_2 \cos \bar{\alpha}\bar{x}] \\ &\quad \times [g_1 \{A_3 \cos \bar{\gamma}\bar{y} + A_4 \sin \bar{\gamma}\bar{y}\} + g_2 \{A_5 \cosh \hat{\mu}\bar{y} + A_6 \sinh \hat{\mu}\bar{y}\}] \\ &\quad + [B_7 \cos \bar{\alpha}\bar{x} + B_8 \sin \bar{\alpha}\bar{x}] \times [B_9 \cosh \hat{\beta}\bar{y} + B_{10} \sinh \hat{\beta}\bar{y}] \end{aligned} \quad (4.85)$$

$$\begin{aligned} \vartheta_y(\bar{x}, \bar{y}) &= \vartheta_{y_1} + \vartheta_{y_2} + \vartheta_{y_s} \\ &= [A_1 \cos \bar{\alpha}\bar{x} + A_2 \sin \bar{\alpha}\bar{x}] \\ &\quad \times [-\bar{\gamma}g_1 \{A_3 \sin \bar{\gamma}\bar{y} - A_4 \cos \bar{\gamma}\bar{y}\} + \hat{\mu}g_2 \{A_5 \sinh \hat{\mu}\bar{y} + A_6 \cosh \hat{\mu}\bar{y}\}] \\ &\quad + \frac{\bar{\alpha}}{\bar{\beta}} [B_7 \sin \bar{\alpha}\bar{x} - B_8 \cos \bar{\alpha}\bar{x}] \times [B_9 \sinh \hat{\beta}\bar{y} + B_{10} \cosh \hat{\beta}\bar{y}] \end{aligned} \quad (4.86)$$

where g_1 is given by Eq. (4.56) and g_2 is given by Eq. (4.69). As noted earlier, if the frequency range of interest is of sufficient magnitude, Eqs. (4.73)-(4.75) must be used when $i\hat{\mu} \rightarrow \bar{\mu}$ and Eqs. (4.82)-(4.83) must be used when $i\hat{\beta} \rightarrow \bar{\beta}$ in combining the individual solutions to get Eqs. (4.84)-(4.86). If for low frequencies there exists solutions such that $\bar{\gamma} \rightarrow i\hat{\gamma}$, Eqs. (4.60)-(4.62) must be used when combining the individual solutions to get Eqs. (4.84)-(4.86).

The solution for the modal functions of the Mindlin boundary value problem presented in Eqs. (4.84)-(4.86) will not yield non-trivial solutions for every possible combination of boundary conditions in the \bar{x} and \bar{y} -directions. If the plate has clamped or free edges in the \bar{x} -direction, it is found when applying boundary conditions that all of the integration constants must vanish, the trivial solution. Hence, the solution presented in Eqs. (4.84)-(4.86) requires the plate to have simply-supported boundaries in the \bar{x} -direction. The solution then allows for any combination of boundaries in the \bar{y} -direction.

A given structure will possess an infinite number of free vibration modes of the form of Eqs. (4.84)-(4.86), corresponding to a specific combination of wave numbers and natural frequency. Upon determining the specific form of the modal functions by the application of boundary conditions, the solution to the eigenvalue problem expressed in Eq. (4.3) results in the general free vibration response of the form

$$\bar{\mathbf{u}}(\bar{x}, \bar{y}, \bar{t}) = \sum_{j=1}^{\infty} \sum_{n=1}^{\infty} \bar{\mathbf{U}}^{(jn)}(\bar{x}, \bar{y}) \bar{A}^{(jn)} \cos(\bar{\omega}_{jn} \bar{t} - \phi_{jn}) \quad (4.87)$$

where $\bar{\mathbf{U}}^{(jn)}(\bar{x}, \bar{y})$ is the matrix of modal functions, $\bar{A}^{(jn)}$ is the amplitude, and ϕ_{jn} is the phase angle. The amplitude and phase angle are determined by the initial conditions imposed upon the plate.

4.4 The Frequency Spectrum and Selection of the Shear Correction Coefficient

In this section, we further examine the frequency equations of the Mindlin plate, Eqs. (4.31), (4.36), and (4.45), to determine the optimal value of the shear correction coefficient to use in applications. The best shear coefficient is determined here by comparison to the elastodynamic frequency spectrum for the infinite plate as presented in Chapter 3. One value considered here is Eq. (2.28), $\kappa = 5/(6 - \nu)$, which Hutchinson [10] and Stephen [29] determined best approximates the lowest *flexural* frequencies of the plate. The other value is $\kappa = \pi^2/12$ from Mindlin [17], which gives exact replication of the lowest *anti-symmetric shear* branch of the elastodynamic spectrum (see Figure 3.1). In Figure 4.1, the frequency spectrum for each of these values of the shear correction coefficient is plotted against the anti-symmetric branches of the elastodynamic spectrum, which is shown in Figure 3.3 for

a Poisson's ratio of $\nu = 0.3$. Poisson's ratio is the only parameter that must be given a numerical value in plotting the frequency spectrum in those figures.

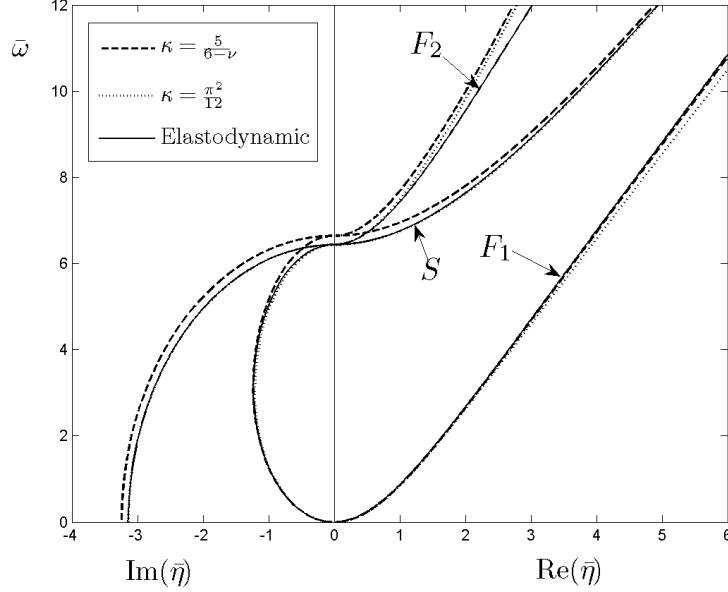


Figure 4.1: Comparison of the Mindlin plate frequency spectrum to that of the infinite elastodynamic plate for two values of the shear coefficient with $\nu = 0.3$, where F_1 and F_2 indicate the *flexural* branches and S indicates the *shear* branch.

Here, we see that $\kappa = 5/(6 - \nu)$ provides a very good approximation of the frequencies associated with the lowest *flexural* branch (F_1) over the entire range of wavelengths and frequencies considered. It does not provide very good agreement with either of the other two elastodynamic branches in Figure 4.1, except for the second *flexural* branch (F_2) at very low frequencies. As mentioned previously, $\kappa = \pi^2/12$ provides exact agreement with the frequencies of the lowest *anti-symmetric shear* branch. It also gives better approximation of the second *flexural* branch to a much higher frequency, while accurately predicting the cut-off frequency for this branch of the elastodynamic spectrum.

Eqs. (4.31), (4.36), and (4.45) each represent a solution to the eigenvalue problem of the Mindlin plate, Eq. (4.9), for a given value of the shear stiffness, \bar{k} . In Section 4.2, the shear stiffnesses corresponding to the solution for each branch were given a subscript to identify which branch they were associated with. The total solution for the Mindlin plate was then taken to be the linear combination of the contributions from each of the three frequency

branches. From Figure 4.1, we see that the most accurate results for the frequency spectrum of the Mindlin plate can be obtained by choosing different values of the shear correction coefficient for the different branches of the spectrum. Hence, the shear stiffness for branch one in Eq. (4.31), is calculated using

$$\kappa_1 = \frac{5}{6 - \nu} \quad (4.88)$$

The shear stiffnesses for the second *flexural* branch and the *shear* branch in Eqs. (4.36) and (4.45) respectively, are calculated using

$$\kappa_2 = \kappa_s = \frac{\pi^2}{12} \quad (4.89)$$

These values will result in the most accurate approximation of the frequency spectrum for a plate using Mindlin theory.

The Mindlin frequency spectrum found using the shear correction coefficients as defined in Eqs. (4.88) and (4.89) is superimposed over the elastodynamic frequency spectrum in Figure 4.2, again for a Poisson's ratio of $\nu = 0.3$. The use of multiple shear correction

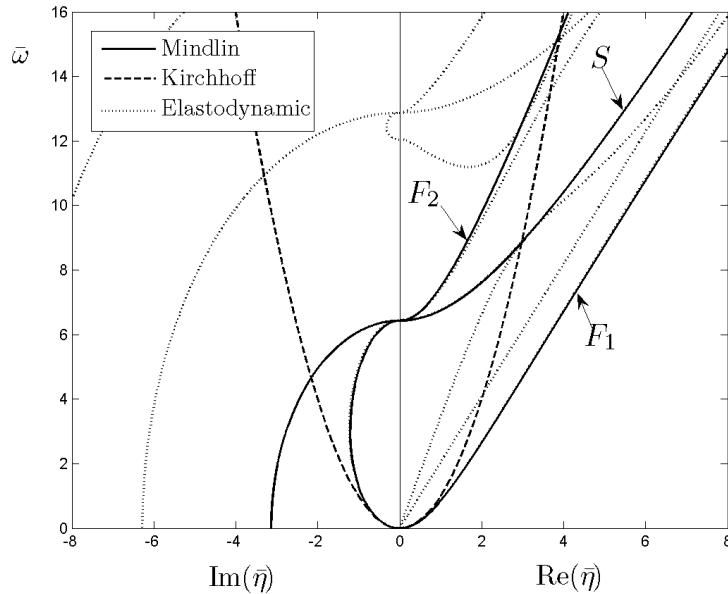


Figure 4.2: Comparison of the frequency spectrum for Kirchhoff plate theory, Mindlin plate theory, and the infinite elastodynamic plate for $\kappa_1 = 5/(6 - \nu)$ and $\kappa_2 = \kappa_s = \pi^2/12$.

coefficients results in good approximation of the lowest *flexural* branch and exact values for

the lowest *anti-symmetric shear* branch. The remaining Mindlin branch given by Eq. (4.36), matches closely with the second *flexural* branch up to approximately a frequency of $\bar{\omega} = 8$ before deviating from that branch. It then later matches closely with a higher *longitudinal* branch of the elastodynamic spectrum for a range of frequencies beginning at approximately $\bar{\omega} = 12$. Stephen [29] argues that due to the “schizophrenic nature” of this Mindlin branch with respect to the elastodynamic spectrum, it should be disregarded. We argue here that this Mindlin branch corresponds to the second *flexural* branch, with the theory losing accuracy once the Mindlin branch deviates from the elastodynamic branch. In this light, the use of multiple shear correction coefficients as presented herein results in highly accurate frequency predictions up to approximately $\bar{\omega} = 8$ for Mindlin plate theory.

The frequency spectrum predicted by Kirchhoff plate theory has also been included in Figure 4.2. Assuming a solution to Eq. (2.49) by separation of variables similar to Eqs. (4.1) and (4.12), results in the frequency equation for the Kirchhoff plate. Hence,

$$\bar{\eta}^2 = \bar{\omega} \tag{4.90}$$

where $\bar{\omega}$ is the same as that given for the non-dimensionalization for the natural frequencies of the Mindlin plate in Eq. (4.7). The frequency branch for Eq. (4.90) in Figure 4.2 shows the well known result that Kirchhoff theory is only accurate for low frequency flexural vibrations. When compared to the elastodynamic theory in the figure, Kirchhoff theory results in significant error beyond approximately $\bar{\omega} = 0.5$ when predicting vibrational frequencies.

The frequency branches for the Mindlin plate in Figure 4.2 are plotted as continuous paths which represent all of the possible vibration modes for a plate. The vibration modes for a specific geometry correspond to a set of discrete points along the branch paths determined when the boundary conditions are applied for a particular geometry and support conditions. In the next chapter, we proceed to apply the general solution for the free vibration modes of the Mindlin plate for specific combinations of boundary conditions.

Chapter 5

Mindlin Theory Applied for Specific Boundary Conditions

In applying boundary conditions to the general solution for the Mindlin plate boundary value problem as derived in Chapter 4, we consider a plate defined over the non-dimensional domain from $\bar{x} = 0$ to $\bar{x} = \bar{a}$ and from $\bar{y} = 0$ to $\bar{y} = \bar{b}$ as shown in Figure 5.1 with thickness, \bar{h} . In accordance with the derived solution procedure, the plate must have simply-supported

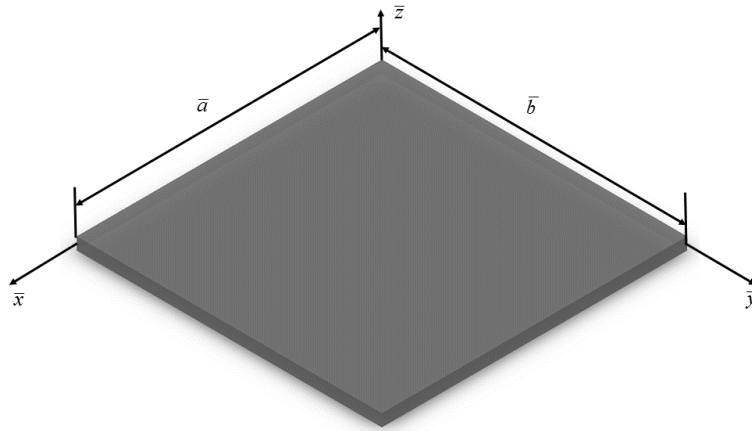


Figure 5.1: Plate with coordinate system and dimensions.

edges in the \bar{x} -direction. We will first apply the boundary conditions for simply-supported edges in the \bar{x} -direction and then proceed to consider simply-supported, clamped, and free boundaries in the \bar{y} -direction. Mixed boundaries in the \bar{y} -direction will not be considered.

5.1 Simply-Supported Boundary Conditions in the \bar{x} -direction

Along simply-supported edges, the structure is free to rotate in the direction perpendicular to the edge but cannot displace or rotate in the direction tangential to the edge. Therefore, in accordance with the possible boundary conditions specified in Section 2.3, the transverse

displacement, the normal bending moment, and the tangential rotation along the edges in the \bar{x} -direction must vanish. Hence, the non-dimensional boundary conditions for the modal functions along $\bar{x} = 0$ follow as

$$\bar{W}(0, \bar{y}) = 0 \quad (5.1a)$$

$$\left[\frac{\partial \vartheta_x}{\partial \bar{x}} + \nu \frac{\partial \vartheta_y}{\partial \bar{y}} \right]_{\bar{x}=0} = 0 \quad (5.1b)$$

$$\vartheta_y(0, \bar{y}) = 0 \quad (5.1c)$$

and along $\bar{x} = \bar{a}$

$$\bar{W}(\bar{a}, \bar{y}) = 0 \quad (5.2a)$$

$$\left[\frac{\partial \vartheta_x}{\partial \bar{x}} + \nu \frac{\partial \vartheta_y}{\partial \bar{y}} \right]_{\bar{x}=\bar{a}} = 0 \quad (5.2b)$$

$$\vartheta_y(\bar{a}, \bar{y}) = 0 \quad (5.2c)$$

Since the tangential rotations of Eqs. (5.1c) and (5.2c) vanish along the edges in the \bar{x} -direction, the following relations will also hold on those edges

$$\frac{\partial \vartheta_y}{\partial \bar{y}} \Big|_{\bar{x}=0} = \frac{\partial \vartheta_y}{\partial \bar{y}} \Big|_{\bar{x}=\bar{a}} = 0 \quad (5.3)$$

Incorporation of Eqs. (5.3) into Eqs. (5.1b) and (5.2b) simplifies those boundary conditions to

$$\frac{\partial \vartheta_x}{\partial \bar{x}} \Big|_{\bar{x}=0} = 0 \quad (5.4a)$$

$$\frac{\partial \vartheta_x}{\partial \bar{x}} \Big|_{\bar{x}=\bar{a}} = 0 \quad (5.4b)$$

Imposing the boundary conditions given by Eqs. (5.1a), (5.1c), and (5.4a) upon the modal functions given by Eqs. (4.84)-(4.86) results in the following respective relations

$$A_1 [A_3 \cos \bar{\gamma} \bar{y} + A_4 \sin \bar{\gamma} \bar{y} + A_5 \cosh \hat{\mu} \bar{y} + A_6 \sinh \hat{\mu} \bar{y}] = 0 \quad (5.5)$$

$$A_1 [-\bar{\gamma} g_1 \{A_3 \sin \bar{\gamma} \bar{y} - A_4 \cos \bar{\gamma} \bar{y}\} + \hat{\mu} g_2 \{A_5 \sinh \hat{\mu} \bar{y} + A_6 \cosh \hat{\mu} \bar{y}\}] - (\bar{\alpha} / \hat{\beta}) B_8 [B_9 \sinh \hat{\beta} \bar{y} + B_{10} \cosh \hat{\beta} \bar{y}] = 0 \quad (5.6)$$

$$-\bar{\alpha} A_1 [g_1 \{A_3 \cos \bar{\gamma} \bar{y} + A_4 \sin \bar{\gamma} \bar{y}\} + g_2 \{A_5 \cosh \hat{\mu} \bar{y} + A_6 \sinh \hat{\mu} \bar{y}\}] + B_8 [B_9 \cosh \hat{\beta} \bar{y} + B_{10} \sinh \hat{\beta} \bar{y}] = 0 \quad (5.7)$$

In order for the relations given in Eqs. (5.5)-(5.7) to vanish identically, we require

$$A_1 = B_8 = 0 \quad (5.8)$$

Next, imposing the boundary conditions along the edge $\bar{x} = \bar{a}$ given by Eqs. (5.2a), (5.2c), and (5.4b) with Eq. (5.8) results in the following respective relations

$$A_2 \sin \bar{\alpha} \bar{a} [A_3 \cos \bar{\gamma} \bar{y} + A_4 \sin \bar{\gamma} \bar{y} + A_5 \cosh \hat{\mu} \bar{y} + A_6 \sinh \hat{\mu} \bar{y}] = 0 \quad (5.9)$$

$$A_2 \sin \bar{\alpha} \bar{a} [-\bar{\gamma} g_1 \{A_3 \sin \bar{\gamma} \bar{y} - A_4 \cos \bar{\gamma} \bar{y}\} + \hat{\mu} g_2 \{A_5 \sinh \hat{\mu} \bar{y} + A_6 \cosh \hat{\mu} \bar{y}\}] \\ + \left(\bar{\alpha}/\hat{\beta}\right) B_7 \sin \bar{\alpha} \bar{a} [B_9 \sinh \hat{\beta} \bar{y} + B_{10} \cosh \hat{\beta} \bar{y}] = 0 \quad (5.10)$$

$$-\bar{\alpha} A_2 \sin \bar{\alpha} \bar{a} [g_1 \{A_3 \cos \bar{\gamma} \bar{y} + A_4 \sin \bar{\gamma} \bar{y}\} + g_2 \{A_5 \cosh \hat{\mu} \bar{y} + A_6 \sinh \hat{\mu} \bar{y}\}] \\ - B_7 \sin \bar{\alpha} \bar{a} [B_9 \cosh \hat{\beta} \bar{y} + B_{10} \sinh \hat{\beta} \bar{y}] = 0 \quad (5.11)$$

The relations given by Eqs. (5.9)-(5.11) will vanish identically if the constants A_2 and B_7 vanish or if

$$\sin \bar{\alpha} \bar{a} = 0 \quad (5.12)$$

If the constants vanish, we will be left with the trivial solution of zero displacement. Hence, for non-trivial modal displacements, Eq. (5.12) is satisfied for

$$\bar{\alpha} = \bar{\alpha}_j = j\pi/\bar{a} \quad (j=1,2,\dots) \quad (5.13)$$

where j is any integer value and the integration constants A_2 and B_7 remain undetermined.

The boundary conditions in the \bar{x} -direction have been fully implemented and incorporation of Eq. (5.8) reduces the modal functions to the following form

$$\bar{W}(\bar{x}, \bar{y}) = A_2 \sin \bar{\alpha} \bar{x} [A_3 \cos \bar{\gamma} \bar{y} + A_4 \sin \bar{\gamma} \bar{y} + A_5 \cosh \hat{\mu} \bar{y} + A_6 \sinh \hat{\mu} \bar{y}] \quad (5.14)$$

$$\vartheta_x(\bar{x}, \bar{y}) = \bar{\alpha} A_2 \cos \bar{\alpha} \bar{x} [g_1 \{A_3 \cos \bar{\gamma} \bar{y} + A_4 \sin \bar{\gamma} \bar{y}\} + g_2 \{A_5 \cosh \hat{\mu} \bar{y} + A_6 \sinh \hat{\mu} \bar{y}\}] \\ + B_7 \cos \bar{\alpha} \bar{x} [B_9 \cosh \hat{\beta} \bar{y} + B_{10} \sinh \hat{\beta} \bar{y}] \quad (5.15)$$

$$\vartheta_y(\bar{x}, \bar{y}) = A_2 \sin \bar{\alpha} \bar{x} [-\bar{\gamma} g_1 \{A_3 \sin \bar{\gamma} \bar{y} - A_4 \cos \bar{\gamma} \bar{y}\} + \hat{\mu} g_2 \{A_5 \sinh \hat{\mu} \bar{y} + A_6 \cosh \hat{\mu} \bar{y}\}] \\ + \left(\bar{\alpha}/\hat{\beta}\right) B_7 \sin \bar{\alpha} \bar{x} [B_9 \sinh \hat{\beta} \bar{y} + B_{10} \cosh \hat{\beta} \bar{y}] \quad (5.16)$$

with $\bar{\alpha}$ given by Eq. (5.13). The reduced modal functions above will hold for a plate with any combination of boundary conditions in the \bar{y} -direction.

5.2 Simply-Supported Boundary Conditions in the \bar{y} -direction

For simply-supported edges in the \bar{y} -direction, the transverse displacement, the normal bending moment, and the tangential rotation must vanish as they did along the edges in the \bar{x} -direction. Hence, the non-dimensional boundary conditions for the modal functions along $\bar{y} = 0$ follow as

$$\bar{W}(\bar{x}, 0) = 0 \quad (5.17a)$$

$$\left[\frac{\partial \vartheta_y}{\partial \bar{y}} + \nu \frac{\partial \vartheta_x}{\partial \bar{x}} \right]_{\bar{y}=0} = 0 \quad (5.17b)$$

$$\vartheta_x(\bar{x}, 0) = 0 \quad (5.17c)$$

and along $\bar{y} = \bar{b}$

$$\bar{W}(\bar{x}, \bar{b}) = 0 \quad (5.18a)$$

$$\left[\frac{\partial \vartheta_y}{\partial \bar{y}} + \nu \frac{\partial \vartheta_x}{\partial \bar{x}} \right]_{\bar{y}=\bar{b}} = 0 \quad (5.18b)$$

$$\vartheta_x(\bar{x}, \bar{b}) = 0 \quad (5.18c)$$

Since the tangential rotations of Eqs. (5.17c) and (5.18c) vanish along the edges in the \bar{y} -direction, the following relations will also hold on those edges

$$\frac{\partial \vartheta_x}{\partial \bar{x}} \Big|_{\bar{y}=0} = \frac{\partial \vartheta_x}{\partial \bar{x}} \Big|_{\bar{y}=\bar{b}} = 0 \quad (5.19)$$

Incorporation of Eqs. (5.19) into Eqs. (5.17b) and (5.18b) simplifies those boundary conditions to

$$\frac{\partial \vartheta_y}{\partial \bar{y}} \Big|_{\bar{y}=0} = 0 \quad (5.20a)$$

$$\frac{\partial \vartheta_y}{\partial \bar{y}} \Big|_{\bar{y}=\bar{b}} = 0 \quad (5.20b)$$

Imposing the boundary conditions given by Eqs. (5.17a), (5.17c), and (5.20a) upon the reduced modal functions given by Eqs. (5.14)-(5.16) results in the following respective relations

$$A_2 \sin \bar{\alpha} \bar{x} [A_3 + A_5] = 0 \quad (5.21)$$

$$\bar{\alpha} A_2 \cos \bar{\alpha} \bar{x} [g_1 A_3 + g_2 A_5] + B_7 B_9 \cos \bar{\alpha} \bar{x} = 0 \quad (5.22)$$

$$A_2 \sin \bar{\alpha} \bar{x} [-\bar{\gamma}^2 g_1 A_3 + \hat{\mu}^2 g_2 A_5] + \bar{\alpha} B_7 B_9 \sin \bar{\alpha} \bar{x} = 0 \quad (5.23)$$

In order for the relations given in Eqs. (5.21)-(5.23) to vanish identically, we require

$$A_3 = A_5 = B_9 = 0 \quad (5.24)$$

Next, imposing the boundary conditions along the edge $\bar{x} = \bar{a}$ given by Eqs. (5.18a), (5.18c), and (5.20b) with Eq. (5.24) results in the following respective relations

$$A_2 \sin \bar{\alpha} \bar{x} [A_4 \sin \bar{\gamma} \bar{b} + A_6 \sinh \hat{\mu} \bar{b}] = 0 \quad (5.25)$$

$$\bar{\alpha} A_2 \cos \bar{\alpha} \bar{x} [g_1 A_4 \sin \bar{\gamma} \bar{b} + g_2 A_6 \sinh \hat{\mu} \bar{b}] + B_7 \cos \bar{\alpha} \bar{x} [B_{10} \sinh \hat{\beta} \bar{b}] = 0 \quad (5.26)$$

$$A_2 \sin \bar{\alpha} \bar{x} [-\bar{\gamma}^2 g_1 A_4 \sin \bar{\gamma} \bar{b} + \hat{\mu}^2 g_2 A_6 \sinh \hat{\mu} \bar{b}] + \bar{\alpha} B_7 \sin \bar{\alpha} \bar{x} [B_{10} \sinh \hat{\beta} \bar{b}] = 0 \quad (5.27)$$

The relations given in Eqs. (5.25)-(5.27) will vanish simultaneously if the following conditions are satisfied

$$A_4 \sin \bar{\gamma} \bar{b} = 0 \quad (5.28)$$

$$A_6 \sinh \hat{\mu} \bar{b} = 0 \quad (5.29)$$

$$B_{10} \sinh \hat{\beta} \bar{b} = 0 \quad (5.30)$$

Equation (5.28) is satisfied for

$$\bar{\gamma} = \bar{\gamma}_n = n\pi/\bar{b} \quad (n=1,2,\dots) \quad (5.31)$$

where n is any integer value and the integration constant A_4 remains undetermined. The other conditions given in Eqs. (5.29) and (5.30) only have roots for imaginary values of the spatial wave numbers, so we take the constants associated with those equations to vanish. Hence,

$$A_6 = B_{10} = 0 \quad (5.32)$$

The wave numbers for the rectangular plate with all four edges simply-supported are given by Eqs. (5.13) and (5.31). The natural frequencies for the free vibration modes are then determined from the term on the right in Eq. (4.35). The natural frequency will be indexed on both j and n and hence, given as $\bar{\omega}_{jn}$.

The natural frequencies and spatial wave numbers are then substituted into the modal functions to obtain the shape for each vibration mode. Substitution of Eqs. (5.24) and

(5.32) into Eqs. (5.14)-(5.16) yields the modal functions for the Mindlin plate with simply-supported edges in the \bar{y} -direction as

$$\bar{W}_1^{(jn)}(\bar{x}, \bar{y}) = A^{(jn)} \sin \bar{\alpha}_j \bar{x} \sin \bar{\gamma}_n \bar{y} \quad (5.33)$$

$$\vartheta_{x_1}^{(jn)}(\bar{x}, \bar{y}) = \bar{\alpha}_j g_1^{(jn)} A^{(jn)} \cos \bar{\alpha}_j \bar{x} \sin \bar{\gamma}_n \bar{y} \quad (5.34)$$

$$\vartheta_{y_1}^{(jn)}(\bar{x}, \bar{y}) = \bar{\gamma}_n g_1^{(jn)} A^{(jn)} \sin \bar{\alpha}_j \bar{x} \cos \bar{\gamma}_n \bar{y} \quad (5.35)$$

where

$$A^{(jn)} = A_2 A_4 \quad (5.36)$$

The modal functions above have been given a subscript of one since only terms from the first *flexural* solution branch, given in Eqs. (4.53), (4.57), and (4.59), remain in the total solution. From Eq. (5.31), we also found that the spatial wave number $\bar{\gamma}_n$ for the first *flexural* branch was the only wave number to yield a natural frequency. Hence, in Eqs. (5.33)-(5.35) only the first *flexural* frequency branch is active, while the other two branches do not effect the vibrational motion for these modes. The modal functions are evaluated using the values of $\bar{\alpha}_j$, $\bar{\gamma}_n$, and $\bar{\omega}_{jn}$ for a given mode.

Consideration is now given to the remaining frequency branches for the simply-supported Mindlin plate. If we allow $i\hat{\mu}_{jn} \rightarrow \bar{\mu}_{jn}$ for the second *flexural* branch, then this branch will also yield propagating solutions of the form

$$\bar{\mu} = \bar{\mu}_n = n\pi/\bar{b} \quad (n=1,2,\dots) \quad (5.37)$$

This relation allows us to solve for the natural frequencies corresponding to the second *flexural* branch through the term on the right of Eq. (4.40). We also see that the general solution for propagating solutions of the second *flexural* branch, given in Eqs. (4.73)-(4.75), takes a similar form to those of the first branch. As a result, they will satisfy the boundary conditions for a rectangular plate with four simply-supported edges. Imposition of the requisite boundary conditions yields the modal functions associated with the vibration modes of the second *flexural* branch as

$$\bar{W}_2^{(jn)}(\bar{x}, \bar{y}) = A^{(jn)} \sin \bar{\alpha}_j \bar{x} \sin \bar{\mu}_n \bar{y} \quad (5.38)$$

$$\vartheta_{x_2}^{(jn)}(\bar{x}, \bar{y}) = \bar{\alpha}_j g_2^{(jn)} A^{(jn)} \cos \bar{\alpha}_j \bar{x} \sin \bar{\mu}_n \bar{y} \quad (5.39)$$

$$\vartheta_{y_2}^{(jn)}(\bar{x}, \bar{y}) = \bar{\mu}_n g_2^{(jn)} A^{(jn)} \sin \bar{\alpha}_j \bar{x} \cos \bar{\mu}_n \bar{y} \quad (5.40)$$

where

$$A^{(jn)} = A_2 A_6 \quad (5.41)$$

The modal functions for this branch are evaluated using the values of $\bar{\alpha}_j$, $\bar{\mu}_n$, and $\bar{\omega}_{jn}$ for a given mode.

Similarly, if we allow $i\hat{\beta}_{jn} \rightarrow \bar{\beta}_{jn}$, then the solutions of the *shear* branch will yield propagating results of the form

$$\bar{\beta} = \bar{\beta}_n = n\pi/\bar{b} \quad (n=1,2,\dots) \quad (5.42)$$

which allows us to solve for the natural frequencies corresponding to the *shear* branch through the term on the right of Eq. (4.49). In this case, the general solution for propagating solutions of the *shear* branch, given in Eqs. (4.82) and (4.83), will also satisfy the boundary conditions for a rectangular plate with four simply-supported edges. Imposition of the requisite boundary conditions yields the modal functions associated with the vibration modes of the *shear* branch as

$$\bar{W}_s^{(jn)}(\bar{x}, \bar{y}) = 0 \quad (5.43)$$

$$\vartheta_{x_s}^{(jn)}(\bar{x}, \bar{y}) = A^{(jn)} \cos \bar{\alpha}_j \bar{x} \sin \bar{\beta}_n \bar{y} \quad (5.44)$$

$$\vartheta_{y_s}^{(jn)}(\bar{x}, \bar{y}) = -(\bar{\alpha}_j/\bar{\beta}_n) A^{(jn)} \sin \bar{\alpha}_j \bar{x} \cos \bar{\beta}_n \bar{y} \quad (5.45)$$

where

$$A^{(jn)} = B_7 B_{10} \quad (5.46)$$

The modal functions for this branch are evaluated using the values of $\bar{\alpha}_j$, $\bar{\beta}_n$, and $\bar{\omega}_{jn}$ for a given mode.

The solution for which $\bar{\gamma} \rightarrow i\hat{\gamma}$ at low frequencies will not yield solutions for simply-supported boundaries. For the case of the simply-supported Mindlin plate, we have found that only one of the three frequency branches is active for a given vibration mode. Since the frequency branches do not interact, we are able to solve for a natural frequency along each of the three branches for a given real valued $\bar{\eta}$ obtained from the modal indices j and n . When considering other combinations of boundary conditions in the \bar{y} -direction we will

find that all three frequency branches must remain active in order for a given vibration mode to satisfy the requisite boundary conditions.

5.3 Clamped Boundary Conditions in the \bar{y} -direction

Along clamped edges, the structure cannot displace or rotate in either direction. Therefore, along the edges in the \bar{y} -direction the displacement, the normal rotation, and the tangential rotation must vanish. Hence, along $\bar{y} = 0$

$$\bar{W}(\bar{x}, 0) = 0 \quad (5.47a)$$

$$\vartheta_x(\bar{x}, 0) = 0 \quad (5.47b)$$

$$\vartheta_y(\bar{x}, 0) = 0 \quad (5.47c)$$

and along the edge $\bar{y} = \bar{b}$

$$\bar{W}(\bar{x}, \bar{b}) = 0 \quad (5.48a)$$

$$\vartheta_x(\bar{x}, \bar{b}) = 0 \quad (5.48b)$$

$$\vartheta_y(\bar{x}, \bar{b}) = 0 \quad (5.48c)$$

We continue by imposing the boundary conditions along the edge $\bar{y} = 0$ given by Eqs. (5.47) upon the reduced modal functions given by Eqs. (5.14)-(5.16), which results in the following respective relations

$$A_2 \sin \bar{\alpha} \bar{x} [A_3 + A_5] = 0 \quad (5.49)$$

$$\cos \bar{\alpha} \bar{x} [\bar{\alpha} A_2 \{g_1 A_3 + g_2 A_5\} + B_7 B_9] = 0 \quad (5.50)$$

$$\sin \bar{\alpha} \bar{x} \left[A_2 \{ \bar{\gamma} g_1 A_4 + \hat{\mu} g_2 A_6 \} + (\bar{\alpha} / \hat{\beta}) B_7 B_{10} \right] = 0 \quad (5.51)$$

Since the trigonometric functions of \bar{x} in the above relations do not vanish identically, Eq. (5.49) yields

$$A_5 = -A_3 \quad (5.52)$$

When Eq. (5.52) is substituted into Eq. (5.50) and the resulting expression is simplified, we obtain the relation

$$B_7 B_9 = \bar{\alpha} A_2 A_3 (g_2 - g_1) \quad (5.53)$$

We also simplify Eq. (5.51) to the following form

$$B_7 B_{10} = -(\hat{\beta}/\bar{\alpha}) A_2 \{ \bar{\gamma} g_1 A_4 + \hat{\mu} g_2 A_6 \} \quad (5.54)$$

which will be used along with Eqs. (5.52) and (5.53) to simplify the relations obtained when imposing the boundary conditions on the final edge of the plate.

We next impose the boundary conditions along the edge $\bar{y} = \bar{b}$ given by Eqs. (5.48) upon the reduced modal functions given by Eqs. (5.14)-(5.16) while also substituting Eq. (5.52) into these expressions, which results in the following respective relations

$$A_2 \sin \bar{\alpha} \bar{x} [A_3 (\cos \bar{\gamma} \bar{b} - \cosh \hat{\mu} \bar{b}) + A_4 \sin \bar{\gamma} \bar{b} + A_6 \sinh \hat{\mu} \bar{b}] = 0 \quad (5.55)$$

$$\begin{aligned} \bar{\alpha} A_2 \cos \bar{\alpha} \bar{x} [A_3 (g_1 \cos \bar{\gamma} \bar{b} - g_2 \cosh \hat{\mu} \bar{b}) + A_4 g_1 \sin \bar{\gamma} \bar{b} + A_6 g_2 \sinh \hat{\mu} \bar{b}] \\ + B_7 \cos \bar{\alpha} \bar{x} [B_9 \cosh \hat{\beta} \bar{b} + B_{10} \sinh \hat{\beta} \bar{b}] = 0 \end{aligned} \quad (5.56)$$

$$\begin{aligned} A_2 \sin \bar{\alpha} \bar{x} [-A_3 (\bar{\gamma} g_1 \sin \bar{\gamma} \bar{b} + \hat{\mu} g_2 \sinh \hat{\mu} \bar{b}) + A_4 \bar{\gamma} g_1 \cos \bar{\gamma} \bar{b} + A_6 \hat{\mu} g_2 \cosh \hat{\mu} \bar{b}] \\ + (\bar{\alpha}/\hat{\beta}) B_7 \sin \bar{\alpha} \bar{x} [B_9 \sinh \hat{\beta} \bar{b} + B_{10} \cosh \hat{\beta} \bar{b}] = 0 \end{aligned} \quad (5.57)$$

In order for Eq. (5.55) to be satisfied, the bracketed terms must vanish since the trigonometric function of \bar{x} does not. Solving that expression for the constant A_6 , results in the following relation

$$A_6 = \frac{1}{\sinh \hat{\mu} \bar{b}} [A_3 (\cosh \hat{\mu} \bar{b} - \cos \bar{\gamma} \bar{b}) - A_4 \sin \bar{\gamma} \bar{b}] \quad (5.58)$$

Substitution of Eqs. (5.53), (5.54), and (5.58) into both Eqs. (5.56) and (5.57) allows us to rewrite Eqs. (5.56) and (5.57) in matrix form as follows

$$\begin{bmatrix} H_{11} & H_{12} \\ H_{21} & H_{22} \end{bmatrix} \begin{Bmatrix} A_2 A_3 \\ A_2 A_4 \end{Bmatrix} = \begin{Bmatrix} 0 \\ 0 \end{Bmatrix} \quad (5.59)$$

where

$$H_{11} = \bar{\alpha}^2 \sinh \hat{\mu} \bar{b} (g_1 - g_2) (\cos \bar{\gamma} \bar{b} - \cosh \hat{\beta} \bar{b}) + \hat{\beta} \hat{\mu} g_2 \sinh \hat{\beta} \bar{b} (\cos \bar{\gamma} \bar{b} - \cosh \hat{\mu} \bar{b}) \quad (5.60)$$

$$H_{12} = \bar{\alpha}^2 (g_1 - g_2) \sinh \hat{\mu} \bar{b} \sin \bar{\gamma} \bar{b} + \hat{\beta} \sinh \hat{\beta} \bar{b} (\hat{\mu} g_2 \sin \bar{\gamma} \bar{b} - \bar{\gamma} g_1 \sinh \hat{\mu} \bar{b}) \quad (5.61)$$

$$\begin{aligned} H_{21} = \sinh \hat{\mu} \bar{b} [\bar{\alpha}^2 (g_2 - g_1) \sinh \hat{\beta} \bar{b} - \hat{\beta} \bar{\gamma} g_1 \sin \bar{\gamma} \bar{b} - \hat{\beta} \hat{\mu} g_2 \sinh \hat{\mu} \bar{b}] \\ + \hat{\beta} \hat{\mu} g_2 (\cosh \hat{\mu} \bar{b} - \cosh \hat{\beta} \bar{b}) (\cosh \hat{\mu} \bar{b} - \cos \bar{\gamma} \bar{b}) \end{aligned} \quad (5.62)$$

$$H_{22} = \hat{\beta}\hat{\mu}g_2 \sin \bar{\gamma} \bar{b} \left(\cosh \hat{\beta} \bar{b} - \cosh \hat{\mu} \bar{b} \right) + \hat{\beta} \bar{\gamma} g_1 \sinh \hat{\mu} \bar{b} \left(\cos \bar{\gamma} \bar{b} - \cosh \hat{\beta} \bar{b} \right) \quad (5.63)$$

To achieve non-trivial solutions for the modal displacements, the determinant of the square matrix appearing in Eq. (5.59) must vanish. The equation that results upon taking the determinant of the matrix is the frequency equation for the simply-supported/clamped Mindlin plate. Hence, the determinant of the square matrix in Eq. (5.59) is

$$F_C = H_{11}H_{22} - H_{12}H_{21} = 0 \quad (5.64)$$

When Eqs. (5.60)-(5.63) are substituted into Eq. (5.64), the final form of the frequency equation for the Mindlin plate with clamped edges in the \bar{y} -direction is obtained as

$$\begin{aligned} F_C = & \left[\left(\hat{\beta} \hat{\mu} g_2 \right)^2 - \left(\hat{\beta} \bar{\gamma} g_1 \right)^2 + \bar{\alpha}^4 (g_2 - g_1)^2 \right] \sin \bar{\gamma} \bar{b} \sinh \hat{\mu} \bar{b} \sinh \hat{\beta} \bar{b} \\ & + 2\bar{\alpha}^2 \hat{\beta} \hat{\mu} g_2 (g_2 - g_1) \sin \bar{\gamma} \bar{b} \left(1 - \cosh \hat{\mu} \bar{b} \cosh \hat{\beta} \bar{b} \right) \\ & + 2\hat{\beta}^2 \hat{\mu} \bar{\gamma} g_1 g_2 \sinh \hat{\beta} \bar{b} \left(1 - \cosh \hat{\mu} \bar{b} \cos \bar{\gamma} \bar{b} \right) \\ & - 2\bar{\alpha}^2 \hat{\beta} \bar{\gamma} g_1 (g_2 - g_1) \sinh \hat{\mu} \bar{b} \left(1 - \cosh \hat{\beta} \bar{b} \cos \bar{\gamma} \bar{b} \right) = 0 \end{aligned} \quad (5.65)$$

The roots of Eq. (5.65) represent the vibration modes of the plate and can be obtained through numerical root solving. There will be an infinite number of modes corresponding to unique combinations of the natural frequencies and spatial wave numbers. In accordance with the solution derived in this chapter there will be a single spatial wave number in the \bar{x} -direction, which is given by Eq. (5.13) and repeated here as

$$\bar{\alpha}_j = j\pi/\bar{a} \quad (5.66)$$

where in physical interpretation, the index j represents the number of half sine waves occurring in the modal displacement of the plate in the \bar{x} -direction. For a given index j in the \bar{x} -direction, there will be an infinite number of combinations of the wave numbers in the \bar{y} -direction, which will be given the index n . Each of the spatial wave numbers in the \bar{y} -direction will be indexed on both j and n ($\bar{\gamma}_{jn}$, $\hat{\mu}_{jn}$, and $\hat{\beta}_{jn}$). The normalized natural frequencies will also be determined for a given $\bar{\alpha}_j$ and hence will also be indexed on both j and n ($\bar{\omega}_{jn}$). In this sense, there will be a single natural frequency for a given pair of $\bar{\alpha}_j$ and the combination of $\bar{\gamma}_{jn}$, $\hat{\mu}_{jn}$, and $\hat{\beta}_{jn}$ that satisfy the roots of Eq. (5.65).

The natural frequencies and spatial wave numbers in the \bar{y} -direction are related by Eqs. (4.35), (4.39) or (4.40), and (4.48) or (4.49) through the wave number $\bar{\alpha}_j$. Hence, from

Eq. (4.35)

$$\bar{\gamma}_{jn} = \sqrt{\bar{\omega}_{jn}^2 F_1 - \bar{\alpha}_j^2} = \sqrt{\bar{\omega}_{jn}^2 F_1 - (j\pi/\bar{a})^2} \quad (5.67)$$

from Eq. (4.39)

$$\hat{\mu}_{jn} = \sqrt{\bar{\alpha}_j^2 - \bar{\omega}_{jn}^2 F_2} = \sqrt{(j\pi/\bar{a})^2 - \bar{\omega}_{jn}^2 F_2} \quad (5.68)$$

and from Eq. (4.48)

$$\hat{\beta}_{jn} = \sqrt{\bar{\alpha}_j^2 - S} = \sqrt{(j\pi/\bar{a})^2 - S} \quad (5.69)$$

where F_1 , F_2 , and S are given by Eqs. (4.32), (4.37), and (4.46), respectively. For each value of j , Eq. (5.65) can be numerically solved to obtain values for $\bar{\omega}_{jn}$, $\bar{\gamma}_{jn}$, $\hat{\mu}_{jn}$, and $\hat{\beta}_{jn}$ using the relations presented in Eqs. (5.67)-(5.69).

When $\bar{\omega}_{jn}$ has reached sufficient magnitude and $i\hat{\mu}_{jn} \rightarrow \bar{\mu}_{jn}$ in Eq. (5.65), then Eq. (5.68) is replaced by the following when root solving

$$\bar{\mu}_{jn} = \sqrt{\bar{\omega}_{jn}^2 F_2 - \bar{\alpha}_j^2} = \sqrt{\bar{\omega}_{jn}^2 F_2 - (j\pi/\bar{a})^2} \quad (5.70)$$

When $\bar{\omega}_{jn}$ has reached sufficient magnitude and $i\hat{\beta}_{jn} \rightarrow \bar{\beta}_{jn}$ in Eq. (5.65), then Eq. (5.69) is replaced by the following when root solving

$$\bar{\beta}_{jn} = \sqrt{S - \bar{\alpha}_j^2} = \sqrt{S - (j\pi/\bar{a})^2} \quad (5.71)$$

If both situations occur simultaneously, then both substitutions must be made when root solving.

If solutions exist such that, $\bar{\gamma} \rightarrow i\hat{\gamma}$ in Eq. (5.65), then Eq. (5.67) is replaced by the following when root solving

$$\hat{\gamma}_{jn} = \sqrt{\bar{\alpha}_j^2 - \bar{\omega}_{jn}^2 F_1} = \sqrt{(j\pi/\bar{a})^2 - \bar{\omega}_{jn}^2 F_1} \quad (5.72)$$

Solutions incorporating Eq. (5.72) will not exist for every combination of boundary conditions.

The natural frequencies and spatial wave numbers are then substituted into the modal functions to obtain the shape for each vibration mode. The first line of Eq. (5.59) yields the relation between the undetermined constants A_2A_3 and A_2A_4 of Eq. (5.59). Hence,

$$A_2A_4 = -\frac{H_{11}^{(jn)}}{H_{12}^{(jn)}}A^{(jn)} \quad (5.73)$$

with

$$A^{(jn)} = A_2 A_3 \quad (5.74)$$

where j and n are the modal indices.

Substitution of Eqs. (5.52)-(5.54), (5.58), and (5.73) into Eqs. (5.14)-(5.16) yields the modal functions for the Mindlin plate with clamped edges in the \bar{y} -direction

$$\bar{W}^{(jn)}(\bar{x}, \bar{y}) = A^{(jn)} \sin \bar{\alpha}_j \bar{x} \left[\cos \bar{\gamma}_{jn} \bar{y} - \frac{H_{11}^{(jn)}}{H_{12}^{(jn)}} \sin \bar{\gamma}_{jn} \bar{y} - \cosh \hat{\mu}_{jn} \bar{y} + \tilde{H}^{(jn)} \sinh \hat{\mu}_{jn} \bar{y} \right] \quad (5.75)$$

$$\begin{aligned} \vartheta_x^{(jn)}(\bar{x}, \bar{y}) = & \bar{\alpha}_j A^{(jn)} \cos \bar{\alpha}_j \bar{x} \left[g_1^{(jn)} \left\{ \cos \bar{\gamma}_{jn} \bar{y} - \frac{H_{11}^{(jn)}}{H_{12}^{(jn)}} \sin \bar{\gamma}_{jn} \bar{y} \right\} \right. \\ & - g_2^{(jn)} \left\{ \cosh \hat{\mu}_{jn} \bar{y} - \tilde{H}^{(jn)} \sinh \hat{\mu}_{jn} \bar{y} \right\} \\ & \left. + \left(g_2^{(jn)} - g_1^{(jn)} \right) \cosh \hat{\beta}_{jn} \bar{y} + \frac{\hat{\beta}_{jn}}{\bar{\alpha}_j^2} \hat{H}^{(jn)} \sinh \hat{\beta}_{jn} \bar{y} \right] \end{aligned} \quad (5.76)$$

$$\begin{aligned} \vartheta_y^{(jn)}(\bar{x}, \bar{y}) = & A^{(jn)} \sin \bar{\alpha}_j \bar{x} \left[-\bar{\gamma}_{jn} g_1^{(jn)} \left\{ \sin \bar{\gamma}_{jn} \bar{y} + \frac{H_{11}^{(jn)}}{H_{12}^{(jn)}} \cos \bar{\gamma}_{jn} \bar{y} \right\} \right. \\ & - \hat{\mu}_{jn} g_2^{(jn)} \left\{ \sinh \hat{\mu}_{jn} \bar{y} - \tilde{H}^{(jn)} \cosh \hat{\mu}_{jn} \bar{y} \right\} \\ & \left. + \frac{\bar{\alpha}_j^2}{\hat{\beta}_{jn}} \left(g_2^{(jn)} - g_1^{(jn)} \right) \sinh \hat{\beta}_{jn} \bar{y} + \hat{H}^{(jn)} \cosh \hat{\beta}_{jn} \bar{y} \right] \end{aligned} \quad (5.77)$$

where

$$\tilde{H}^{(jn)} = \frac{H_{11}^{(jn)}}{H_{12}^{(jn)}} \frac{\sin \bar{\gamma}_{jn} \bar{b}}{\sinh \hat{\mu}_{jn} \bar{b}} + \frac{\cosh \hat{\mu}_{jn} \bar{b} - \cos \bar{\gamma}_{jn} \bar{b}}{\sinh \hat{\mu}_{jn} \bar{b}} \quad (5.78)$$

and

$$\hat{H}^{(jn)} = \bar{\gamma}_{jn} g_1^{(jn)} \frac{H_{11}^{(jn)}}{H_{12}^{(jn)}} - \hat{\mu}_{jn} g_2^{(jn)} \tilde{H}^{(jn)} \quad (5.79)$$

The modal functions are evaluated using the values for $\bar{\omega}_{jn}$, $\bar{\gamma}_{jn}$, $\hat{\mu}_{jn}$, and $\hat{\beta}_{jn}$ obtained from Eq. (5.65) for a given mode. When $\bar{\omega}_{jn}$ has reached sufficient magnitude, $i\hat{\mu}_{jn} \rightarrow \bar{\mu}_{jn}$ and $i\hat{\beta}_{jn} \rightarrow \bar{\beta}_{jn}$ in the above set of equations. If such solutions exist, $\bar{\gamma} \rightarrow i\hat{\gamma}$ in the above set of modal equations. In the modal functions for the Mindlin plate with clamped edges in the \bar{y} -direction, the solutions corresponding to each of the three frequency branches are active in comprising a given vibration mode. The implications of this in solving for the natural frequencies will be discussed further when presenting numerical results in the next chapter.

5.4 Free Boundary Conditions in the \bar{y} -direction

Along free edges, the structure is free to displace and rotate in either direction. Therefore, along the edges in the \bar{y} -direction the resultant normal bending moment, twisting moment,

and transverse shear force must vanish. Hence, along $\bar{y} = 0$

$$\left[\frac{\partial \vartheta_y}{\partial \bar{y}} + \nu \frac{\partial \vartheta_x}{\partial \bar{x}} \right]_{\bar{y}=0} = 0 \quad (5.80a)$$

$$\left[\frac{\partial \vartheta_y}{\partial \bar{x}} + \frac{\partial \vartheta_x}{\partial \bar{y}} \right]_{\bar{y}=0} = 0 \quad (5.80b)$$

$$\left[\bar{k}_1 \left(\frac{\partial \bar{W}_1}{\partial \bar{y}} - \vartheta_{y_1} \right) + \bar{k}_2 \left(\frac{\partial \bar{W}_2}{\partial \bar{y}} - \vartheta_{y_2} \right) - \bar{k}_2 \vartheta_{y_s} \right]_{\bar{y}=0} = 0 \quad (5.80c)$$

and along the edge $\bar{y} = \bar{b}$

$$\left[\frac{\partial \vartheta_y}{\partial \bar{y}} + \nu \frac{\partial \vartheta_x}{\partial \bar{x}} \right]_{\bar{y}=\bar{b}} = 0 \quad (5.81a)$$

$$\left[\frac{\partial \vartheta_y}{\partial \bar{x}} + \frac{\partial \vartheta_x}{\partial \bar{y}} \right]_{\bar{y}=\bar{b}} = 0 \quad (5.81b)$$

$$\left[\bar{k}_1 \left(\frac{\partial \bar{W}_1}{\partial \bar{y}} - \vartheta_{y_1} \right) + \bar{k}_2 \left(\frac{\partial \bar{W}_2}{\partial \bar{y}} - \vartheta_{y_2} \right) - \bar{k}_2 \vartheta_{y_s} \right]_{\bar{y}=\bar{b}} = 0 \quad (5.81c)$$

where in Eqs. (5.80c) and (5.81c) the resultant transverse shear force is taken to be the linear combination of the three solution branches substituted into the non-dimensional form of the transverse shear force given by Eq. (2.23b). In those equations, the shear stiffness for the *shear* branch, \bar{k}_s , has been set equal to \bar{k}_2 in accordance with Eq. (4.89).

We continue by imposing the boundary conditions along the edge $\bar{y} = 0$ given by Eqs. (5.80) upon the reduced modal functions given by Eqs. (5.14)-(5.16), which results in the following respective relations

$$\sin \bar{\alpha} \bar{x} [A_2 \{-g_1 Z_1 A_3 + g_2 Z_2 A_5\} + \bar{\alpha}(1 - \nu) B_7 B_9] = 0 \quad (5.82)$$

$$\cos \bar{\alpha} \bar{x} \left[\bar{\alpha} A_2 \{2\bar{\gamma} g_1 A_4 + 2\hat{\mu} g_2 A_6\} + \left(\frac{\bar{\alpha}^2}{\hat{\beta}} + \hat{\beta} \right) B_7 B_{10} \right] = 0 \quad (5.83)$$

$$\sin \bar{\alpha} \bar{x} \left[A_2 \{ \bar{k}_1 \bar{\gamma} (1 - g_1) A_4 + \bar{k}_2 \hat{\mu} (1 - g_2) A_6 \} - \bar{k}_2 \left(\bar{\alpha} / \hat{\beta} \right) B_7 B_{10} \right] = 0 \quad (5.84)$$

where

$$Z_1 = \bar{\gamma}^2 + \nu \bar{\alpha}^2 \quad (5.85)$$

$$Z_2 = \hat{\mu}^2 - \nu \bar{\alpha}^2 \quad (5.86)$$

Since the trigonometric function of \bar{x} in Eq. (5.82) does not vanish identically, the bracketed term in that equation yields

$$B_7 B_9 = \frac{1}{\bar{\alpha}(1 - \nu)} [g_1 Z_1 A_2 A_3 - g_2 Z_2 A_2 A_5] \quad (5.87)$$

Similarly, Eqs. (5.83) and (5.84) yield

$$A_2 A_6 = -\frac{\bar{\gamma} Z_4}{\hat{\mu} Z_5} A_2 A_4 \quad (5.88)$$

and

$$B_7 B_{10} = \frac{2\hat{\beta}\bar{\alpha}\bar{\gamma}}{Z_3 Z_5} (g_2 Z_4 - g_1 Z_5) A_2 A_4 \quad (5.89)$$

where

$$Z_3 = \bar{\alpha}^2 + \hat{\beta}^2 \quad (5.90)$$

$$Z_4 = 2\bar{k}_2 \bar{\alpha}^2 g_1 + \bar{k}_1 (1 - g_1) Z_3 \quad (5.91)$$

$$Z_5 = 2\bar{k}_2 \bar{\alpha}^2 g_2 + \bar{k}_2 (1 - g_2) Z_3 \quad (5.92)$$

We next impose the boundary conditions along the edge $\bar{y} = \bar{b}$ given by Eqs. (5.81) upon the reduced modal functions given by Eqs. (5.14)-(5.16) while also substituting Eqs. (5.87)-(5.89) into these expressions. This results in the following system of equations

$$\begin{bmatrix} \Lambda_{11} & \Lambda_{12} & \Lambda_{13} \\ \Lambda_{21} & \Lambda_{22} & \Lambda_{23} \\ \Lambda_{31} & \Lambda_{32} & \Lambda_{33} \end{bmatrix} \begin{Bmatrix} A_2 A_3 \\ A_2 A_4 \\ A_2 A_5 \end{Bmatrix} = \begin{Bmatrix} 0 \\ 0 \\ 0 \end{Bmatrix} \quad (5.93)$$

where

$$\Lambda_{11} = \hat{\mu} g_1 Z_1 Z_3 Z_5 \left[\cosh \hat{\beta} \bar{b} - \cos \bar{\gamma} \bar{b} \right] \quad (5.94)$$

$$\Lambda_{12} = 2(1 - \nu) \bar{\alpha}^2 \hat{\beta} \bar{\gamma} \hat{\mu} (g_2 Z_4 - g_1 Z_5) \sinh \hat{\beta} \bar{b} - \hat{\mu} g_1 Z_1 Z_3 Z_5 \sin \bar{\gamma} \bar{b} - \bar{\gamma} g_2 Z_2 Z_3 Z_4 \sinh \hat{\mu} \bar{b} \quad (5.95)$$

$$\Lambda_{13} = \hat{\mu} g_2 Z_2 Z_3 Z_5 \left[\cosh \hat{\mu} \bar{b} - \cosh \hat{\beta} \bar{b} \right] \quad (5.96)$$

$$\Lambda_{21} = g_1 Z_5 \left[Z_1 Z_3 \sinh \hat{\beta} \bar{b} - 2(1 - \nu) \bar{\alpha}^2 \hat{\beta} \bar{\gamma} \sin \bar{\gamma} \bar{b} \right] \quad (5.97)$$

$$\Lambda_{22} = 2(1 - \nu) \bar{\alpha}^2 \hat{\beta} \bar{\gamma} \left[g_1 Z_5 \cos \bar{\gamma} \bar{b} - g_2 Z_4 \cosh \hat{\mu} \bar{b} + (g_2 Z_4 - g_1 Z_5) \cosh \hat{\beta} \bar{b} \right] \quad (5.98)$$

$$\Lambda_{23} = g_2 Z_5 \left[2(1 - \nu) \bar{\alpha}^2 \hat{\beta} \hat{\mu} \sinh \hat{\mu} \bar{b} - Z_2 Z_3 \sinh \hat{\beta} \bar{b} \right] \quad (5.99)$$

$$\Lambda_{31} = Z_3 Z_5 \left[-\bar{k}_1 (1 - \nu) \hat{\beta} \bar{\gamma} (1 - g_1) \sin \bar{\gamma} \bar{b} - \bar{k}_2 g_1 Z_1 \sinh \hat{\beta} \bar{b} \right] \quad (5.100)$$

$$\Lambda_{32} = (1 - \nu) \hat{\beta} \bar{\gamma} \left[\bar{k}_1 (1 - g_1) Z_3 Z_5 \cos \bar{\gamma} \bar{b} - \bar{k}_2 (1 - g_2) Z_3 Z_4 \cosh \hat{\mu} \bar{b} - 2\bar{k}_2 \bar{\alpha}^2 (g_2 Z_4 - g_1 Z_5) \cosh \hat{\beta} \bar{b} \right] \quad (5.101)$$

$$\Lambda_{33} = \bar{k}_2 Z_3 Z_5 \left[g_2 Z_2 \sinh \hat{\beta} \bar{b} + (1 - \nu) \hat{\beta} \hat{\mu} (1 - g_2) \sinh \hat{\mu} \bar{b} \right] \quad (5.102)$$

To achieve non-trivial solutions for the modal displacements, the determinant of the square matrix appearing in Eq. (5.93) must vanish. The equation that results from this is the frequency equation for the simply-supported/free Mindlin plate. Hence, the determinant of the square matrix in Eq. (5.93) is

$$F_F = \Lambda_{11} (\Lambda_{22}\Lambda_{33} - \Lambda_{32}\Lambda_{23}) - \Lambda_{12} (\Lambda_{21}\Lambda_{33} - \Lambda_{23}\Lambda_{31}) + \Lambda_{13} (\Lambda_{21}\Lambda_{32} - \Lambda_{22}\Lambda_{31}) = 0 \quad (5.103)$$

When Eqs. (5.94)-(5.102) are substituted into Eq. (5.103), the final form of the frequency equation for the Mindlin plate with free edges in the \bar{y} -direction is obtained as

$$\begin{aligned} F_F = & \left[Z_3 \left\{ (g_1 \hat{\mu} Z_1 Z_5)^2 - (g_2 \bar{\gamma} Z_2 Z_4)^2 \right\} \right. \\ & \left. + 4\bar{\alpha}^4 Z_6 (g_2 Z_4 - g_1 Z_5) \left\{ \hat{\beta} \bar{\gamma} \hat{\mu} (1 - \nu) \right\}^2 \right] \sin \bar{\gamma} \bar{b} \sinh \hat{\mu} \bar{b} \sinh \hat{\beta} \bar{b} \\ & - 2\bar{\alpha}^2 \bar{\gamma}^2 \hat{\beta} \hat{\mu} (1 - \nu) g_2 Z_2 Z_4 \{ Z_3 Z_6 - g_2 Z_4 + g_1 Z_5 \} \sin \bar{\gamma} \bar{b} \left(\cosh \hat{\mu} \bar{b} \cosh \hat{\beta} \bar{b} - 1 \right) \\ & + 2\bar{\alpha}^2 \hat{\mu}^2 \hat{\beta} \bar{\gamma} (1 - \nu) g_1 Z_1 Z_5 \{ Z_3 Z_6 - g_2 Z_4 + g_1 Z_5 \} \sinh \hat{\mu} \bar{b} \left(\cosh \hat{\beta} \bar{b} \cos \bar{\gamma} \bar{b} - 1 \right) \\ & + 2\hat{\mu} \bar{\gamma} g_1 g_2 Z_1 Z_2 Z_3 Z_4 Z_5 \sinh \hat{\beta} \bar{b} \left(\cosh \hat{\mu} \bar{b} \cos \bar{\gamma} \bar{b} - 1 \right) = 0 \end{aligned} \quad (5.104)$$

where

$$Z_6 = \bar{k}_2 g_1 - \bar{k}_1 g_2 + g_1 g_2 (\bar{k}_1 - \bar{k}_2) \quad (5.105)$$

The roots of Eq. (5.104) represent the vibration modes of the plate and can be obtained through numerical root solving. There will be an infinite number of modes corresponding to unique combinations of the natural frequencies and spatial wave numbers. The method of solving for pairs of $\bar{\omega}_{jn}$, $\bar{\gamma}_{jn}$, $\hat{\mu}_{jn}$, and $\hat{\beta}_{jn}$ for a given $\bar{\alpha}_j$ is the same as described in the previous section for plates with clamped edges in the \bar{y} -direction.

The natural frequencies and spatial wave numbers for the simply-supported/free plate are then substituted into the modal functions to obtain the shape for each vibration mode. The undetermined coefficients from Eq. (5.93) are related as follows

$$A_2 A_4 = \frac{\Lambda_{23}^{(jn)} \Lambda_{11}^{(jn)} - \Lambda_{21}^{(jn)} \Lambda_{13}^{(jn)}}{\Lambda_{22}^{(jn)} \Lambda_{13}^{(jn)} - \Lambda_{23}^{(jn)} \Lambda_{12}^{(jn)}} A^{(jn)} = \Lambda_1^{(jn)} A^{(jn)} \quad (5.106)$$

and

$$A_2 A_5 = - \left[\frac{\Lambda_{12}^{(jn)}}{\Lambda_{13}^{(jn)}} \Lambda_1^{(jn)} + \frac{\Lambda_{11}^{(jn)}}{\Lambda_{13}^{(jn)}} \right] A^{(jn)} = -\Lambda_2^{(jn)} A^{(jn)} \quad (5.107)$$

with

$$A^{(jn)} = A_2 A_3 \quad (5.108)$$

where j and n are the modal indices.

Substitution of Eqs. (5.87)-(5.89), (5.106), and (5.107) into Eqs. (5.14)-(5.16) yields the modal functions for the Mindlin plate with free edges in the \bar{y} -direction

$$\bar{W}^{(jn)}(\bar{x}, \bar{y}) = A^{(jn)} \sin \bar{\alpha}_j \bar{x} \left[\cos \bar{\gamma}_{jn} \bar{y} + \Lambda_1^{(jn)} \sin \bar{\gamma}_{jn} \bar{y} - \Lambda_2^{(jn)} \cosh \hat{\mu}_{jn} \bar{y} - \Lambda_1^{(jn)} \frac{\bar{\gamma}_{jn} Z_4^{(jn)}}{\hat{\mu}_{jn} Z_5^{(jn)}} \sinh \hat{\mu}_{jn} \bar{y} \right] \quad (5.109)$$

$$\begin{aligned} \vartheta_x^{(jn)}(\bar{x}, \bar{y}) = & \bar{\alpha}_j A^{(jn)} \cos \bar{\alpha}_j \bar{x} \left[g_1^{(jn)} \left\{ \cos \bar{\gamma}_{jn} \bar{y} + \Lambda_1^{(jn)} \sin \bar{\gamma}_{jn} \bar{y} \right\} \right. \\ & - g_2^{(jn)} \left\{ \Lambda_2^{(jn)} \cosh \hat{\mu}_{jn} \bar{y} + \Lambda_1^{(jn)} \frac{\bar{\gamma}_{jn} Z_4^{(jn)}}{\hat{\mu}_{jn} Z_5^{(jn)}} \sinh \hat{\mu}_{jn} \bar{y} \right\} \\ & \left. + \frac{1}{\bar{\alpha}_j^2 (1-\nu)} \tilde{\Lambda}^{(jn)} \cosh \hat{\beta}_{jn} \bar{y} + \hat{\beta}_{jn} \hat{\Lambda}^{(jn)} \sinh \hat{\beta}_{jn} \bar{y} \right] \end{aligned} \quad (5.110)$$

$$\begin{aligned} \vartheta_y^{(jn)}(\bar{x}, \bar{y}) = & A^{(jn)} \sin \bar{\alpha}_j \bar{x} \left[-\bar{\gamma}_{jn} g_1^{(jn)} \left\{ \sin \bar{\gamma}_{jn} \bar{y} - \Lambda_1^{(jn)} \cos \bar{\gamma}_{jn} \bar{y} \right\} \right. \\ & - \hat{\mu}_{jn} g_2^{(jn)} \left\{ \Lambda_2^{(jn)} \sinh \hat{\mu}_{jn} \bar{y} + \Lambda_1^{(jn)} \frac{\bar{\gamma}_{jn} Z_4^{(jn)}}{\hat{\mu}_{jn} Z_5^{(jn)}} \cosh \hat{\mu}_{jn} \bar{y} \right\} \\ & \left. + \frac{1}{\hat{\beta}_{jn} (1-\nu)} \tilde{\Lambda}^{(jn)} \sinh \hat{\beta}_{jn} \bar{y} + \bar{\alpha}_j^2 \hat{\Lambda}^{(jn)} \cosh \hat{\beta}_{jn} \bar{y} \right] \end{aligned} \quad (5.111)$$

where

$$\tilde{\Lambda}^{(jn)} = g_1^{(jn)} Z_1^{(jn)} + \Lambda_2^{(jn)} g_2^{(jn)} Z_2^{(jn)} \quad (5.112)$$

and

$$\hat{\Lambda}^{(jn)} = \Lambda_1^{(jn)} \frac{2\bar{\gamma}_{jn}}{Z_3^{(jn)} Z_5^{(jn)}} \left(g_2^{(jn)} Z_4^{(jn)} - g_1^{(jn)} Z_5^{(jn)} \right) \quad (5.113)$$

The modal functions are evaluated using the values for $\bar{\omega}_{jn}$, $\bar{\gamma}_{jn}$, $\hat{\mu}_{jn}$, and $\hat{\beta}_{jn}$ obtained from Eq. (5.104) for a given mode. When $\bar{\omega}_{jn}$ has reached sufficient magnitude, $i\hat{\mu}_{jn} \rightarrow \bar{\mu}_{jn}$ and $i\hat{\beta}_{jn} \rightarrow \bar{\beta}_{jn}$ in the above set of equations. If such solutions exist, $\bar{\gamma} \rightarrow i\hat{\gamma}$ in the above set of modal equations. As for the case of clamped edges in the \bar{y} -direction, all three frequency branches remain active in calculating a given natural frequency for free edges in the \bar{y} -direction. In the next chapter, numerical results are presented for each of the three combinations of boundary conditions considered in this chapter.

Chapter 6

Results and Discussion

This chapter presents numerical simulations for the Mindlin plate with the various boundary conditions covered in the previous chapter. Analysis of both the modal frequency spectrum and the modal displacement functions is performed for representative values of Poisson's ratio and the thickness to length ratio of the plate.

6.1 Simply-Supported Boundary Conditions in the \bar{y} -direction

We begin by solving for the natural frequencies of the simply-supported Mindlin plate. For the first *flexural* branch, the frequencies are obtained from the term on the right in Eq. (4.35), with $\bar{\alpha}_j$ and $\bar{\gamma}_n$ given by Eqs. (5.13) and (5.31), respectively. Hence,

$$\left(\frac{j\pi}{a}\right)^2 + \left(\frac{n\pi}{b}\right)^2 = \left(\bar{\omega}_{jn}^{(1)}\right)^2 F_1 \quad (6.1)$$

where j and n are integers identifying the vibration modes and F_1 is given in Eq. (4.32). In the above equation $\bar{\omega}_{jn}$ has been given a superscript of (1) to identify it with the first *flexural* branch.

The calculated values for the natural frequencies of this branch appear in Table 6.1 in the rows labeled as Present. Since the frequencies are symmetric with respect to the indices j and n , only half of the figure has been populated with values. In Table 6.1, the results from several other studies found in the literature have also been included, the most important of which being the work of Srinivas *et al.* [28]. Srinivas *et al.* presented a solution for the simply-supported plate that satisfies the three-dimensional elastodynamic equations. The resulting natural frequencies computed from their solution are therefore taken to be the exact values. The non-dimensional natural frequencies used in the present study are related

to the non-dimensional values used in Srinivas *et al.* by

$$\tilde{\omega} = \bar{\omega} \sqrt{\frac{1}{6(1-\nu)}} = \omega h \sqrt{\frac{\rho}{G}} \quad (6.2)$$

where $\tilde{\omega}$ is the non-dimensionalization appearing in Srinivas *et al.*.

The results found in the literature from three additional studies have been included in Table 6.1. The results of Mindlin *et al.* [18] and Hashemi and Arsanjani [7] are, like the present study, calculated using the first-order shear deformation theory of Mindlin [17]. Mindlin *et al.* [18] were the first to present frequency results and has been included as a

	j	$\bar{\omega}_{j1}^{(1)}$	$\bar{\omega}_{j2}^{(1)}$	$\bar{\omega}_{j3}^{(1)}$	$\bar{\omega}_{j4}^{(1)}$	$\bar{\omega}_{j5}^{(1)}$
Present	1	0.1909	0.4562	0.8546	1.3458	1.8975
Srinivas <i>et al.</i> [28]		0.1909	0.4562	0.8549	1.3466*	1.8993
Mindlin <i>et al.</i> [18]		0.1906	0.4545	0.8493	1.3337*	1.8756
Reddy and Phan [24]		0.1908	0.4554	0.8521	1.3413	1.8916
Hashemi and Arsanjani [7]		0.1908	0.4558	0.8537	1.3436	1.8934*
Present	2		0.7009	1.0733	1.5382	2.0662
Srinivas <i>et al.</i> [28]			0.7010	1.0737	1.5393	2.0685*
Mindlin <i>et al.</i> [18]		-	0.6972	1.0652	1.5229	2.0410*
Reddy and Phan [24]			0.6990	1.0700	1.5331	2.0603
Hashemi and Arsanjani [7]			0.7002	1.0718	1.5354*	2.0616*
Present	3			1.4110	1.8397	2.3339
Srinivas <i>et al.</i> [28]				1.4119	1.8414*	2.3370*
Mindlin <i>et al.</i> [18]		-	-	1.3978	1.8189*	2.3030*
Reddy and Phan [24]				1.4063	1.8340	2.3283
Hashemi and Arsanjani [7]				1.4086*	1.8359*	2.3282*
Present	4				2.2287	2.6843
Srinivas <i>et al.</i> [28]					2.2315	2.6885*
Mindlin <i>et al.</i> [18]		-	-	-	2.2001	2.6454*
Reddy and Phan [24]					2.2230	-
Hashemi and Arsanjani [7]					2.2234*	2.6771*
Present	5					3.1005
Srinivas <i>et al.</i> [28]						3.1064
Mindlin <i>et al.</i> [18]		-	-	-	-	3.0515
Reddy and Phan [24]						-
Hashemi and Arsanjani [7]						3.0914*

Table 6.1: Natural frequencies for the first *flexural* branch of the simply-supported Mindlin plate with sides $\bar{a} = \bar{b} = 10$ and $\nu = 0.3$ (*values did not appear in publication and have been calculated).

historical benchmark. A shear correction coefficient of $\kappa = \pi^2/12$, was used in Mindlin *et al.* to obtain the tabulated natural frequencies. The results of Hashemi and Arsanjani [7] have been included as it is the only study found that considers all other combinations of

boundary conditions in addition to the plate that is simply-supported on all four of its edges. Hashemi and Arsanjani used a shear correction coefficient of $\kappa = 0.86667$ in calculating the tabulated natural frequencies. Reddy and Phan [24] used a higher-order shear deformation theory that allows for a parabolic distribution of the shear stress through the thickness of the plate and hence, does not require a shear correction coefficient.

In analyzing Table 6.1, we see that the results of the present study best match with the exact results of Srinivas *et al.* [28]. While the higher-order shear theory of Reddy and Phan [24] did improve upon the results of Mindlin *et al.* [18], it falls behind the results of the present study and Hashemi and Arsanjani [7]. Hence, use of a first-order shear theory with the proper selection of the shear correction coefficient can lead to more accurate frequency results than those of a higher-order theory. As the natural frequency increases in magnitude, each of the approximate studies deviate further from the exact value. However, this still only results in a maximum percentage difference of 0.18% for $\bar{\omega}_{55}^{(1)}$ of the present study for the first *flexural* branch.

For the second *flexural* branch, the frequencies are obtained from the term on the right in Eq. (4.40), with $\bar{\alpha}_j$ and $\bar{\mu}_n$ given by Eqs. (5.13) and (5.37), respectively. Hence,

$$\left(\frac{j\pi}{\bar{a}}\right)^2 + \left(\frac{n\pi}{\bar{b}}\right)^2 = \left(\bar{\omega}_{jn}^{(2)}\right)^2 F_2 \quad (6.3)$$

where j and n are integers identifying the vibration modes and F_2 is given in Eq. (4.36). In the above equation $\bar{\omega}_{jn}$ has been given a superscript of (2) to identify it with the second *flexural* branch.

The calculated values for the natural frequencies of this branch appear in Table 6.2 in the rows labeled as Present. Since the frequencies are again symmetric with respect to the indices j and n , only half of the figure has been populated with values. The results from Srinivas *et al.* [28] are again taken to be the exact values for the natural frequencies of this branch. The results from Mindlin *et al.* [18] do not appear in Table 6.2 because the shear correction coefficient selected in Section 4.4 for the second *flexural* branch was $\kappa = \pi^2/12$, which is the same value used by Mindlin *et al.*. With the same value used for the shear correction coefficient, the same value is calculated for the natural frequencies of this branch. Table 6.2 does not provide results from Reddy and Phan [24] either, since values were not

	j	$\bar{\omega}_{j1}^{(2)}$	$\bar{\omega}_{j2}^{(2)}$	$\bar{\omega}_{j3}^{(2)}$	$\bar{\omega}_{j4}^{(2)}$	$\bar{\omega}_{j5}^{(2)}$
Present		6.6683	6.9909	7.4822	8.0996	8.8086
Srinivas <i>et al.</i> [28]	1	6.6533	6.9542	7.4106	7.9801*	8.6277
$\kappa = 0.86667^{**}$		6.8360	7.1547	7.6412	8.2533	8.9571
Present			7.2917	7.7554	8.3450	9.0288
Srinivas <i>et al.</i> [28]	2	-	7.2339	7.6632	8.2051	8.8272*
$\kappa = 0.86667^{**}$			7.4524	7.9119	8.4968	9.1758
Present				8.1825	8.7336	9.3813
Srinivas <i>et al.</i> [28]	3	-	-	8.0562	8.5596*	9.1448*
$\kappa = 0.86667^{**}$				8.3355	8.8826	9.5259
Present					9.2423	9.8484
Srinivas <i>et al.</i> [28]	4	-	-	-	9.0199	9.5622*
$\kappa = 0.86667^{**}$					9.3879	9.9901
Present						10.4118
Srinivas <i>et al.</i> [28]	5	-	-	-	-	10.0596
$\kappa = 0.86667^{**}$						10.5501

Table 6.2: Natural frequencies for the second *flexural* branch of the simply-supported Mindlin plate with sides $\bar{a} = \bar{b} = 10$ and $\nu = 0.3$ (*values did not appear in publication and have been calculated, **shear coefficient used in Hashemi and Arsanjani [7]).

provided for the natural frequencies of the second *flexural* branch in that study.

The final set of data included in Table 6.2 is labeled as $\kappa = 0.86667$, corresponding to the shear correction coefficient used in Hashemi and Arsanjani [7]. The authors of that study did not discuss the second *flexural* branch for the simply-supported plate, but those are the natural frequencies they would have obtained. The values have been included to further illustrate numerically the improved accuracy of the frequency predictions when using branch dependent shear correction coefficients. By employing κ_1 and κ_2 as defined in Eqs. (4.88) and (4.89), respectively, the present study has led to the results that best match the exact values for both *flexural* branches. The calculated values again lose accuracy as the magnitude of the natural frequency increases with a maximum percentage difference of 3.5% for $\bar{\omega}_{55}^{(2)}$ of the present study for the second *flexural* branch.

For the *shear* branch, the frequencies are obtained from the term on the right in Eq. (4.49), with $\bar{\alpha}_j$ and $\bar{\beta}_n$ given by Eqs. (5.13) and (5.42), respectively. Hence,

$$\left(\frac{j\pi}{\bar{a}}\right)^2 + \left(\frac{n\pi}{\bar{b}}\right)^2 = S \quad (6.4)$$

where j and n are integers identifying the vibration modes and S is given in Eq. (4.46). In S , $\bar{\omega}_{jn}$ is given a superscript of (s) to identify it with the *shear* branch.

The calculated values for the natural frequencies of this branch appear in Table 6.3 in the rows labeled as Present. With this branch again using a shear correction coefficient of $\kappa = \pi^2/12$ for the present study, it gives identical values to the results of Mindlin *et al.* [18]. When employing this value of the shear correction coefficient for the *shear* branch, the

	j	$\bar{\omega}_{j1}^{(s)}$	$\bar{\omega}_{j2}^{(s)}$	$\bar{\omega}_{j3}^{(s)}$	$\bar{\omega}_{j4}^{(s)}$	$\bar{\omega}_{j5}^{(s)}$
Present		6.5024	6.5973	6.7526	6.9641	7.2270
Srinivas <i>et al.</i> [28]	1	6.5024	6.5973	6.7526	6.9641*	7.2270
$\kappa = 0.86667^{**}$		6.6715	6.7641	6.9156	7.1223	7.3796
Present			6.6909	6.8441	7.0529	7.3126
Srinivas <i>et al.</i> [28]	2	-	6.6909	6.8441	7.0529	7.3126*
$\kappa = 0.86667^{**}$			6.8554	7.0049	7.2091	7.4633
Present				6.9938	7.1983	7.4529
Srinivas <i>et al.</i> [28]	3	-	-	6.9938	7.1983*	7.4529*
$\kappa = 0.86667^{**}$				7.1513	7.3514	7.6009
Present					7.3971	7.6451
Srinivas <i>et al.</i> [28]	4	-	-	-	7.3971	7.6451*
$\kappa = 0.86667^{**}$					7.5462	7.7895
Present						7.8853
Srinivas <i>et al.</i> [28]	5	-	-	-	-	7.8853
$\kappa = 0.86667^{**}$						8.0254

Table 6.3: Natural frequencies for the *anti-symmetric shear* branch of the simply-supported Mindlin plate with sides $\bar{a} = \bar{b} = 10$ and $\nu = 0.3$ (*values did not appear in publication and have been calculated, **shear coefficient used in Hashemi and Arsanjani [7]).

calculated values for the natural frequencies also match identically with the exact values of Srinivas *et al.* [28]. As with the second *flexural* branch, Reddy and Phan [24] does not provide frequency values for the *shear* branch and Hashemi and Arsanjani [7] does not discuss this frequency branch. The rows labeled $\kappa = 0.86667$ are the frequencies Hashemi and Arsanjani would have obtained if the authors had considered the frequencies for this branch and have been included to again emphasize the improved accuracy of employing branch dependent shear correction coefficients.

The natural frequencies for the present study tabulated in Tables 6.1-6.3 correspond to the vibration modes for the Mindlin plate. The vibration modes are plotted superimposed upon the frequency branches from Eqs. (4.31), (4.36), and (4.45) in Figure 6.1. This illustrates how the frequency branches correspond to an infinite number of possible vibration modes, with the active vibration modes labeled as discrete points along the path determined

through imposition of the boundary conditions for the plate.

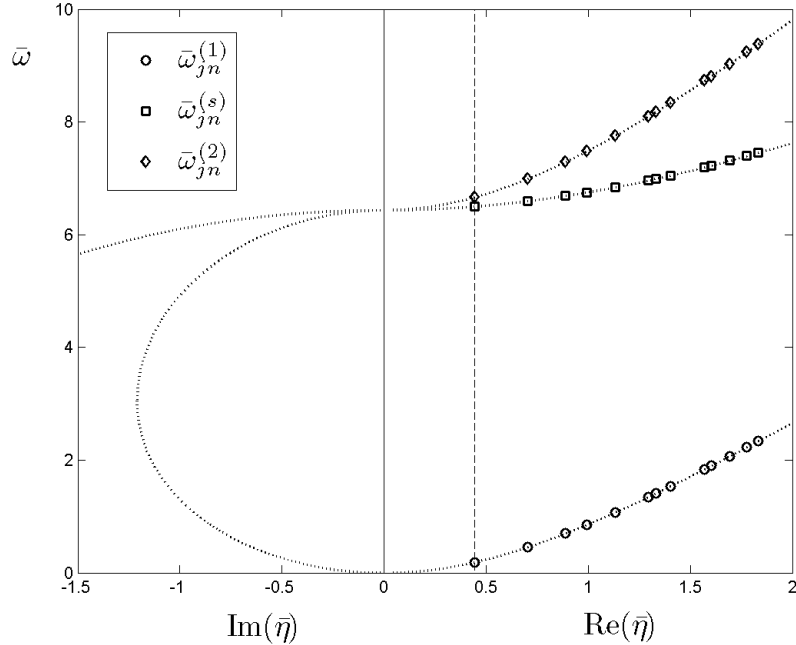


Figure 6.1: The vibration modes for the simply-supported Mindlin plate with sides $\bar{a} = \bar{b} = 10$ and $\nu = 0.3$.

Figure 6.1 also illustrates how the vibration modes for a given real valued $\bar{\eta}$ will align vertically along each of the three branches for the simply-supported plate. This is shown in the figure by a dashed vertical line for mode $j = 1$ and $n = 1$, which corresponds to $\bar{\eta} = (\sqrt{2}\pi)/10$. The line passes through the modes corresponding to the natural frequencies $\bar{\omega}_{11}^{(1)}$, $\bar{\omega}_{11}^{(s)}$, and $\bar{\omega}_{11}^{(2)}$ as it intersects with each respective frequency branch. For each of the vibration modes, only the branch which the mode lies upon is active and the mode does not interact with the other two branches. This behavior is unique to the plate simply-supported on all four of its edges. For other combinations of boundary conditions, all three branches of the frequency spectrum are active for a given mode and the interpretation of the vibration modes changes significantly.

6.1.1 Modal Plots

We now proceed to an analysis of the modal plots corresponding to the vibration modes of the simply-supported Mindlin plate tabulated in Tables 6.1-6.3. The modal functions for

the first *flexural* branch are given in Eqs. (5.33)-(5.35) and are plotted for the first mode, $j = 1$ and $n = 1$, in Figure 6.2. The modal functions for the second *flexural* branch are given in Eqs. (5.38)-(5.40) and are plotted for the first mode in Figure 6.3. The modal functions for the *shear* branch are given in Eqs. (5.43)-(5.45) and are plotted for the first mode in Figure 6.4. All of the modal plots presented are scaled by their maximum value in order to compare the distribution of the functions over the span of the plate for a given mode.

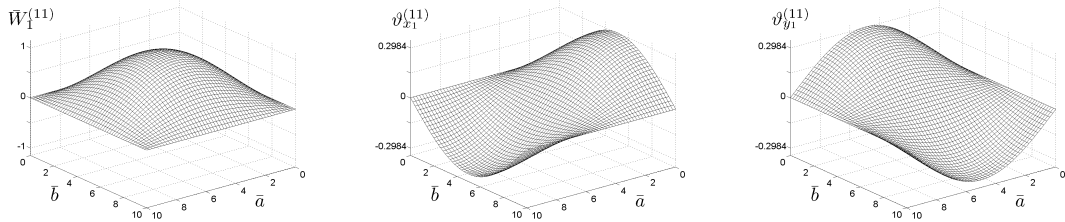


Figure 6.2: The modal functions for the first vibration mode of the first *flexural* branch for the simply-supported Mindlin plate with sides $\bar{a} = \bar{b} = 10$ and $\nu = 0.3$.

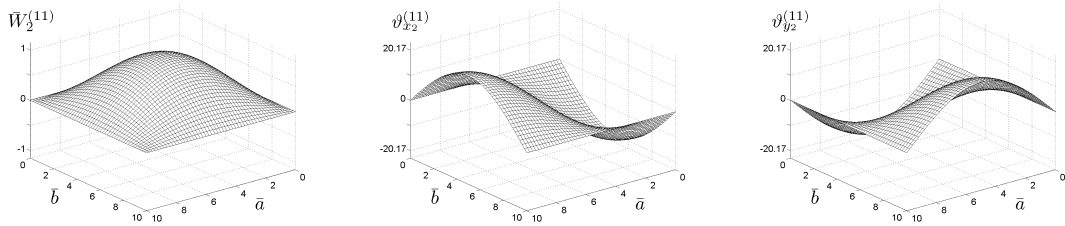


Figure 6.3: The modal functions for the first vibration mode of the second *flexural* branch for the simply-supported Mindlin plate with sides $\bar{a} = \bar{b} = 10$ and $\nu = 0.3$.

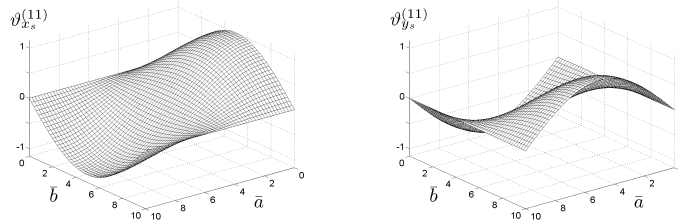


Figure 6.4: The modal functions for the first vibration mode of the *anti-symmetric shear* branch for the simply-supported Mindlin plate with sides $\bar{a} = \bar{b} = 10$ and $\nu = 0.3$.

The modal displacements for the first and second *flexural* branches are seen to be of the same shape, since they are given by the same function for a given modal index. The

differences in behavior between the branches is identified through the modal bending rotation. From Figures 6.2 and 6.3, we find that the bending rotations for these branches have opposite sign and vastly differ in magnitude. To better understand this discrepancy, it is also instructive to examine the distribution of the shear angle over the span of the Mindlin plate. To do this, we first define the modal shear angles in the \bar{x} and \bar{y} -directions as $\Gamma_x^{(jn)}$ and $\Gamma_y^{(jn)}$, respectively. In accordance with Eqs. (2.10) and (2.11) for the transverse shear angle we obtain the modal shear angles as

$$\Gamma_x^{(jn)} = \frac{\partial \bar{W}^{(jn)}}{\partial \bar{x}} - \vartheta_x^{(jn)} \quad (6.5)$$

and

$$\Gamma_y^{(jn)} = \frac{\partial \bar{W}^{(jn)}}{\partial \bar{y}} - \vartheta_y^{(jn)} \quad (6.6)$$

Substitution of the modal functions into Eqs. (6.5) and (6.6) for a given mode yields the function for the shear angle of that mode.

The modal shear angles for the first and second *flexural* branches are plotted in Figures 6.5 and 6.6, respectively. Comparison of the modal shear angles with the modal bending rotations shows the full picture of how the deformation mechanisms for the first and second *flexural* branches manifest themselves and yet result in the same shape for the modal displacement. For the first branch, the shear angle and bending rotation act in the same direction and combine together to form the total angle change of the plate. For the second branch, the shear angle and bending rotation act in opposite directions and compete with each other. The shear angle has a larger magnitude and hence determines the direction of the overall angle change.

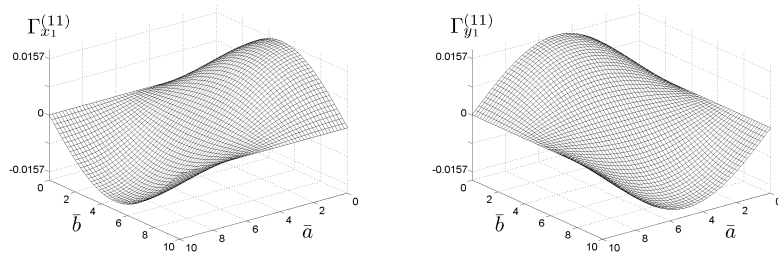


Figure 6.5: The modal shear angles for the first vibration mode of the first *flexural* branch for the simply-supported Mindlin plate with sides $\bar{a} = \bar{b} = 10$ and $\nu = 0.3$.

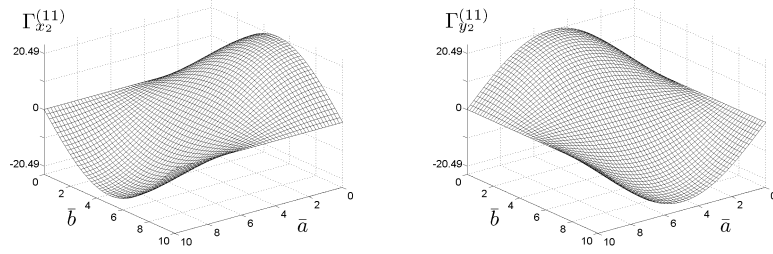


Figure 6.6: The modal shear angles for the first vibration mode of the second *flexural* branch for the simply-supported Mindlin plate with sides $\bar{a} = \bar{b} = 10$ and $\nu = 0.3$.

For the *shear* branch in Figure 6.4, the distribution for the modal bending rotations is given, although for this branch the modal displacement vanishes. In taking into account the modal shear angles given in Eqs. (6.5) and (6.6), we see that for this branch the bending rotation must act in the opposite direction of the shear angle with equal magnitude. As a result the bending rotation will cancel out the effects of the shear angle deformation and the displacement of the plate is zero.

In concluding the discussion of the modal plots for the simply-supported Mindlin plate, the modal displacements for several other vibration modes are displayed in Figure 6.7. All of the displacement modes shown are for the first *flexural* branch, although we have previously established these will also be the shapes for the second *flexural* branch as well. It is evident from the figure, as well as from inspection of the modal functions, that the indices of the vibration mode determine the number of half-sine waves appearing in the modal displacement distribution. For example, vibration mode $j = 2$ and $n = 3$ has two half-sine waves in the \bar{x} -direction and three half sine waves in the \bar{y} -direction.

The modal bending rotations in the \bar{x} and \bar{y} -directions of the first *flexural* branch are displayed in Figures 6.8 and 6.9, respectively. The modal bending rotations for the other two branches have been omitted for brevity. The physical interpretation of the relationship between the modal displacements, bending rotations, and shear angles is the same for these vibration modes as it was for the lowest vibration mode discussed in detail earlier. In the next section, we proceed to an analysis of the numerical simulations for the Mindlin plate with clamped edges in the \bar{y} -direction.

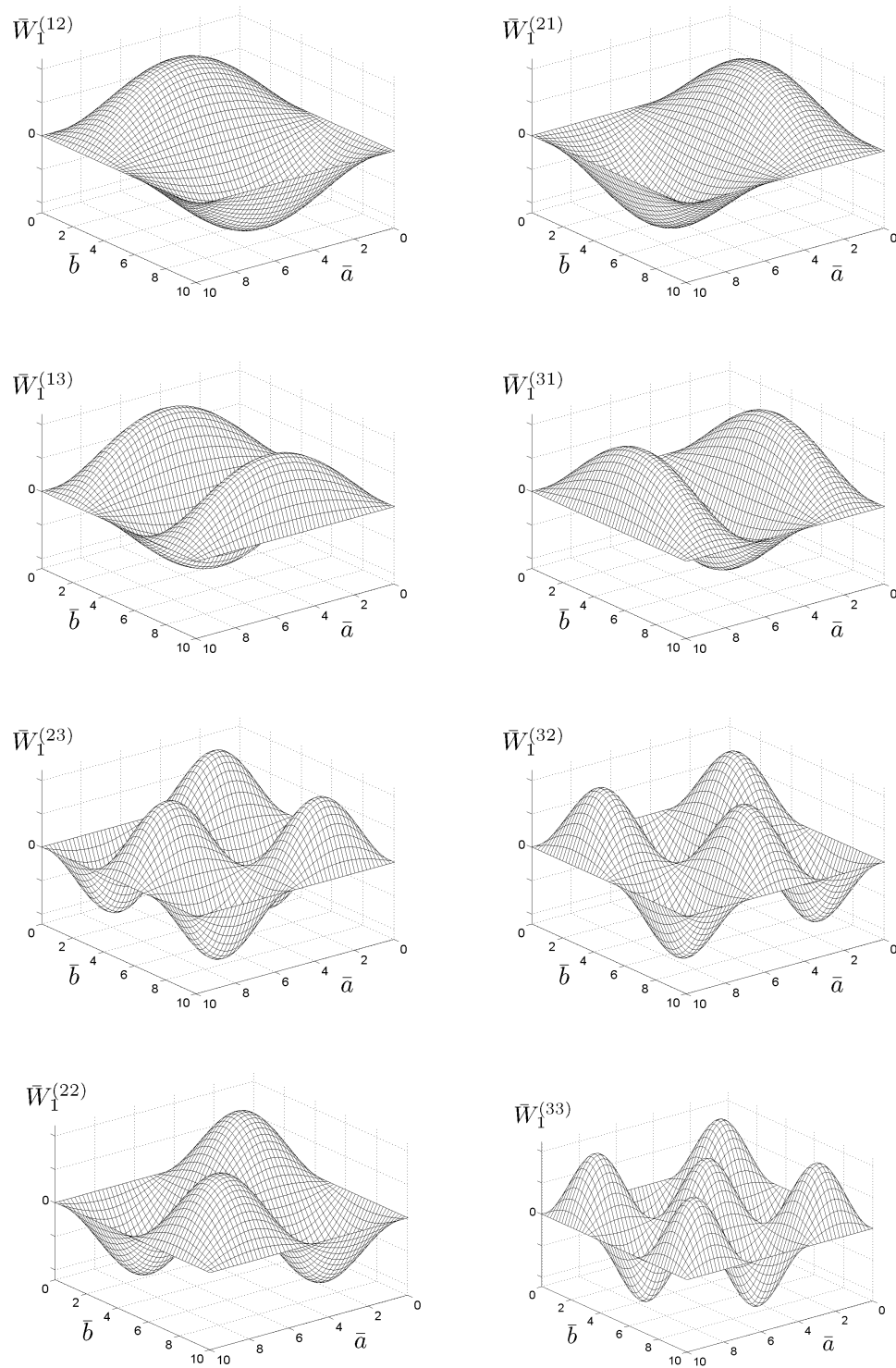


Figure 6.7: The modal displacements for several representative vibration modes of the first *flexural* branch for the simply-supported Mindlin plate with sides $\bar{a} = \bar{b} = 10$ and $\nu = 0.3$.

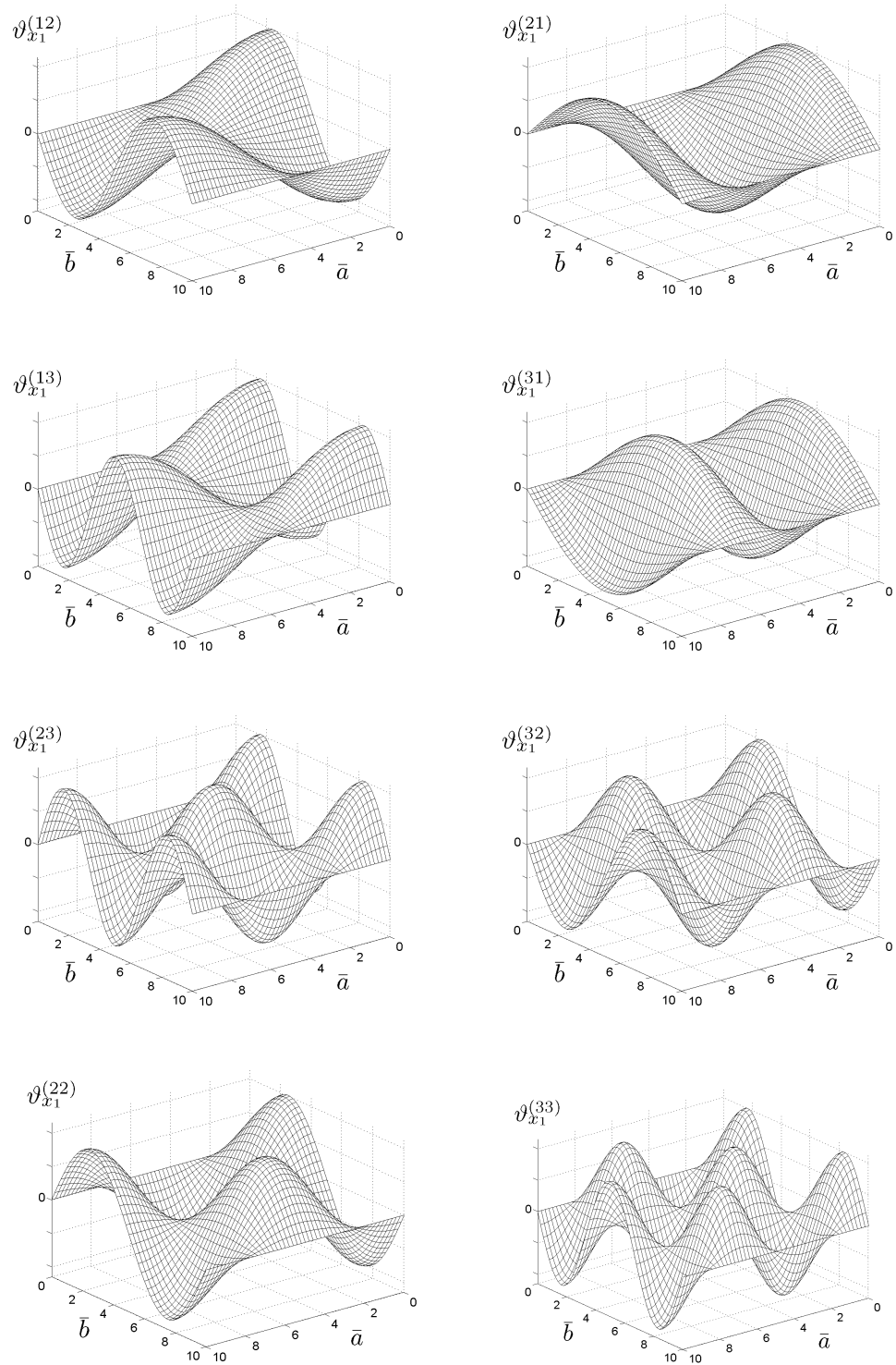


Figure 6.8: The modal bending rotations in the \bar{x} -direction for several representative vibration modes of the first *flexural* branch for the simply-supported Mindlin plate with sides $\bar{a} = \bar{b} = 10$ and $\nu = 0.3$.

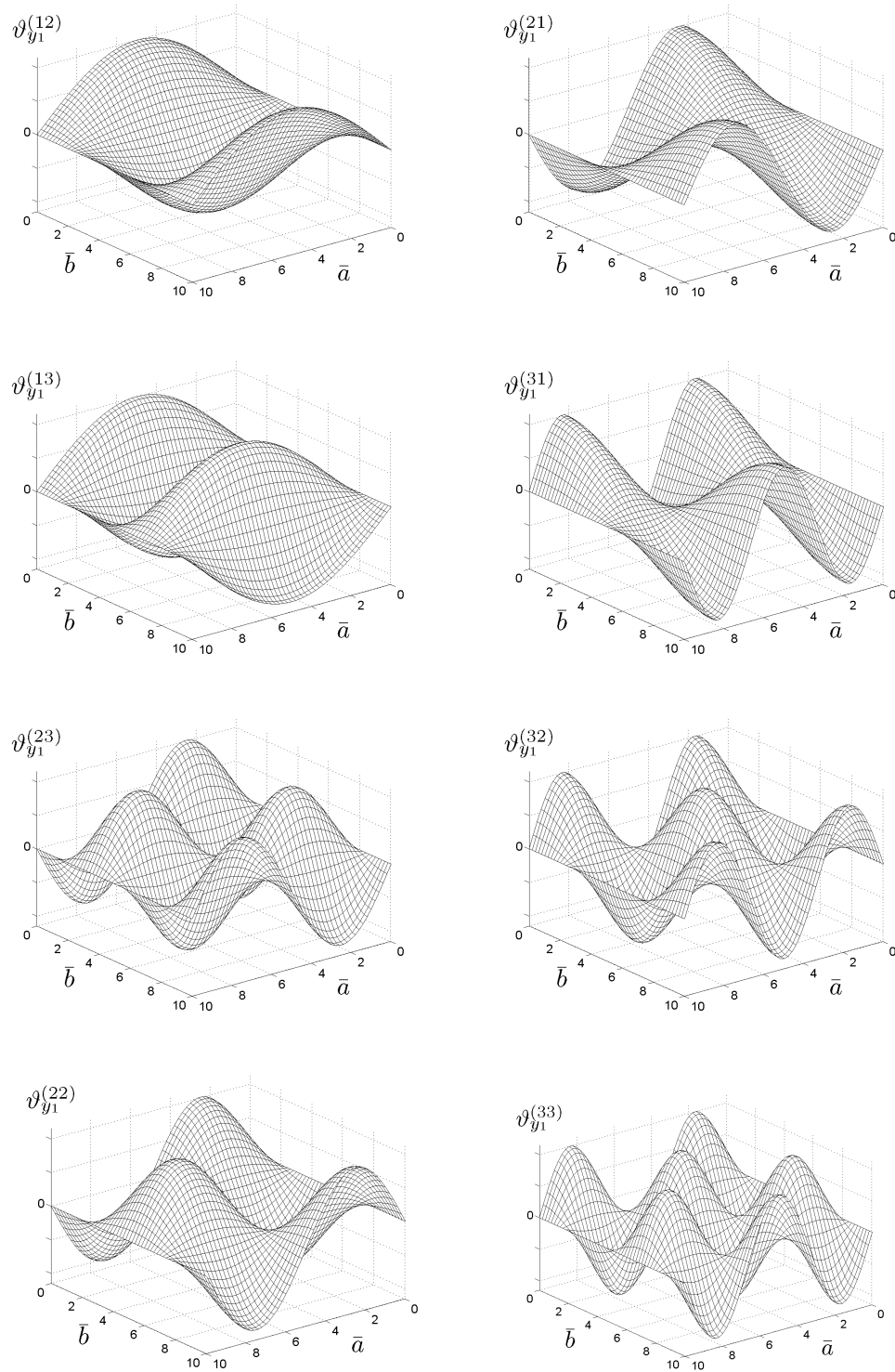


Figure 6.9: The modal bending rotations in the \bar{y} -direction for several representative vibration modes of the first *flexural* branch for the simply-supported Mindlin plate with sides $\bar{a} = \bar{b} = 10$ and $\nu = 0.3$.

6.2 Clamped Boundary Conditions in the \bar{y} -direction

We begin with a detailed explanation of the process of solving for the natural frequencies for the simply-supported/clamped Mindlin plate. The process is different when compared to the plate that is simply-supported on all four of its edges, as all three branches of the frequency spectrum governing the free vibration of the plate must be active for a given vibration mode when considering mixed boundary conditions. In order to obtain the natural frequencies, we must numerically solve for the roots of the frequency equation given by Eq. (5.65). For a given natural frequency there will be a unique combination of three wave numbers in the \bar{y} -direction to pair with $\bar{\alpha}_j$ in the \bar{x} -direction. We seek solutions where the wave numbers associated with the \bar{y} -direction are given by Eqs. (5.67)-(5.69).

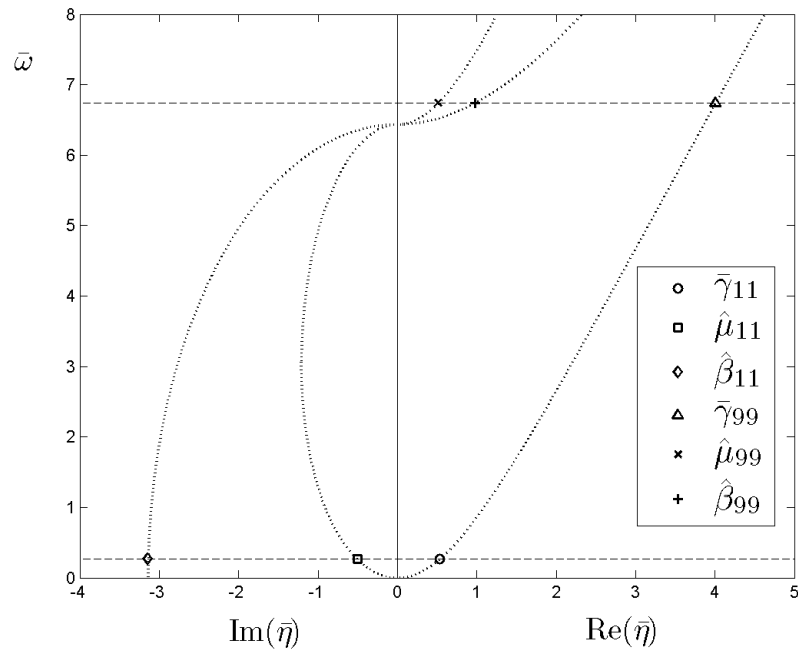


Figure 6.10: Modal wave number combinations for the simply-supported/clamped Mindlin plate with sides $\bar{a} = \bar{b} = 10$ and $\nu = 0.3$.

The process of solving for the natural frequencies and modal wave number pairings is further explained graphically by Figure 6.10. A natural frequency that satisfies Eq. (5.65) is found when a specific combination of the wave numbers $\bar{\gamma}_{jn}$, $\hat{\mu}_{jn}$, and $\hat{\beta}_{jn}$ form horizontally aligned intersection points on each of the three branches. The intersection point with one of

the branches represents its contribution to that vibration mode. The solution combination for the lowest mode is labeled in Figure 6.10. Each of the wave numbers in the \bar{y} -direction interact with $\bar{\alpha}_1 = \pi/\bar{a}$ to calculate real or imaginary values of $\bar{\eta}$, such that a point intersects with each of the three branches in horizontal alignment. The dashed line through the points for mode $j = 1$ and $n = 1$ corresponds to the magnitude of $\bar{\omega}_{11}$.

Figure 6.10 also includes the wave number combinations for mode $j = 9$ and $n = 9$, used to determine the magnitude of $\bar{\omega}_{99}$. This is the lowest natural frequency for which the frequency value surpasses the “cut-off” frequency (the frequency at which $\bar{\eta}$ transitions from imaginary to real valued) for the *shear* and second *flexural* branches. In this case, the wave numbers associated with these branches are still related to $\bar{\alpha}_j$ by Eqs. (5.68) and (5.69). They are however, now governed by the term on the left in Eqs. (4.40) and (4.49) rather than by Eqs. (4.39) and (4.48).

If we continued to solve for increasing values of $\bar{\omega}_{jn}$, there will reach a magnitude of $\bar{\omega}_{jn}$ for which $i\hat{\mu}_{jn} \rightarrow \bar{\mu}_{jn}$ and also a magnitude for which $i\hat{\beta}_{jn} \rightarrow \bar{\beta}_{jn}$. When this occurs, Eq. (5.70) replaces Eq. (5.68) and/or Eq. (5.71) replaces Eq. (5.69), respectively as the wave number combinations used for solving the frequency equation. The geometry and material properties considered herein for the simply-supported/clamped Mindlin plate will not result in solutions for which $\bar{\gamma}_{jn} \rightarrow i\hat{\gamma}_{jn}$, and Eq. (5.72) is not needed. For other geometries and material properties the solution may exist, so it should be considered when solving for the natural frequencies in those cases.

The calculated values for the natural frequencies of the simply-supported/clamped Mindlin plate are tabulated in Table 6.4. Unlike for simply-supported boundary conditions, the frequencies are no longer symmetric with respect to the indices j and n so the entire figure has been populated with frequency values. The frequencies calculated by Hashemi and Arsanjani [7], using a shear correction coefficient of $\kappa = 0.86667$ are tabulated in Table 6.5. An exact analysis for the simply-supported/clamped Mindlin plate does not exist in the literature for comparison. It is believed that Hashemi and Arsanjani was the first to consider all possible boundary conditions for the Mindlin plate in closed analytical form.

In comparing Tables 6.4 and 6.5, it is evident that the calculated natural frequencies in the present study are very close to the values found by Hashemi and Arsanjani. The

j	$\bar{\omega}_{j1}$	$\bar{\omega}_{j2}$	$\bar{\omega}_{j3}$	$\bar{\omega}_{j4}$	$\bar{\omega}_{j5}$
1	0.2673	0.5947	1.0203	1.5126	2.0501
2	0.4928	0.7923	1.1977	1.6727	2.1950
3	0.8730	1.1279	1.4953	1.9386	2.4342
4	1.3558	1.5707	1.8944	2.2979	2.7585
5	1.9032	2.0860	2.3693	2.7316	3.1541

Table 6.4: Natural frequencies for the present study of the simply-supported/clamped Mindlin plate with sides $\bar{a} = \bar{b} = 10$ and $\nu = 0.3$.

j	$\bar{\omega}_{j1}$	$\bar{\omega}_{j2}$	$\bar{\omega}_{j3}$	$\bar{\omega}_{j4}$	$\bar{\omega}_{j5}$
1	0.2674	0.5948	1.0202	1.5118*	2.0482*
2	0.4926	0.7920	1.1970	1.6713*	2.1923*
3	0.8721	1.1268	1.4935*	1.9359*	2.4301*
4	1.3536	1.5681*	1.8912*	2.2935*	2.7527*
5	1.8992*	2.0815*	2.3640*	2.7252*	3.1461*

Table 6.5: Natural frequencies from Hashemi and Arsanjani [7] for the simply-supported/clamped Mindlin plate with sides $\bar{a} = \bar{b} = 10$ and $\nu = 0.3$ (*values did not appear in publication and have been calculated).

results between these studies match much more closely than did the frequencies for the *shear* and second *flexural* branches of the simply-supported plate. Hence, even when all three branches of the frequency spectrum are required to be active simultaneously, the accuracy of the frequency prediction is largely determined for these cases by the accuracy of the first *flexural* branch of the spectrum. As the frequency increases in magnitude, there is an increase in the difference between the calculated frequency between the two studies, but even up to the mode $j = 10$ and $n = 10$ the percentage difference is under 0.5%. Though an exact study is not available in the literature for comparison for these boundary conditions, it is assumed that the present study results in slightly more accurate frequency results due to its increased accuracy for the simply-supported plate.

Since all frequency branches for these boundary conditions must be active for a given mode, the frequency spectrum cannot be plotted as a function of $\bar{\eta}$ as it was for the simply-supported case. Hence, we postulate plotting the frequency spectrum as a function of the wave number in the \bar{x} -direction, $\bar{\alpha}_j$. The suggested frequency spectrum is displayed in Figure 6.11 using the values tabulated in Table 6.4. Here we are able to clearly identify the natural frequencies in a way that cannot be represented on a plot of the branches of the

frequency spectrum due to the interaction of the branches in forming a vibration mode.

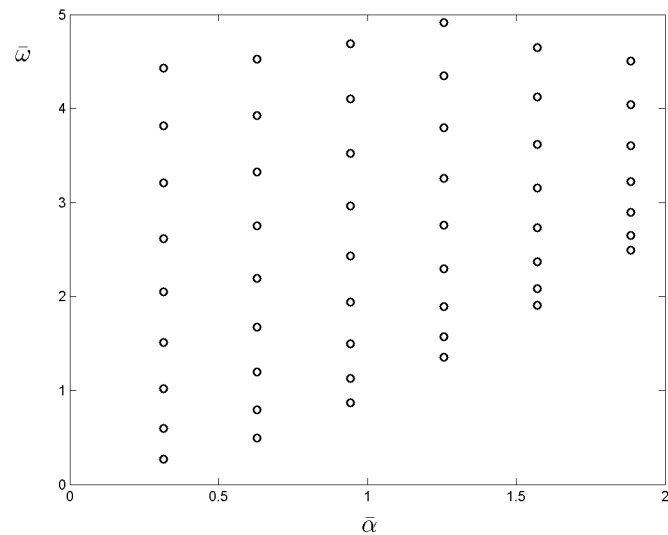


Figure 6.11: Frequency spectrum for the simply-supported/clamped Mindlin plate with sides $\bar{a} = \bar{b} = 10$ and $\nu = 0.3$.

6.2.1 Modal Plots

We proceed to an analysis of the modal functions for the simply-supported/clamped Mindlin plate. To obtain the modal functions for a given mode, the natural frequency and the corresponding wave number pairs found from the roots of Eq. (5.65) are substituted into Eqs. (5.75)-(5.77).

The modal displacement and bending rotations corresponding to the mode $j = 1$ and $n = 1$ appear in Figure 6.12. For this mode, we note that a single half-sine wave is formed in the \bar{x} -direction of the modal displacement plot, since this is specified by the parameter j in $\bar{\alpha}_j$. The displacement in the \bar{y} -direction also retains the appearance of a single half-sine wave but it is not a true half-sine wave due to the interaction of the three wave numbers in this direction.

Even though Eqs. (5.75) and (5.76) for the modal displacement and the modal bending rotation in the \bar{x} -direction, respectively, are more complex for the clamped case as compared to those for the simply-supported case, their plots in Figure 6.12 appear very similar to the corresponding plots in Figure 6.2. This is due to the fact that the boundary conditions

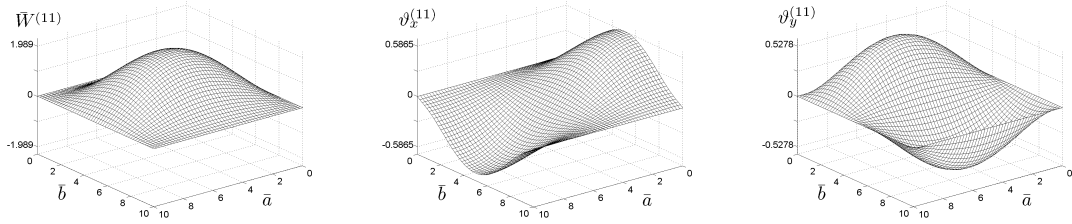


Figure 6.12: The modal functions for the first vibration mode of the simply-supported/clamped Mindlin plate with sides $\bar{a} = \bar{b} = 10$ and $\nu = 0.3$.

imposed on those two functions specifically have not changed as the simply-supported edges were replaced with clamped edges. The distribution of the modal bending rotation in the \bar{y} -direction has changed shape, since with clamped edges the function must now vanish on all four edges.

The modal shear angles for clamped boundaries in the \bar{y} -direction are obtained through substitution of the modal displacement and bending rotation functions given in Eqs. (5.75)-(5.77) into Eqs. (6.5) and (6.6). Figure 6.13 gives the distribution of the modal shear angles for mode $j = 1$ and $n = 1$. The modal shear angle in the \bar{x} -direction, $\Gamma_x^{(11)}$, exhibits a more complex distribution than it did for the case of the fully simply-supported plate. We now see increased shear behavior near the boundaries $\bar{y} = 0$ and $\bar{y} = \bar{b}$ where the clamped edges have replaced the simply-supported edges.

We also compare the modal bending rotation in the \bar{y} -direction, $\vartheta_y^{(11)}$, and the modal shear angle in that direction, $\Gamma_y^{(11)}$. The bending rotation is seen to be zero on all edges of the plate as simply-supported edges do not allow for tangential bending rotation and clamped edges do not allow for normal bending rotation. The shear angle is also zero over the edges $\bar{x} = 0$ and $\bar{x} = \bar{a}$ as there cannot be an angle change due to shear in the tangential direction of a simply-supported edge. Along the edges $\bar{y} = 0$ and $\bar{y} = \bar{b}$ we see that the shear angle remains non-zero on these edges. While clamped boundaries resist normal bending rotations, they do not provide resistance to normal shear rotation. Hence, a plate theory that does not account for the effects of transverse shear deformation would yield different results near an edge of this type. In general, the effects of including transverse shear deformation will have the most influence near the boundaries of the plate.

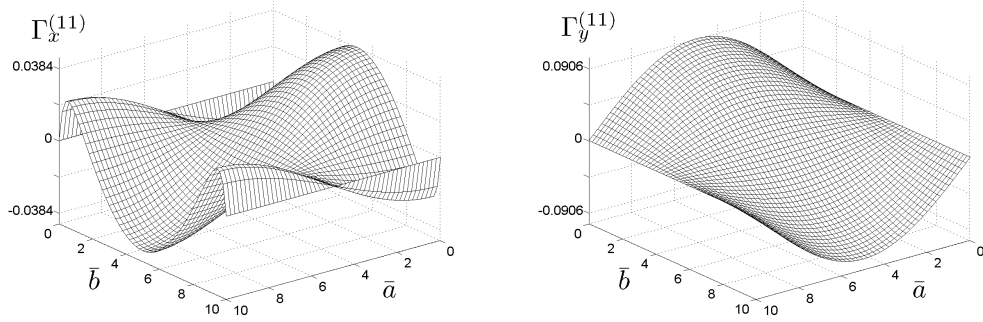


Figure 6.13: The modal shear angles for the first vibration mode of the simply-supported/clamped Mindlin plate with sides $\bar{a} = \bar{b} = 10$ and $\nu = 0.3$.

The modal plots for various other vibration modes given in Figure 6.4 for the simply-supported/clamped Mindlin plate follow, with the modal displacements in Figure 6.14, the modal bending rotations in the \bar{x} -direction in Figure 6.15, and the modal bending rotations in the \bar{y} -direction in Figure 6.16. The modal displacements and the modal bending rotations in the \bar{x} -direction again show similar behavior to their counterparts for the fully simply-supported case. The distribution of the modal bending rotations in the \bar{y} -direction is different in order to satisfy the new condition of zero normal rotation on the clamped edges in the \bar{y} -direction.

Substitution of any of the natural frequency and wave number pairs found from the roots of Eq. (5.65) into the modal functions given in Eqs. (5.75)-(5.77) will give the modal plots for that vibration mode of the simply-supported/clamped Mindlin plate. However, additional plots have been omitted for brevity. In the next section, we consider the Mindlin plate with free boundaries in the \bar{y} -direction.

6.3 Free Boundary Conditions in the \bar{y} -direction

For the simply-supported/free Mindlin plate, all three of the frequency branches must be active for a given vibration mode when solving for the natural frequencies. The natural frequencies are calculated by numerically solving for the roots of Eq. (5.104) in the same manner as was described for the plate with clamped edges in the \bar{y} -direction. As for those boundary conditions, for a given natural frequency there is a unique combination of the

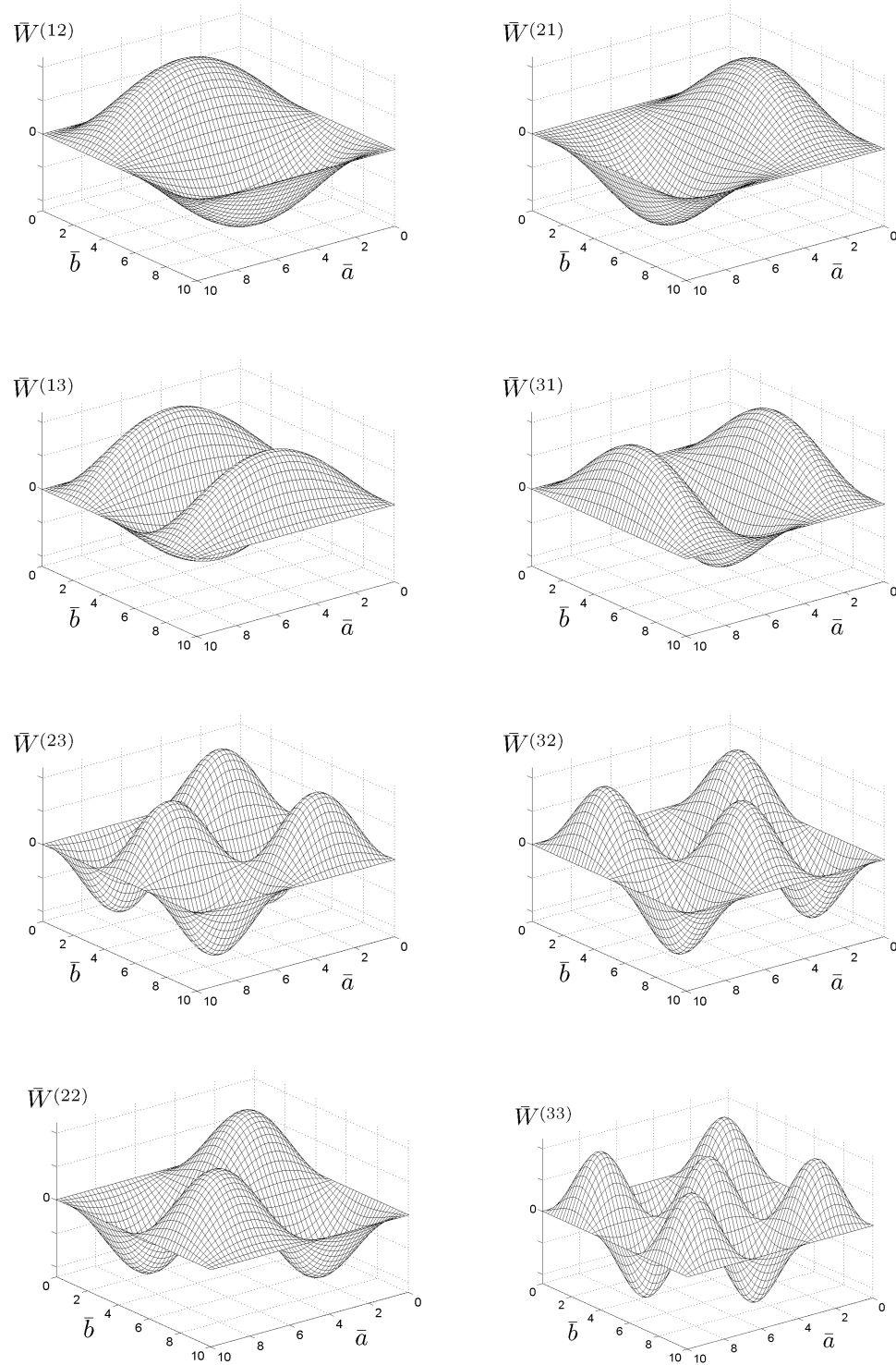


Figure 6.14: The modal displacements for several representative vibration modes of the simply-supported/clamped Mindlin plate with sides $\bar{a} = \bar{b} = 10$ and $\nu = 0.3$.

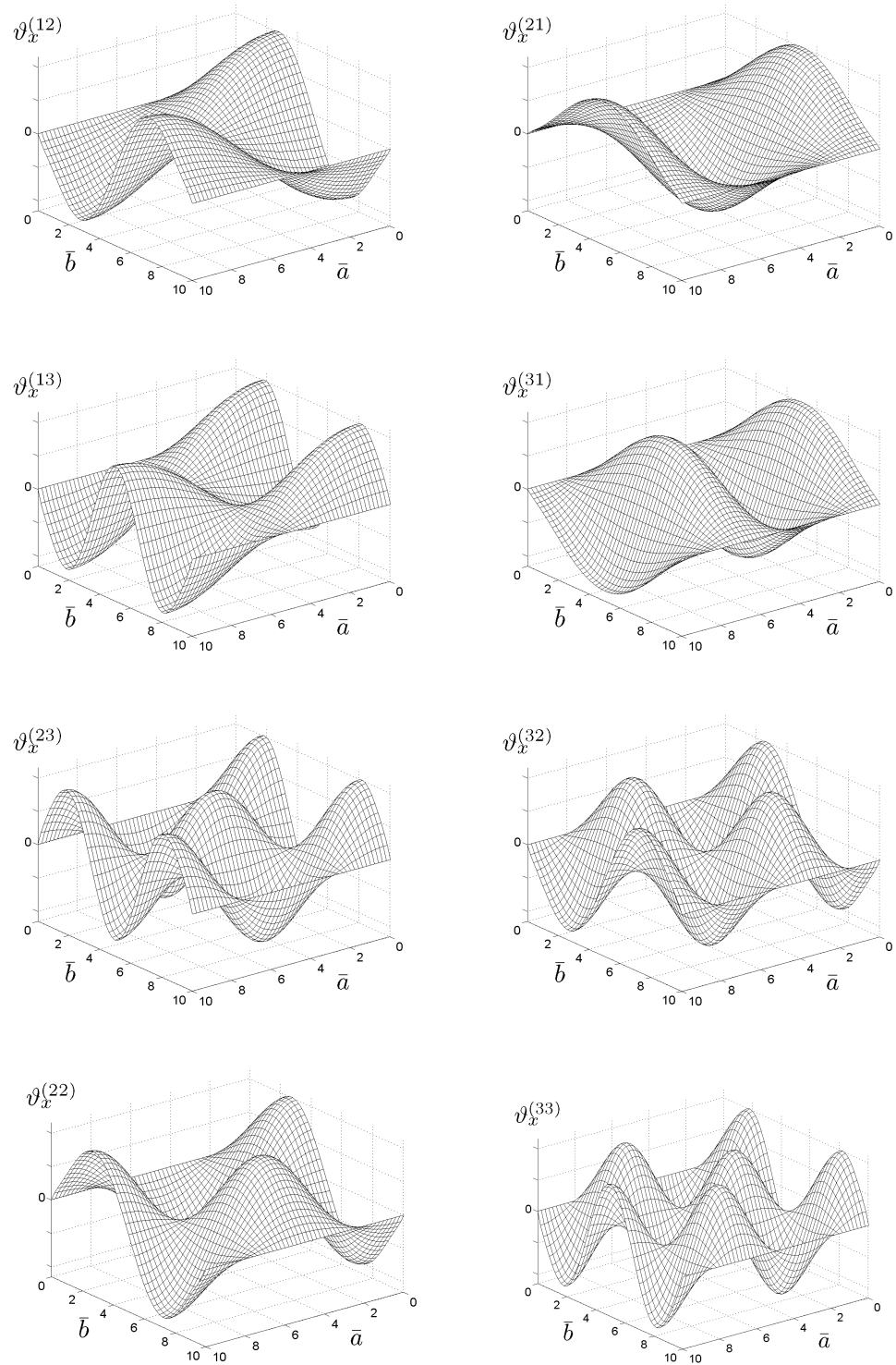


Figure 6.15: The modal bending rotations in the \bar{x} -direction for several representative vibration modes of the simply-supported/clamped Mindlin plate with sides $\bar{a} = \bar{b} = 10$ and $\nu = 0.3$.

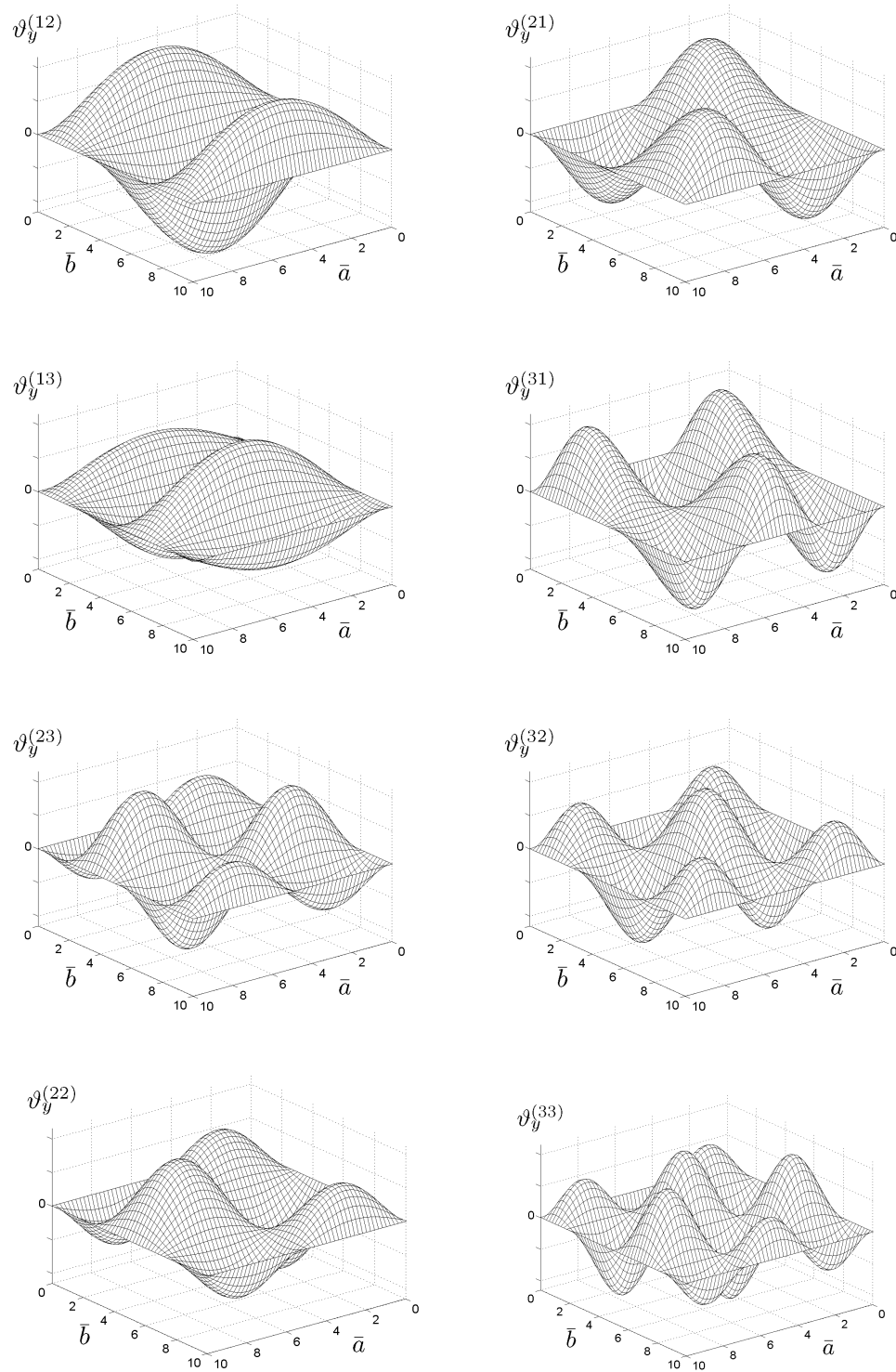


Figure 6.16: The modal bending rotations in the \bar{y} -direction for several representative vibration modes of the simply-supported/clamped Mindlin plate with sides $\bar{a} = \bar{b} = 10$ and $\nu = 0.3$.

three wave numbers in the \bar{y} -direction to pair with $\bar{\alpha}_j$ in the \bar{x} -direction.

A graphical depiction of the wave number combination for the lowest vibration mode, $\bar{\omega}_{jn}$, is shown in Figure 6.17 superimposed upon the frequency branches for the Mindlin plate. For free boundary conditions, a solution exists such that $\bar{\gamma}_{jn} \rightarrow i\hat{\gamma}_{jn}$ for low values of the modal index n . Hence, in solving for $\bar{\omega}_{11}$, Eq. (5.72) is used to relate $\hat{\gamma}_{11}$ to $\bar{\alpha}_1$ and $\bar{\omega}_{11}$. The combination of wave numbers leading to the next highest natural frequency, $\bar{\omega}_{12}$,

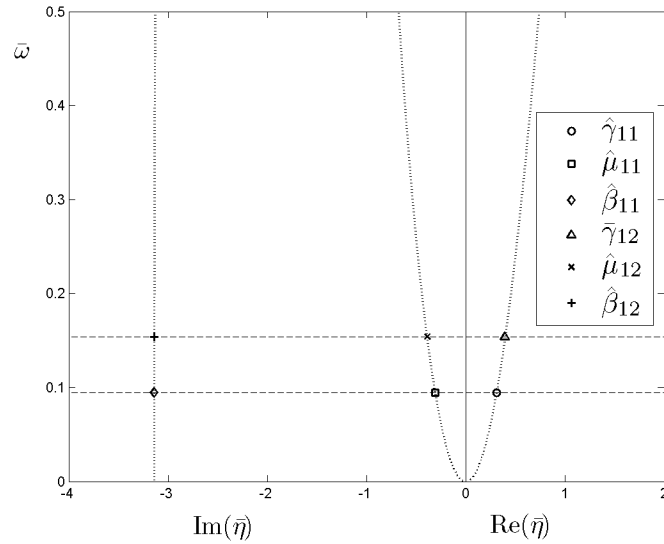


Figure 6.17: Modal wave number combinations for the simply-supported/free Mindlin plate with sides $\bar{a} = \bar{b} = 10$ and $\nu = 0.3$.

is also shown in Figure 6.17. This is the lowest frequency for $j = 1$ in which the solution moves to $\bar{\gamma}_{jn}$ and the natural frequency-wave number relation is again given by Eq. (5.67). For a given modal index j , we must check for solutions for which $\bar{\gamma}_{jn} \rightarrow i\hat{\gamma}_{jn}$ for the lowest modal indices of n when considering this combination of boundary conditions.

As for the case of clamped edges, if we continued to solve for increasing values of $\bar{\omega}_{jn}$, there will reach a magnitude of $\bar{\omega}_{jn}$ for which $i\hat{\mu}_{jn} \rightarrow \bar{\mu}_{jn}$ and also a magnitude for which $i\hat{\beta}_{jn} \rightarrow \bar{\beta}_{jn}$. When this occurs, Eq. (5.70) replaces Eq. (5.68) and/or Eq. (5.71) replaces Eq. (5.69), respectively as the wave number combinations used for solving the frequency equation.

The calculated values for the natural frequencies of the simply-supported/free Mindlin plate are tabulated in Table 6.6. In a manner similar to that for the simply-supported/

clamped boundary conditions, the frequencies are no longer symmetric with respect to the indices j and n so the entire figure has been populated with frequency values. The frequencies calculated from the solutions for which $\bar{\gamma}_{jn} \rightarrow i\hat{\gamma}_{jn}$ have been denoted in Table 6.6 by an asterisk.

The frequencies calculated by Hashemi and Arsanjani [7], using a shear correction coefficient of $\kappa = 0.86667$ are tabulated in Table 6.7. As with clamped boundaries, an exact analysis for the simply-supported/free Mindlin plate does not exist in the literature for comparison. In comparing Tables 6.6 and 6.7, it is again evident that the calculated natural frequencies in the present study are very close to the values found by Hashemi and Arsanjani for free boundaries. It is seen that, as the frequency increases in magnitude, there is an increase in the difference between the calculated frequency between the two studies, but now the percentage difference is under 0.4% up to the mode $j = 10$ and $n = 10$. Though an exact study is not available in the literature for comparison for these boundary conditions, it is again assumed that the present study results in slightly more accurate frequency values due to its increased accuracy for the simply-supported plate.

j	$\bar{\omega}_{j1}$	$\bar{\omega}_{j2}$	$\bar{\omega}_{j3}$	$\bar{\omega}_{j4}$	$\bar{\omega}_{j5}$
1	0.0945*	0.1540	0.3392	0.6643	1.1064
2	0.3644*	0.4289	0.6234	0.9304	1.3394
3	0.7697*	0.8277	1.0154	1.3048	1.6824
4	1.2679*	1.3171	1.4898	1.7568	2.1042
5	1.8256*	1.8666	2.0227	2.2654	2.5831

Table 6.6: Natural frequencies for the present study of the simply-supported/free Mindlin plate with sides $\bar{a} = \bar{b} = 10$ and $\nu = 0.3$ (*correspond to solutions for which $\bar{\gamma}_{jn} \rightarrow i\hat{\gamma}_{jn}$).

j	$\bar{\omega}_{j1}$	$\bar{\omega}_{j2}$	$\bar{\omega}_{j3}$	$\bar{\omega}_{j4}$	$\bar{\omega}_{j5}$
1	0.0945	0.1541	0.3392	0.6637	1.1047*
2	0.3642	0.4289	0.6233	0.9297*	1.3374*
3	0.7690	0.8272	1.0147*	1.3035*	1.6799*
4	1.2662*	1.3157*	1.4880*	1.7543*	2.1005*
5	1.8224*	1.8638*	2.0194*	2.2613*	2.5778*

Table 6.7: Natural frequencies from Hashemi and Arsanjani [7] for the simply-supported/free Mindlin plate with sides $\bar{a} = \bar{b} = 10$ and $\nu = 0.3$ (*values did not appear in publication and have been calculated).

As for the case of clamped boundaries, the frequency spectrum cannot be plotted as a function of $\bar{\eta}$ due to the interaction of the frequency branches in forming a vibration mode for these boundary conditions. The frequency spectrum is plotted as a function of the wave number in the \bar{x} -direction, $\bar{\alpha}_j$, in Figure 6.18 using the values tabulated in Table 6.6. Here we are able to clearly identify the natural frequencies that cannot be represented on a plot of the branches of the frequency spectrum due to the requirement that all branches are active for a given vibration mode. For a given value of $\bar{\alpha}_j$, the two lowest natural frequencies are very close in value as the solution changes from employing $\hat{\gamma}_{jn}$ to employing $\bar{\gamma}_{jn}$.

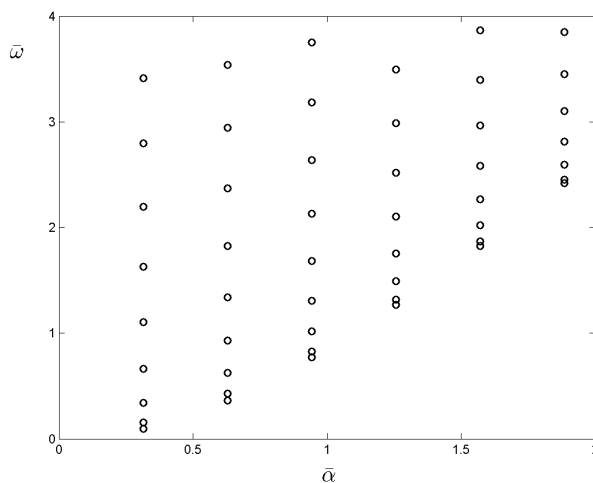


Figure 6.18: Frequency spectrum for the simply-supported/free Mindlin plate with sides $\bar{a} = \bar{b} = 10$ and $\nu = 0.3$.

6.3.1 Modal Plots

We proceed to an analysis of the modal functions for the simply-supported/free Mindlin plate. To obtain the modal functions for a given mode, the natural frequency and the corresponding wave number pairs found from the roots of Eq. (5.104) are substituted into Eqs. (5.109)-(5.111).

The modal displacement and bending rotations corresponding to the mode $j = 1$ and $n = 1$ appear in Figure 6.19. For this mode, we note that a single half-sine wave is formed in the \bar{x} -direction of the modal displacement plot, since this is specified by the parameter j in $\bar{\alpha}_j$. This has not changed for any of the cases considered, as the boundaries in the

\bar{x} -direction are simply-supported for all three cases. The displacement in the \bar{y} -direction no longer retains the appearance of a single half-sine wave for the mode $j = 1$ and $n = 1$ with free boundaries. The modal displacement has a slight bend in the \bar{y} -direction, but

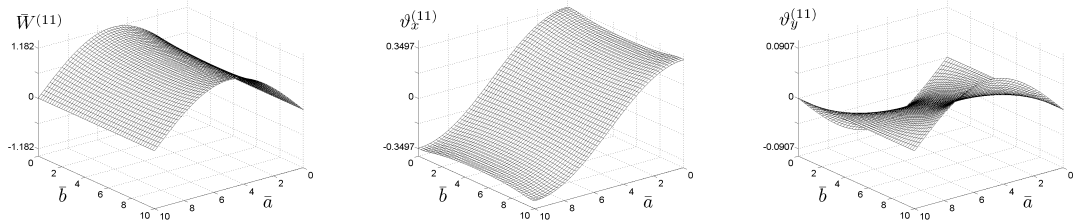


Figure 6.19: The modal functions for the first vibration mode of the simply-supported/free Mindlin plate with sides $\bar{a} = \bar{b} = 10$ and $\nu = 0.3$.

more closely resembles a zeroth mode in this direction. For consistency with the other boundary conditions considered, we shall leave the mode indexed as $j = 1$ and $n = 1$ but it would more appropriately be labeled as mode $j = 1$ and $n = 0$ corresponding to a natural frequency labeled $\bar{\omega}_{10}$.

As with the other boundary conditions, the modal bending rotations are better understood in conjunction with the modal shear angles which are obtained through substitution of the modal displacement and bending rotation functions for free boundaries in the \bar{y} -direction given in Eqs. (5.109)-(5.111) into Eqs. (6.5) and (6.6). Figure 6.20 gives the distribution of the modal shear angles for mode $j = 1$ and $n = 1$. Here, we again see the most significant

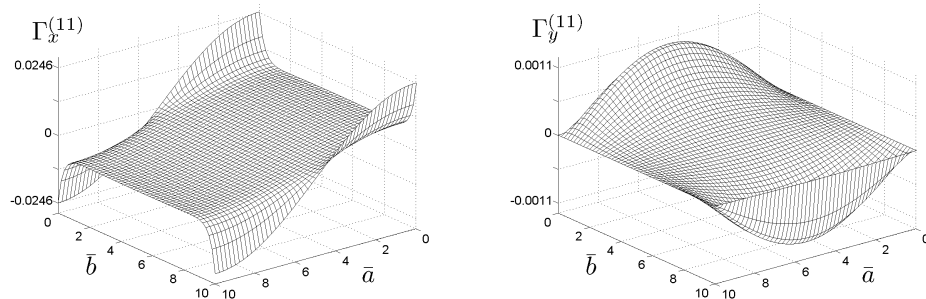


Figure 6.20: The modal shear angles for the first vibration mode of the simply-supported/free Mindlin plate with sides $\bar{a} = \bar{b} = 10$ and $\nu = 0.3$.

contributions of the shear angle in the vicinity of the bounding edges. The modal shear angle in the \bar{x} -direction, $\Gamma_x^{(11)}$, is zero over most of the span and then takes on a non-zero

value near the free edges at $\bar{y} = 0$ and $\bar{y} = \bar{b}$. The modal shear angle in both directions has a small magnitude when compared to the modal bending rotations in Figure 6.19, signifying the contribution of the shear angle is small for the plate with free edges in the \bar{y} -direction.

The modal plots for various other vibration modes given in Table 6.6 for the simply-supported/free Mindlin plate follow, with the modal displacements in Figure 6.21, the modal bending rotations in the \bar{x} -direction in Figure 6.22, and the modal bending rotations in the \bar{y} -direction in Figure 6.23. Substitution of any of the natural frequency and wave number pairs found from the roots of Eq. (5.104) into the modal functions given in Eqs. (5.109)-(5.111) will give the modal plots for that vibration mode of the simply-supported/free Mindlin plate. Additional plots have been omitted for brevity. Conclusions from the numerical simulations presented herein follow in the final chapter of this thesis.

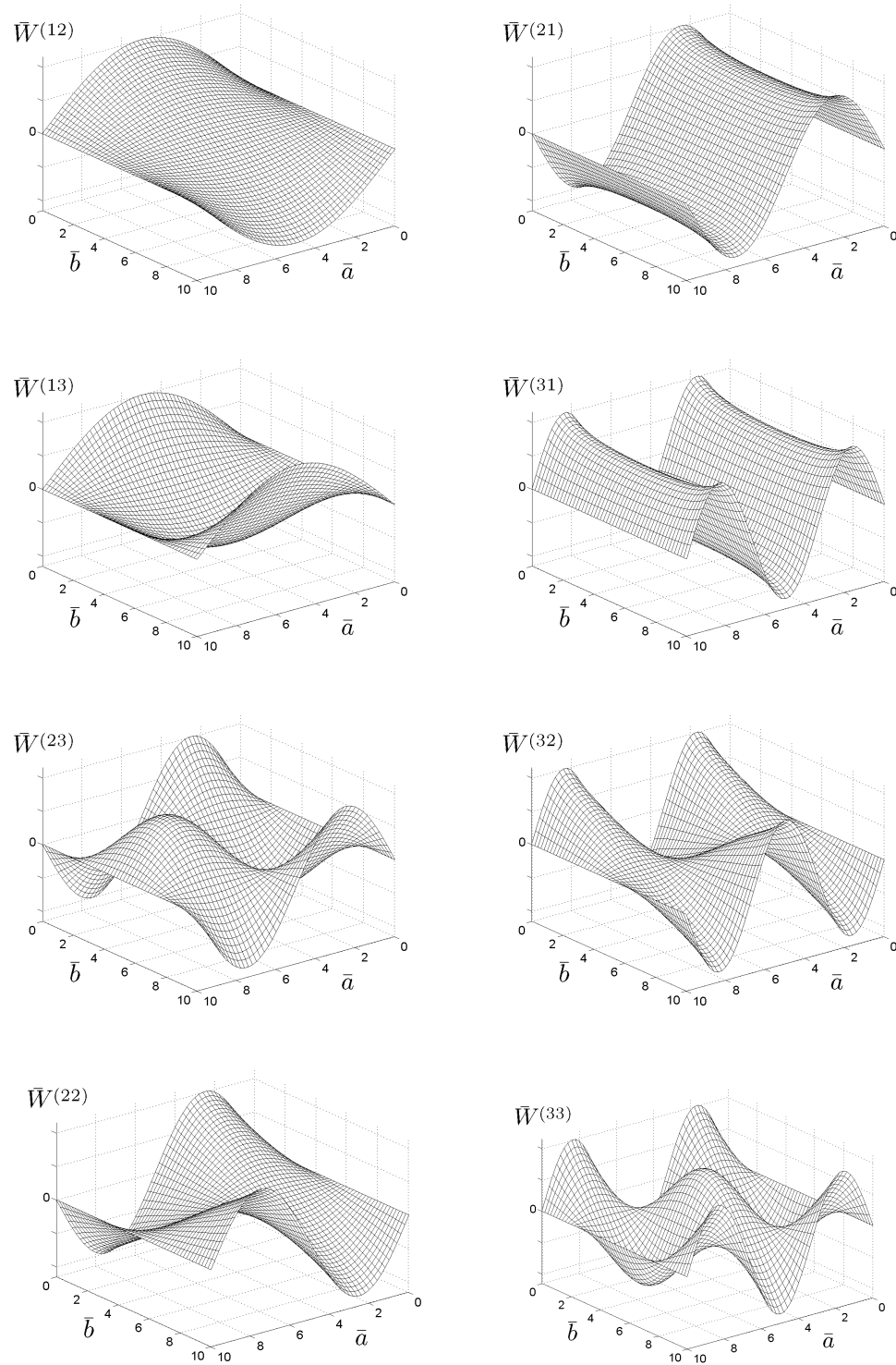


Figure 6.21: The modal displacements for several representative vibration modes of the simply-supported/free Mindlin plate with sides $\bar{a} = \bar{b} = 10$ and $\nu = 0.3$.

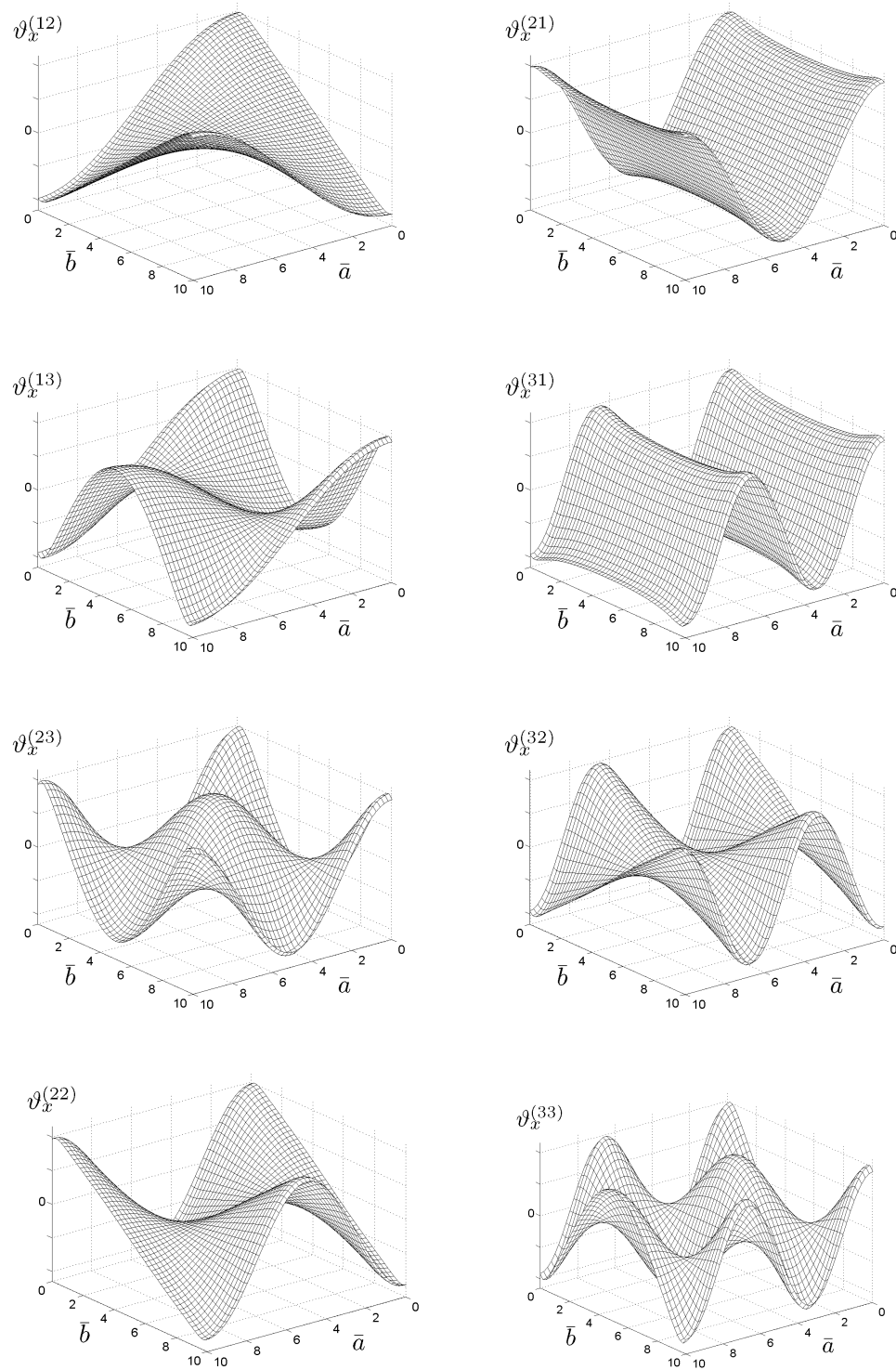


Figure 6.22: The modal bending rotations in the \bar{x} -direction for several representative vibration modes of the simply-supported/free Mindlin plate with sides $\bar{a} = \bar{b} = 10$ and $\nu = 0.3$.

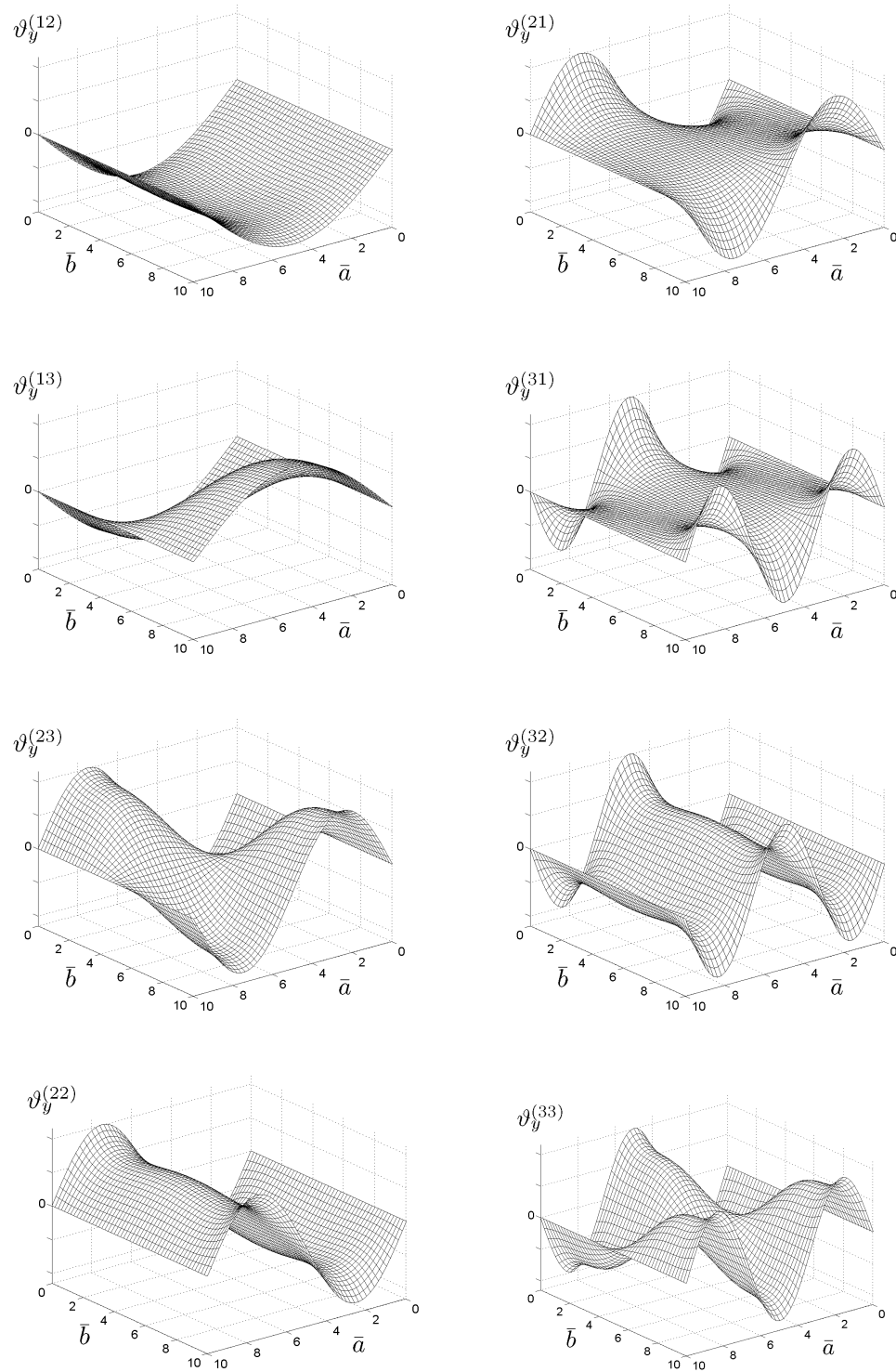


Figure 6.23: The modal bending rotations in the \bar{y} -direction for several representative vibration modes of the simply-supported/free Mindlin plate with sides $\bar{a} = \bar{b} = 10$ and $\nu = 0.3$.

Chapter 7

Conclusions

The free vibration of a plate using Mindlin plate theory has been studied. The kinematic, constitutive, and kinetic relations for Mindlin plate theory are presented, with a summary of prominent values for the shear correction coefficient used in the literature included. A review of the frequency spectrum for the elastodynamic plate is presented in order to analyze the accuracy of the frequency spectrum for the Mindlin plate.

A general analytical solution is presented for the equations of motion governing the free vibration of the Mindlin plate. The three branches of the frequency spectrum for this plate theory are identified through comparison with the frequency spectrum of the infinite elastodynamic plate. Based on physical interpretation and correspondence with the elastodynamic branches, the use of branch dependent shear correction coefficients is proposed. The branch dependent coefficients bring each of the three branches of the Mindlin plate into best agreement with the elastodynamic branches.

The general solution is applied to plates with simply-supported, simply-supported/clamped, and simply-supported/free edges. Upon imposition of the boundary conditions for the simply-supported plate, it is found that only one of the three branches of the frequency spectrum is active for a given vibration mode. Since the frequency branches do not interact for a given vibration mode, natural frequencies for each of the branches are calculated for a given propagating value of the wave number $\bar{\eta}$. The modal behavior corresponding to each of the branches is analyzed and distinctions in the mechanisms of deformation for each branch are drawn. When compared to other studies in the literature, the predicted natural frequencies calculated using branch dependent shear correction coefficients best matched those assessed through the exact elastodynamic analysis for all three branches.

For both the cases of the plate with simply-supported/clamped and with simply-supported/free edges, all three branches of the frequency spectrum are active for a given vibration mode. That is, each mode is seen to be comprised of a contribution from each of the three wave numbers in the \bar{y} -direction of the plate. Hence, a point is found on each of the branches that aligned horizontally upon the branches of the frequency spectrum, which corresponds to the natural frequencies for these boundary conditions. The natural frequency spectrum is presented as a functional component of the wave number $\bar{\alpha}$ in the \bar{x} -direction, and modal plots are also presented for both cases. An elastodynamic analysis is not available in the literature for comparison for these cases but, based on the results from the simply-supported plate, it is assumed that branch dependent shear correction coefficients slightly improved the frequency results.

In conclusion, the use of branch dependent shear correction coefficients has improved the frequency predictions for the free vibrations of Mindlin plates. The thesis has also provided insight into the nuances that must be considered when solving for the natural frequencies of the Mindlin plate for various boundary conditions. The insight provided into the interactions of the frequency branches improves upon the physical understanding and interpretation, as well as the analysis of the free vibration of the Mindlin plate even for the classical case when a single shear correction coefficient is employed. The most important of which is the recognition that when considering simply-supported boundaries a single branch of the frequency spectrum is active for a given vibration mode while for mixed boundaries all three branches of the frequency spectrum must be active to form a given vibration mode.

References

- [1] Bottega, W.J., 2015. *Engineering Vibrations*, 2nd ed., CRC Press, Boca Raton.
- [2] Cowper, G.R., 1966. The shear coefficient in Timoshenko's beam theory. *J. Appl. Mechs.*, 33, 2, 335-340.
- [3] Endo, M. and Kimura, N., 2007. An alternative formulation of the boundary value problem for the Timoshenko beam and Mindlin plate. *J. Sound Vib.*, 301, 355-373.
- [4] Filon, L.N.G., 1903. On an approximate solution for the bending of a beam of rectangular cross-section under any system of load, with special reference to points of concentrated or discontinuous loading. *Phil. Trans. R. Soc. (Ser. A)*, 201, 63-155.
- [5] Filon, L.N.G., 1912. Investigation of stresses in a rectangular bar by means of polarized light. *Phil. Mag.*, 6, 23, 1-25.
- [6] Graff, K.F., 1991. *Wave motion in elastic solids*. Dover, New York.
- [7] Hashemi, S.H. and Arsanjani, M., 2005. Exact characteristic equations for some of classical boundary conditions of vibrating moderately thick rectangular plates. *Internat. J. Solids Structures*, 42, 819-853.
- [8] Higuchi, S., Saito, H., and Hashimoto, C., 1957. A study of the approximate theory of an elastic thick beam. *Can. J. Phys.*, 35, 757-765.
- [9] Hutchinson, J.R., 1980. Vibrations of solid cylinders. *J. Appl. Mechs.*, 47, 901-907.
- [10] Hutchinson, J.R., 1984. Vibrations of thick free circular plates, exact versus approximate solutions. *J. Appl. Mechs.*, 51, 581-585.
- [11] Kaneko, T., 1975. On Timoshenko's correction for shear in vibrating beams. *J. Phys. D: Appl. Phys.*, 8, 1927-1936.
- [12] Kirchhoff, G., 1850. Uber das Gleichgewicht und die Bewegung einer Elastischen Scheibe. *J. Reine Angew. Math.*, 40, 51-88.
- [13] Lamb, H., 1889. On the flexure of an elastic plate. *Proc. Lond. Math. Soc.*, 23-24, 70-91.
- [14] Lange, K.A. and Bottega, W.J., 1998. On the elastodynamic response of thick multi-layered plates subjected to impact loads. *J. Sound Vib.*, 211, 1, 39-93.
- [15] Liew, K. M., Xiang, Y. and Kitipornchai, S., 1995. Research on thick plate vibration: A literature survey. *J. Sound Vib.*, 180, 163-176.
- [16] Meeker, T.R. and Meitzler, A.H., 1964. Guided wave propagation in elongated cylinders and plates, in *Physical Acoustics*, Mason, W.P., ed., Vol. 1, Part A, Chap. 2. Academic Press, New York.

- [17] Mindlin, R.D., 1951. Influence of rotatory inertia and shear on flexural motions of isotropic, elastic plates. *J. Appl. Mechs.*, 18, 1, 31-58.
- [18] Mindlin, R.D., Schacknow, A., and Deresiewicz, H., 1956. Flexural vibrations of rectangular plates. *J. Appl. Mechs.*, 23, 430-436.
- [19] Mindlin, R.D. and Medick, M.A., 1959. Extensional vibrations of elastic plates. *J. Appl. Mechs.*, 26, 561-569.
- [20] Mindlin, R.D., 1960. Waves and vibrations in isotropic, elastic plates. *Structural Mechanics*, Pergamon Press, New York, 199-232.
- [21] Pao, Y.-H., 1983. Elastic waves in solids. *J. Appl. Mechs.*, 50, 1152-1164.
- [22] Lord Rayleigh, 1889. On the free vibrations of an infinite plate of homogenous isotropic elastic matter. *Proc. Lond. Math. Soc.*, 20, 1, 225-237.
- [23] Reddy, J.N., 1984. A simple higher-order theory for laminated composite plates. *J. Appl. Mechs.*, 51, 745-752.
- [24] Reddy, J.N. and Phan, N.D., 1985. Stability and vibration of isotropic, orthotropic and laminated plates according to a higher-order shear deformation theory. *J. Sound Vib.*, 98, 157-170.
- [25] Reissner, E., 1944. On the theory of bending of elastic plates. *J. Math. Phys.*, 23, 184-191.
- [26] Reissner, E., 1945. The effect of transverse shear deformation on bending of elastic plates. *J. Appl. Mechs.*, 12, 69-77.
- [27] Shimpi, R.P. and Patel, H.G., 2006. Free vibrations of plate using two variable refined plate theory. *J. Sound Vib.*, 296, 979-999.
- [28] Srinivas, S., Rao, C.V. Joga, and Rao, A.K., 1970. An exact analysis for vibration of simply-supported homogeneous and laminated thick rectangular plates. *J. Sound Vib.*, 12, 187-199.
- [29] Stephen, N.G., 1997. Mindlin plate theory: Best shear coefficient and higher spectra validity. *J. Sound Vib.*, 202, 4, 539-553.
- [30] Timoshenko, S.P., 1921. On the correction for shear of the differential equations for transverse vibrations of prismatic bars. *Phil. Mag.*, 6, 41, 744-746.
- [31] Timoshenko, S.P., 1922. On the transverse vibrations of bars of uniform cross-section. *Phil. Mag.*, 6, 43, 125-131.
- [32] Xiang, W. and Xing, Y., 2015. A new first-order shear deformation theory for free vibrations of rectangular plate. *Int. J. Appl. Mechanics*, 7, 1.